Post processing of raw data recorded with an ECG-vest

by

Øyvind Aardal

THESIS

for the degree of

MASTER OF SCIENCE

in

Computational Science and Engineering

Department of Mathematics
Faculty of Mathematics and Natural Sciences
University of Oslo

November 2008

Matematisk institutt
Det matematisk- naturvitenskapelige fakultet
Universitetet i Oslo

Acknowledgements

I would like to thank my three excellent supervisors for all their support in my work with this thesis. First of all, I would like to thank my main supervisor Marius Lysaker who has guided me through the writing of this thesis, and for always being inspiring and helpful. Andreas Austeng; for all his contributions throughout the thesis and help with signal processing techniques. Bjørn Fredrik Nielsen; for his valuable feedback on the presentation of my thesis and the final chapters.

For the help in recording and acquiring real BSPM data for use in this thesis, I would like to thank Per Grøttum from Simula and Kristina H. Haugaa and Jan G. Fjeld from Rikshospitalet HF.

Thank you, Camilla Kirkemo, for being so supportive and for the input on my thesis. For making the studies at the University of Oslo pleasant and enjoyable; a great thank you to H.K.H. Ursus Major. Finally, I would like to thank my parents for all their love and for always being here for me.

Contents

List of Figures

List of Tables

A short explanation of the abbreviations and terms used in the thesis

ECG is the abbreviation for electrocardiogram and is the term used for the 12-lead ECG. ECG is also used for the recording in a single channel of the 12-lead ECG.

12-lead is another term for the standard ECG recording.

BSPM is an abbreviation for body surface potential mapping, which is a collection of electrical potential differences recorded at many points on the upper body. In this thesis a 64 channel BSPM is used. The term BSPM will also be used on single channels in the 64 channel BSPM.

WCT is the abbreviation for the Wilson Central Terminal.

Electrode is the term used for a single recording node used in BSPM/ECG.

Channel is used for the recording in one of the electrodes of an ECG/BSPM that have been modified by the WCT.

Lead is the term used for a combination of electrode recordings. For the BSPM recordings in this thesis, a lead will be the same as a channel.

V is often used as the term for a channel of the BSPM. V^i is then the ith channel out of the 64 channels.

V_j^i is often used as the term for the jth heartbeat of the ith channel of a BSPM. V_j^i is then a vector containing the measurement of one channel V^i between onset value j and $j+1$.

ST segment is a segment of the heartbeat. In this thesis, shifts in the ST segment between a rest and exercise recording is used as an indication of ischemia.

BSSTM is an abbreviation for body surface ST segment mapping. This is a mapping of the difference in ST segment shifts at the spatial locations of the channels of the BSPM.

Chapter 1

Introduction

1.1 Ischemia and the electrocardiogram (ECG)

Ischemic heart disease is the single most frequent cause of death in the world today [42]. It occurs when the oxygen demand of the heart muscle exceeds the supply, often caused by an occlusion in the blood vessels. Diagnosing ischemia is a difficult task, with the illness being undetected in many patients [15]. Even the tiniest improvement of the methods for diagnosing this disease will have great effect on the number of people receiving treatment in time. The electrocardiogram (ECG) is the most commonly used tool for diagnosing heart diseases, including ischemia. The ECG is a recording of the electrical activity in the heart at selected points on the body surface.

1.1.1 ST shift measurement

ECG exercise testing can be used to detect ischemia by comparing a rest and exercise ECG recording of a patient. A shift in a part of the heartbeat called the ST segment is used as an indication of the presence of ischemia [15]. In the standard ECG, three limb electrodes in addition to six electrodes placed close to each other on the chest is used. The small number of measuring points in the traditional 12-lead ECG limits it's diagnostic capabilities [22]. The use of an ECG vest, more commonly called a body surface potential mapping (BSPM), which has more electrodes spread over a greater area of the upper body provides better detection and localisation properties than the traditional ECG [25, 43]. In addition, cardiac computation methods using such ST segment shifts as input values will benefit from the BSPM as it measures the ST segment shifts at points spread out on the upper body.

Before these ST segment shifts can be measured precisely, the raw data recorded in a BSPM must be processed. While the ECG is a standardised and well researched tool, there exists, to the author's knowledge, no complete BSPM post processing algorithm. In this thesis an automatic algorithm for post processing and measuring ST segment shifts in a 64 lead BSPM has been developed. Both methods developed in this thesis, and modifications of existing ECG processing methods will be made. These will utilise the increased spatial information provided by the BSPM.

1.2 BSPM signal processing

The BSPM is a body surface recording of the electrical activity originating from the heart. However, not only the signal from the heart will be recorded in a BSPM. A simple model for the content of a recorded BSPM is made:

$$BSPM = BSPM_{signal} + BSPM_{noise} + BSPM_{drift}.$$

The model classifying the contributing parts of a BSPM as a signal originating from the heart, noise or baseline drift (slow varying changes in the recording). The noise and baseline drift will result in inaccurate and sometimes even false measurements of the BSPM characteristics if computed from the raw data. Post processing BSPM recordings is a task of reducing the amount of $BSPM_{noise}$ and $BSPM_{drift}$ while at the same time keeping $BSPM_{signal}$ unchanged.

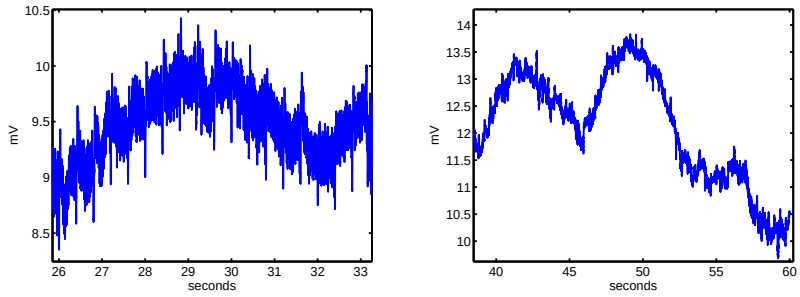

Figure 1.1: Two examples of raw data recordings in a BSPM.

1.3 Development of automatic algorithm

Manual processing and ST segment shift measurement of BSPM raw data is time consuming and can be inaccurate. This motivates the need for a complete automatic algorithm for post processing BSPM data. An automatic BSPM processing algorithm is developed in this thesis. It will use raw data recordings as input, and produce both the processed BSPM and computed ST segment shifts as output. Methods are developed and tested to both remove a priori known noise content, and unclassified disturbances in the signal.

The following methods have been developed, implemented and tested as part of the algorithm: First, noise reduction methods using frequency based filtering techniques was implemented and tested. Second, an algorithm for detecting the BSPM signal peaks was developed. This method was used to locate the interesting parts of each heartbeat. Third, methods for removing the baseline drift is discussed. Four methods were selected, implemented and evaluated against each other. A method using cubic spline interpolation as an approximation to the drift was deemed best and used in the automatic algorithm. Even after this initial processing, there may be noisy or corrupted signal parts present in a BSPM. Hence a framework for removing such parts of the BSPM was developed as the fourth step of the algorithm. In the fifth step, a robust method for computing the ST segment shifts at each electrode location from a processed BSPM was made. Finally, a tool for visualising these shifts was created.

1.4 Outline of results

The algorithm developed in this thesis was applied to BSPM recordings of real patients. Before processing, it was not possible to compute neither reliable nor correct ST segment shifts from these recordings. In addition most recordings showed variations between neighbouring points on the body too great to be physically possible. After the automatic algorithm was applied to these recordings, all BSPMs became smoother with neighbouring ST segment shift values being relatively close to each other in value. The visualisation tool developed in this thesis, can also be used to confirm that the processed BSPMs are physically possible.

A comparison between the standard ECG and processed BSPM was made. Finally, each processed BSPM could be recognised as belonging to either a healthy patient or an ischemic patient. With the exception of one unclear BSPM, the decisions on the presence of ischemia or not in a patient were all correct.

Each step of the automatic algorithm developed has been evaluated and discussed. In addition, the algorithm shows promising results when applied to real life BSPMs. However, only a small number of BSPMs were available for testing in this thesis. The results found by applying the algorithm to these BSPMs are therefore not statistically significant, but rather an indication to the effectiveness of the algorithm developed.

Chapter 2

Electrical activity in the heart, the ECG and the BSPM

This thesis will have it's focus on post processing body surface potential mappings. Differences in certain segments of the BSPM of patients during rest and exercise is computed from these for use in detecting ischemia. Before attention is turned to these problems, a description of the background for the later computations will be given. The physiology and electrophysiology of the heart is briefly described. The 12-lead ECG has for decades been the leading tool for recording the electrical activity in the heart, and still is today. The ECG will be described as a motivation for the body surface potential mappings that have been used in this study. The BSPM and the recordings used will then be introduced to the reader. This chapter will be rounded off by a description of ischemic heart disease, and its effect on the recordings of the electrical activity from the heart.

2.1 The physiology and electrical activity of the heart

In this section an introduction to the physiology and electrical activity in the heart will be given. This will serve as a background for the computations on the electrical signals originating in the heart that will be described later. [20, 37, 5] all contain chapters on the subject, and can be read for a more thorough introduction.

2.1.1 The physiology of the heart

The heart contains four chambers, divided into two upper chambers called the atria, and two lower chambers called the ventricles. Each of these is also divided into left and right sides (see Figure 2.1). A typical heartbeat starts in the sinoatrial node (SA node) located just above the right atrium. It initiates the contraction of the atria, pushing blood into the ventricles. When the atrial

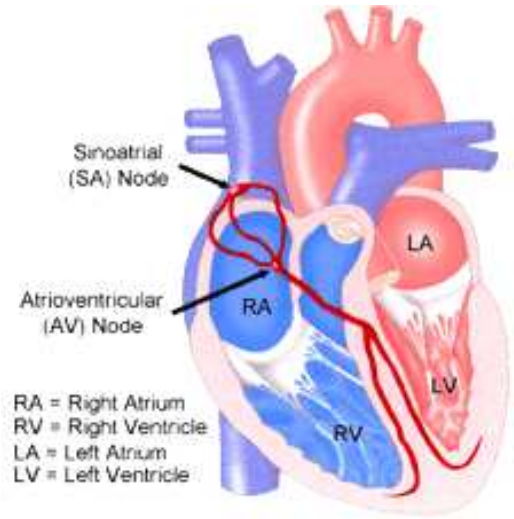

Figure 2.1: A schematic figure of the human heart. (Figure from [4].)

contraction is finished, the ventricles contract. The left ventricle pushes blood rich on oxygen into the arterial system, while the right pushes blood to the lungs. Then the heart muscles relax, allowing the atria and ventricles to be refilled with blood.

The contractions of the heart muscles during a heartbeat is controlled by a series of electrical signals which will be described in the next section.

2.1.2 Electrical activity in the heart

The pumping of the heart is controlled by a system of electrical signals originating in the SA node. The cells in the SA node are autonomous oscillators, which means that they create electrical action potentials without any external sources. The heart muscle cells (myocardium) has the ability to carry an action potential (conduct electricity), which means that the electrical signals initiated in the SA node can be carried throughout the heart muscles. Heart muscle cells in their resting state have a negative potential. The action potential initiated in the SA node spreads across both atria as a wave of depolarisation, causing them to contract. The atria and ventricles are separated by a septum (layer) of non-excitable cells, so the action potential does not spread directly to the ventricles[1]. Instead it is passed through the only conductive passage between the two layers; the atrioventricular node (AV node) located at the bottom of the atria. The propagation of electricity through the AV node is quite slow, so there is a small delay between the signal propagating through the atria and reaching the ventricles. This allows the ventricles to be filled with blood before contracting. The action potential exits the AV node through it's distal portion, called the atrioventricular bundle or the bundle of His, and into the ventricles. At last the muscles of the heart relax and repolarise, readying for the next heartbeat.

[1] This is the case in the majority of hearts. Heart conditions or illnesses such as ventricular fibrillation will result in different electrophysiological behaviour

2.2 The electrocardiogram

2.2.1 History

The electrical potential that cause the heart to pump, spread through the body and can be measured at the body surface. The electrocardiogram (ECG) records the difference of this potential at the body surface. The first ECG was published in 1887 by Augustus D. Waller. He recorded the electrical potential differences in the paws of his bulldog using a capillary electrometer. 14 years later Willem Einthoven invented a better and more sensitive device called the string galvanometer. He also assigned the letter P,Q,R,S and T to the different deflections in the ECG, which are still used today (see Section 2.2.3). Einthoven used electrodes on the left and right arm and the left leg to produce three bipolar leads, where each lead is the potential difference between two electrodes. (see Section 2.2.2 for more info). In 1933 Wilson introduced the concept of unipolar leads by tying the three limb leads together to create a common reference point for all leads. The ECG has been standardised and improved over several decades after this. In the last decades, digital computers have been used to a greater and greater extent to process the ECG signals. Today the ECG is a well known and much used tool around the world for monitoring the electrical activity in the heart.

2.2.2 The standard 12-lead ECG

During the course of a heartbeat, the electrical current spreading form the heart throughout the body changes in orientation and magnitude. The human body functions as a passive volume conductor. While not producing any electrical potential of its own, it allows the electrical signals originating from the heart to travel to the surface. By measuring the potential difference between electrodes at the body surface, one can approximate this electrical activity.

The measurement of the potential difference between electrodes is called a lead. Two types of leads will be described below; bipolar and unipolar leads. Unipolar leads are the potential difference between a point and a constructed reference potential. Einthoven used his three electrodes on the right arm (RA), left arm (LA) and left leg (LL) called V_{RA}, V_{LA} and V_{LL} respectively to form three leads. These leads measure the potential difference between two points, and are called lead I, II and III. Leads measuring the potential difference between two points are called bipolar.

$$\begin{aligned} I &= V_{LA} - V_{RA} \\ II &= V_{LL} - V_{RA} \\ III &= V_{LL} - V_{LA}. \end{aligned}$$

The standard ECG used in hospitals worldwide consists of three or four limb electrodes and six chest electrodes. These are combined to form 12 leads (see Figure 2.2) called I, II, III, AVR, AVL, AVF and V1-V6. Only lead I, II and III are bipolar, the others are unipolar. Differing from the three bipolar leads, the unipolar ones are not the potential difference between just two points. Instead, they are electrodes referenced to a constructed "neutral" potential. Table 2.1

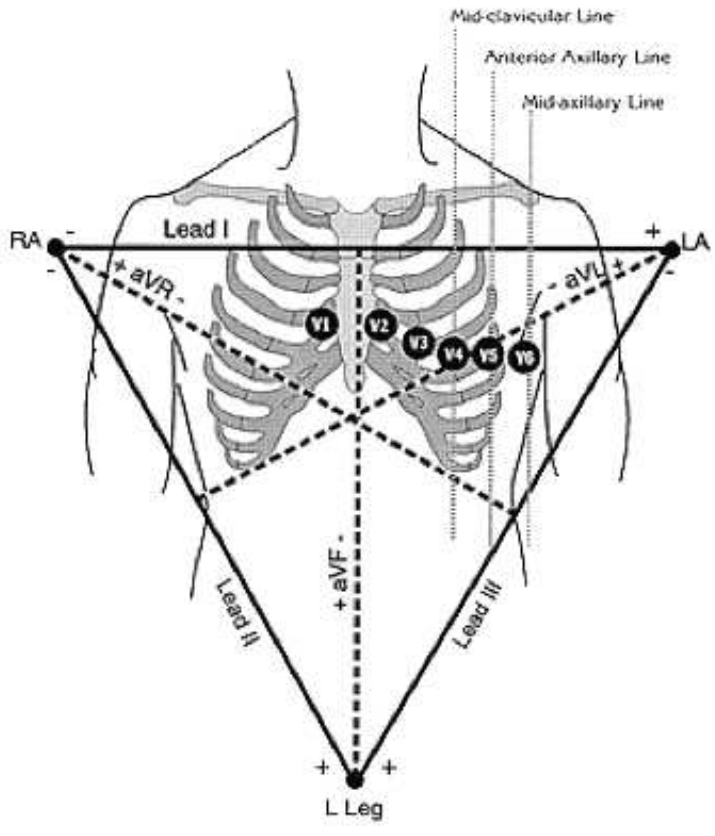

Figure 2.2: The electrode placement in the standard 12-lead ECG. Figure taken from [5]

[37] gives an overview of the electrodes and reference potentials used to produce each lead. For leads V1-V6 the reference potential is the arithmetic average of the three limb electrodes V_{RA}, V_{LA} and V_{LL}, and is called the Wilson Central Terminal (WCT). The idea is to create a "zero" electrode which ideally has small changes during a heartbeat.

Lead	electrode	reference
I	V_{LA}	V_{RA}
II	V_{LL}	V_{RA}
III	V_{LL}	V_{LA}
aVR	V_{RA}	V_{LA} and V_{LL}
aVL	V_{LA}	V_{RA} and V_{LL}
aVF	V_{LL}	V_{RA} and V_{LA}
V1-V6	1-6	V_{RA}, V_{LA} and V_{LL}

Table 2.1: The construction of the leads in 12-lead ECG

Hence, the unipolar leads referenced to the WCT approximately describes the electronic potential changes in each electrode. In the BSPM used in this study, all leads used will be unipolar leads referenced to the Wilson Central Terminal.

2.2.3 The ECG signal

Figure 2.3 shows the characteristics of a typical heartbeat, plotted with time on the horizontal axis and potential difference on the vertical axis. The straight line segments represents periods of time when there are no sources of electrical activity in the heart, and are referred to as the baseline or isoelectric line. The waveform deflections from the baseline are caused by electrical activity in the heart tissue. Each phase in the ECG represents a certain electrical activity in the heart. A detailed description is given below. In practice, the magnitude, duration and orientation (positive vs. negative deflections) will wary over different leads, and not all characteristics are sure to be present in the ECG of every lead.

P wave : The electrical activity of a heartbeat starts with the propagation of action potential from the SA node through the atria. This triggers depolarisation of the atria, resulting in a contraction. This depolarisation produces the P wave. The normal duration of a P wave is 100 ms, and the magnitude is low relative to the QRS complex and T wave.

PR interval : The PR interval is the period starting with the onset of the P wave, and ending with the onset of the QRS complex. It normally has a duration of 120-200 ms.

PR segment : The PR segment is the period between the offset of the P wave and the onset of the QRS complex. This segment should be on the baseline, as no electrical activity normally occurs in this segment.

QRS complex : The QRS complex is caused by the depolarisation of the ventricles, and the repolarisation of the atria. The deflection caused by

repolarisation of the atria is small relative to the deflection from depolarisation of the ventricles. The complex is quite steep because of high velocity of propagation of the electrical signals through the ventricles. It also is the part of a heartbeat with the largest magnitude (normally around 1-3 mV) due to the great muscle mass of the ventricles. Normal duration for the QRS complex is 60-100 ms.

ST segment : The ST segment is the period from the offset of the QRS complex to the onset of the T wave. It corresponds to the time between depolarisation and repolarisation in the ventricles, a time period in which there is little to none electrical activity in the heart. Typical duration of the ST segment is 120 ms or less.

T wave : The T wave is a result of repolarisation of the ventricles, where the cells return to their resting potential. It has longer duration (normally 200 ms or less) than the QRS complex since repolarisation is a slower process than depolarisation. It has a magnitude of up to 0.5 mV, and usually is larger than the P wave.

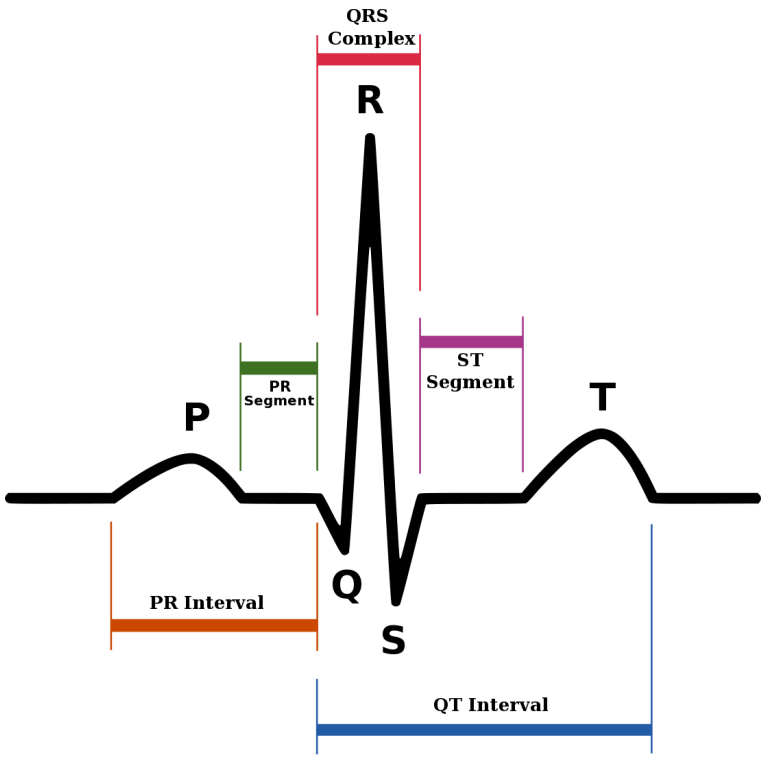

Figure 2.3: Schematic representation of ECG during one heart cycle. Time along the horizontal axis, voltage along the vertical axis. The figure is from [7].

2.3 Body surface potential mappings

For several decades ECG has been, and still is, the number one tool for recording the electrical activity in the heart at the body surface. Even though the 12-lead ECG is a well standardised and known test to medical personnel, it has it's limitations. Since the ECG only records the body surface potential differences in six locations on the thorax it's spatial coverage limits it's ability to detect several heart diseases, such as ischemia [26, 22]. The BSPM covering an extensive area of the upper body provides better spatial sampling and is also more sensitive in detecting ischemia [38, 17], even in patients with no characteristic findings in the standard 12-lead [26]. The BSPM may also prove better suited for localising an ischemic region of the heart [26]. This motivates the use of BSPMs for early diagnosis of ischemia. It is also a useful tool for cardiac computations and inverse problems, as the increased spatial sampling provides more data. From a signal processing point of view the increased amount of data and spatial sampling compared to the 12-lead is an advantage that will be used in this thesis.

2.3.1 Outline of the BSPM

So far in this chapter, the traditional 12 lead ECG has been described. This standard ECG mapping uses six electrodes placed at the chest as shown in Figure 2.2 in addition to the reference electrodes. The standard 12 lead ECG will not be used in this thesis. Instead a 64 lead BSPM will be used. The BSPM consists of 64 electrodes placed evenly in strips on the torso, in addition to three reference electrodes placed at the limbs (see Figure 2.4 and 2.5). While the

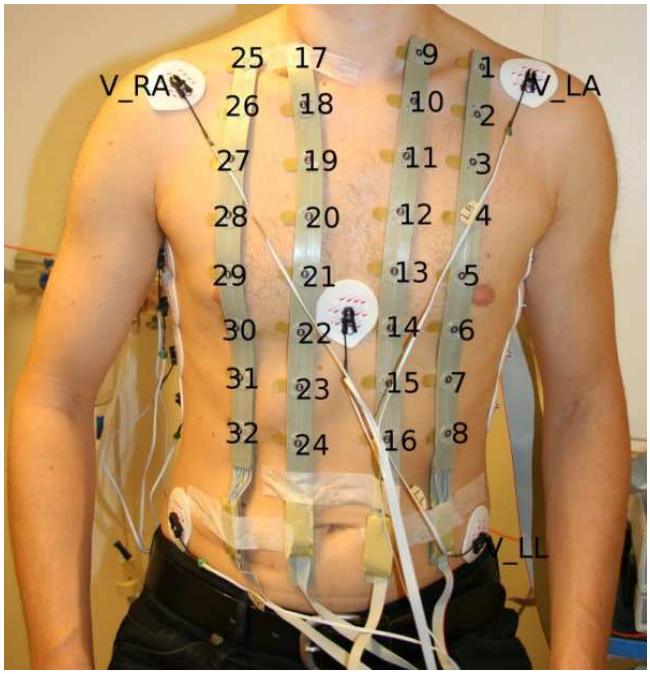

Figure 2.4: The 32 front leads in the 64 lead Body surface potential mapping used in this thesis.

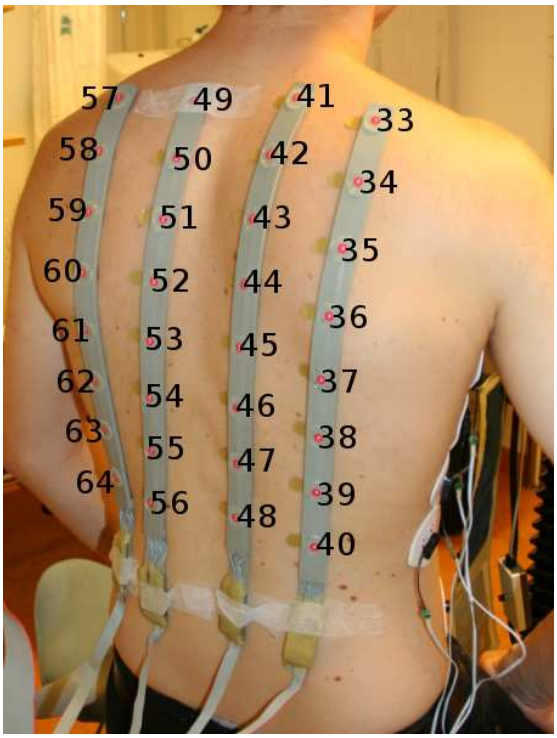

Figure 2.5: The 32 back leads in the 64 lead Body surface potential mapping used in this thesis.

traditional ECG only records the electric action potential originating from the heart at six points on the chest, the BSPM records the action potential at both the front and back of the upper body. 32 electrodes are placed in four strips of eight at the front of the torso, and 32 electrodes are placed in four strips of eight at the back. These totals to 64 channels that will be denoted V^i, $i = 1, \ldots, 64$ throughout the thesis.

As written in Section 2.2.2, the leads of a BSPM are unipolar leads. This means that each lead of a BSPM is the difference between the recording at the current electrode, and the WCT (Remember that the WCT is the arithmetic average of the three limb electrodes V_{LA}, V_{RA} and V_{LL}). Each of the BSPM leads measure a signal similar to those in a traditional ECG (both cases are recordings of the electrical potential difference at points on the body surface). Although each lead will have the characteristics illustrated in Figure 2.3, the variation in shape and amplitude between some of the leads in a BSPM will be greater than for 12 lead ECG due to the large difference in spatial placement between some of the electrodes.

2.3.2 The equipment and recordings used in this study

Throughout the study, BSPMs of real patients will be presented and used. The BSPMs have been recorded at Rikshospitalet [1] in cooperation with Simula research laboratory [2]. The equipment used for the recording of the BSPMs, is the Biosemi ActiveTwo Mk2-system [8]. Two 4×8 electrode panels shown in

Figure 2.6 are used; one on the front and one on the back of the upper body.

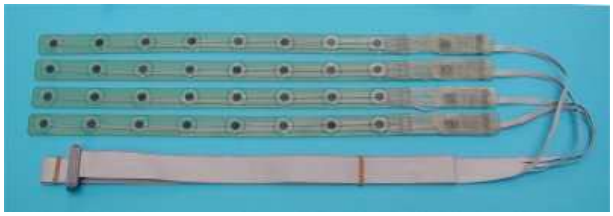

Figure 2.6: The 4×8 electrode strips that are attached to the front and back of the torso for the BSPMs used in this thesis. Picture is from [3].

Electrical signals spread continuously through the body. To do computations on these signals, they have to be recorded and stored digitally. Thus, the continuous electrical action potentials that reach the electrodes at the body surface are sampled in time by the BSPM measuring equipment. A sampling rate of $2048Hz$ is used, which means that the continuous analog signal is stored as a discrete digital signal with 2048 data values (samples) per second. All of this is done by the Biosemi system. The output of the equipment is a matrix of numbers, where each column is a recording of a BSPM channel in time.

The focus of this thesis is to calculate information about the ST and PR segments of the BSPM of a patient for usage in diagnosing ischemia. To get the information needed, a BSPM of each patient has to be recorded both during rest and during exercise. For these recordings, the electrodes are first attached to the patient. For some time, the patient sits without moving to get the "rest"-data. Then, without stopping the measurements, the patient mounts a stationary bicycle and starts cycling. When the patient reaches a certain heartbeat rate (220 minus age beats per minutes, adjusted by clinical decisions by the medical personnel), or starts to feel pain in the chest, the time is noted and the following part of the recording is termed the "exercise"-data. Throughout the rest of the thesis, when terms like "recording during rest" and "BSPM of the patient during exercise" are used, they refer to these time periods.

Due to a limited set of recordings available, this thesis will be limited to using six different BSPMs. Two of these are recordings of healthy patients[2] (which will be called patient5 and patient6), and four are recordings of patients with ischemic heart disease diagnosed by additional medical testing (called patient1, patient2, patient3 and patient4).

2.4 Heart diseases

The electrical signals generated by the heart change in response to different heart conditions. Heart diseases and their effect on ECGs/BSPMs is a large field, and many diseases with corresponding changes to the ECG has been surveyed. This makes the ECG a powerful diagnostic tool, as different heart diseases can be recognised by characteristic changes in the signal recorded at the body surface.

[2]The two healthy patients were not actually patients, but volunteers which with certainty did not suffer from ischemia. For the sake of convenience though, they will be referred to as patients for the rest of the thesis.

There exist a great number of different heart diseases and conditions, and so a multitude of effects on ECG signals. Attention will soon be turned to ischemia, which is the disease this thesis will focus on. First a few examples of ECG abnormalities as a result of illnesses will be given [5], to illustrate that heart conditions can change ECG recordings in many different ways: Heartbeat rhythms deviating from normal heartbeat rhythm (60-100 regularly spaced beats per minutes) are called arrhythmias. These come in many forms, like changes and irregularities in heartbeat rate, missing heartbeats, changes in P wave, T wave and QRS complex morphologies. In the extreme case of ventricular fibrillation, the normal ECG waveform seen in Figure 2.3 is unrecognisable in the ECG. Illnesses like pericarditis and hyperkalemia will change the morphology of the ST phase and T wave, while illnesses like hypertrophy changes the P wave. Also, a range of other diseases and heart conditions will produce other variations in the ECG morphology. Thus a patient suffering from heart diseases other than ischemia can complicate the detection of ischemic heart disease in the BSPM. Compensating for individual other heart diseases in the processing of BSPM data for ischemia detection falls beyond the scope of this master's thesis. Instead the BSPM processing algorithms used and developed will be designed to be robust against various changes in the electrocardial morphology.

Myocardial infarction and ischemic heart disease will also show characteristic changes in the ECG, although not always easy to detect. A further description of ischemia and it's effect on BSPMs is given below.

2.4.1 Ischemia

Ischemic heart disease, or ischemia, is a mismatch between demand and supply of oxygen to heart muscle cells. This is most often the case when an occlusion or narrowed part in one or more of the coronary arteries is present. Such an occlusion will result in diminished blood supply to the heart muscle, and so insufficient oxygen supply. In many cases this will happen when the oxygen demand in the heart muscle increases, for example when the heart is exposed to increased stress because the patient exercises. The lack of oxygen supply leads to changes in the electrophysiological behaviour in the myocardial cells, which can be recorded in a BSPM or ECG.

An oxygen demand greater than the supply in heart muscles for longer periods of time will result in injury. This will eventually lead to myocardial infarction, which is the death of heart muscle cells.

2.4.2 Changes in BSPM caused by ischemia

Since the electrophysiological behaviour of the myocardium is changed for a person with ischemia, there will also be changes in the electrical signal recorded at the body surface using a BSPM. These changes can in many cases be seen as changes in the ST segment of each heartbeat. In a healthy heart, the ST segment is the time between ventricular depolarisation and repolarisation. Thus, no electrical activity should occur during this time, and the BSPM recording should be on level with the baseline. However, ischemia causes a delay in the depolarisation and repolarisation of the myocardial cells. This delay results in shifts in the ST segment of the BSPM.

The shifts in the signal from a patient with ischemia can be seen as elevations or depressions in the ST segments, as seen in Figure 2.7. These shifts is present

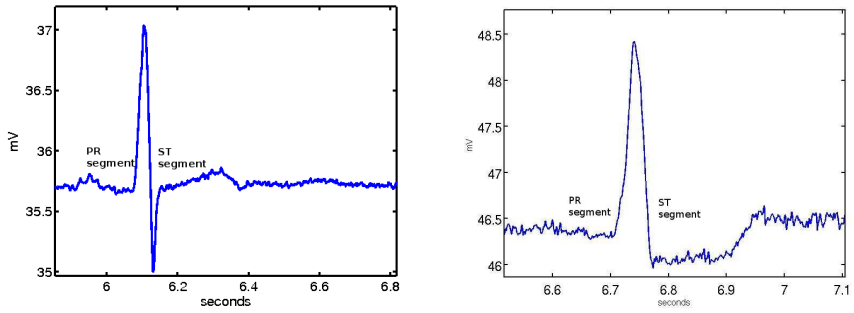

Figure 2.7: To the left is a heartbeat of a patient suffering from ischemia during rest. To the right is a heartbeat of the same channel of the same patient during exercise. Note that the ST segment is depressed relative to the PR segment during exercise while it is not during rest. This is a characteristic change in the BSPM/ECG of a patient with ischemia.

in the BSPM of a patient with ischemia when the blood supply to the heart muscle is insufficient. This leads to the following conclusion: A patient with a heart that gets sufficient blood supply during rest, but insufficient during stress should have a "normal" BSPM during rest and ST segment shifts during stress. This is common in patients with early stages of ischemia, where some arteries may be partially obstructed. It is then possible to find indications of ischemia by measuring the difference in ST segment elevation in BSPMs recorded during rest and and stress. It is not the ischemia itself that is detected this way, but the ST segment shifts that usually is a consequence of the ischemia. Other conditions or circumstances may also cause shifts in the ST segment. Thus there may occur false diagnostications no matter how well the BSPM is processed, if ST segment shifts alone is used.

Shifts in the ST segment in the BSPM of a patient with ischemia will not be present in all channels of the BSPM. The size and location of the ischemic zone varies with which arteries are narrowed, and to what extent. The position and number of channels with ST segment depression and elevation in a BSPM will also vary. Since each channel is "looking" at the heart from different directions, the locations of ST segment changes may be used to determine the location of the ischemic region of the heart [26]. In traditional 12-lead ECG, there are only six electrodes placed on the chest in addition to the reference electrodes. This limits the 12-lead's usefulness in detecting the region of ischemia. In some cases, the ST segment shifts will only be present in electrodes placed at other locations on the torso than where the 12-lead electrodes are placed. These two factors makes the BSPM an attractive tool for detecting ischemia. The BSPM can record ST segment shifts that may not be present in traditional ECG because of the spatial location of the electrodes, and also provides data that is better suited for determining the location of the ischemia. A further description of measuring the ST phase differences to detect ischemia will be given in Section 3.2.

Chapter 3

Working with real data, and theoretical background

In the previous chapter the electrophysiology of the heart and the concept of body surface potential mappings were introduced. This chapter will further describe the problems involved when working with real life BSPM data, and the processing needed. Measuring of ST segment shift differences between rest and exercise recordings to detect ischemia will be further addressed. Finally an introduction to the Discrete Fourier Transform and the filtering techniques used in this thesis will given.

3.1 Noise, drift and artefacts in BSPM recordings

When thinking about ECG, most people will think of a smooth graph with spikes every second or so, such as in Figure 3.1. If the only electrical activity

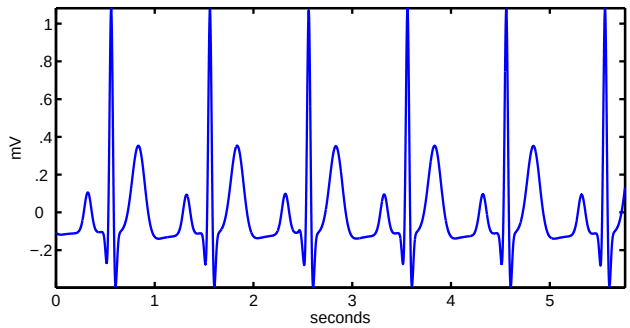

Figure 3.1: Plot of an ideal ECG recording

recorded had been the one originating from the heart, this would indeed be what the ECG of a healthy person looks like. However, in real life recordings this is not the case. Figure 3.2 shows some real ECGs contaminated by noise in different ways. Clearly, most of these signals can't provide information helpful

in diagnosing deceases in their raw form, and need to be processed first to get useful results. Some channels, like the lower right in Figure 3.2 will not provide any information at all even after processing, and need to be removed. There are

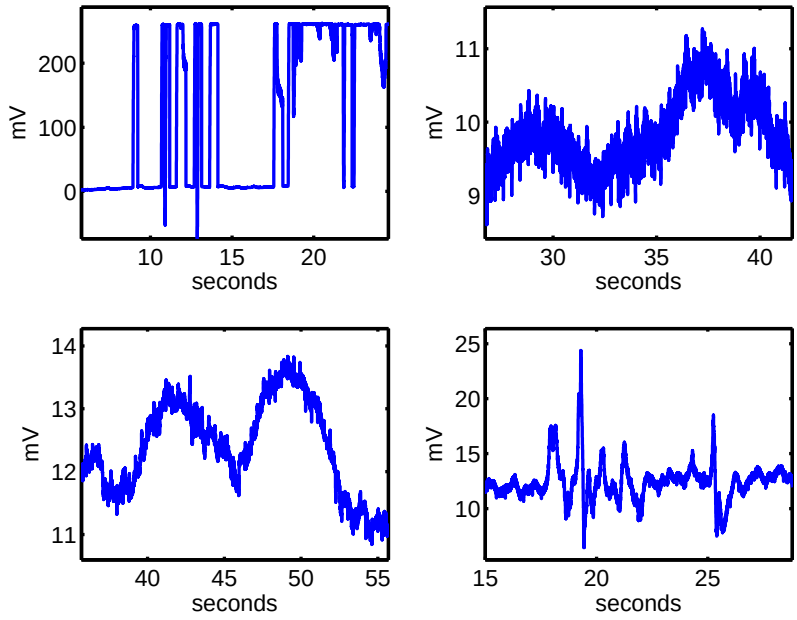

Figure 3.2: Plot of ECGs distorted by noise in different ways. The upper left ECG is a result of loss of contact between the electrode and the skin of the patient. Note the magnitude on the y-axis. The upper right ECG is a typical example of an ECG with lots of $50Hz$ and white noise present. The lower left figure, is an ECG with lots of drift, varying differently in time. Note the magnitude of the axis on the lower right figure. This signal has no characteristics of an ECG.

many sources of noise that can degrade the signal. The most important ones and their effect on the recordings will be discussed in Section 3.1.2.

3.1.1 Noise and drift in the measured BSPM

The measurement in a channel of a BSPM consists of the actual electrical signals originating from the heart combined with noise and baseline drift. Written in another way:

$$BSPM = BSPM_{signal} + BSPM_{noise} + BSPM_{drift}. \tag{3.1}$$

Equation (3.1) is composed of:

- $BSPM$ is the measurement of one channel in a BSPM.
- $BSPM_{signal}$ is the part of the measurement that consists of the electrical signals from the heart. The amplitude of $BSPM_{signal}$ usually varies within a range of 1-3 mV.

- $BSPM_{drift}$ is the slow varying high amplitude parts of the measured $BSPM$. The magnitude of the drift can be many times the magnitude of $BSPM_{signal}$. A more thorough description of drift and its impact on the BSPM is given in Section 3.1.3.

- $BSPM_{noise}$ consists of every part of the measurement that is not $BSPM_{signal}$ nor $BSPM_{drift}$. The noise varies much in both form and amount, which means that BSPMs even from the same patient can look complete different. See Section 3.1.2 for a classification of different noise sources.

To illustrate how drift and noise can affect the signal, a set of synthetic data has been generated. A synthetic BSPM signal has been generated using the technique described in [24]. Random noise and baseline drift have been generated separately from the signal. This noise and drift have been given typical characteristics, i.e. high amplitude and low frequency for the drift, and low amplitude and high frequency for the noise. These three parts have been added together according to (3.1). The resulting BSPM can be seen in Figure 3.3. This is what a real life BSPM may look like. In this illustrating example, $BSPM_{signal}$, $BSPM_{drift}$ and $BSPM_{noise}$ as seen in Figure 3.4 have been added to produce the BSPM. The inverse process of splitting a BSPM measurement into these three parts is much more complex.

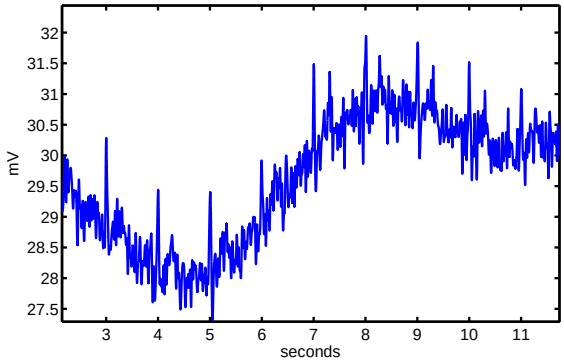

Figure 3.3: A typical looking BSPM signal created by adding $BSPM_{signal}$, $BSPM_{drift}$ and $BSPM_{noise}$. Each of the three synthetically generated components of this BSPM can be seen in Figure 3.4.

All measured channels in a BSPM will be such a combination of signal, drift and noise in many variations. Because all the diagnostic information in a BSPM lies in the $BSPM_{signal}$ parts, an important task in BSPM post processing will be to separate the information in a signal from the contaminating noise and drift. Due to the randomness and the complexity of drift and noise in real measurements, this is a nontrivial task. In a measured BSPM, one does not know what parts of the measurements that are signal, noise or drift, as was the case in Figure 3.3 and Figure 3.4. There are especially two problems connected to reducing the noise and drift in a BSPM: One is that some noise and drift may be difficult to remove, and hence will still be present in the BSPM after drift and noise reducing algorithms have been applied. The other is that drift and noise

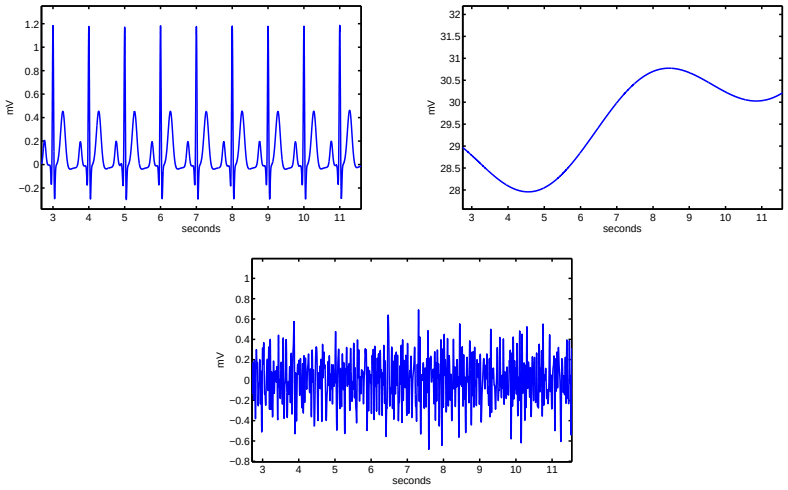

Figure 3.4: These three figures show synthetically generated BSPM signal, drift and noise. The upper left is a plot of $BSPM_{signal}$, the upper right is $BSPM_{drift}$ and the lower is $BSPM_{noise}$.

reducing algorithms can distort the signal part of the BSPM measurement. Reducing noise and drift in BSPM measurements, while minimising the two problems described above will be an important part of this thesis.

3.1.2 Description of noise sources, and their impact on the BSPM

A short description of the most common noise and drift sources and how they affect the ECG is given in [14]. Experimental testing with real BSPM recordings has also been performed. Below is an overview of the noise sources that may be present in a BSPM recording. An illustration of some of these can be seen in Figure 3.2 and Figure 3.5:

Power line interference consists of 50 Hz harmonics, with amplitude of up to 50% of BSPM amplitude. Often these characteristics will not change much during a recording.

Muscle contraction noise is caused by artificial potentials generated by muscle contractions. The signals resulting from muscle contractions can simplified be viewed as zero mean band-limited Gaussian noise. Typical parameters are; standard deviation of 10 % of BSPM amplitude and frequency content of up to 10 kHz.

Electrode contact noise is interference caused by loss of contact between electrode and skin. This may happen temporarily, or during the whole recording. The amplitude may be over 100 times that of normal BSPM amplitude.

Patient movement produce transient baseline changes caused by variations in the electrode skin impedance when the electrode moves. These changes

are sometimes slow varying, and can have amplitudes many times as high as normal BSPM amplitude.

Baseline wandering/BSPM amplitude variation due to respiration. The amplitude of the BSPM may vary by about 15 %, and slow baseline wandering occur due to respiration by the patient.

Instrument noise generated by electronic devices used in signal processing may disturb the recorded signal.

Electrosurgical noise will destroy the signal, since it normally consists of large amplitude noise with frequencies between 100 kHz and 1 MHz. The aliasing effect caused by lower sampling rate than this, will disturb the signal.

Other sources such as perspiration, flawed electrodes, coughing or talking during recording etc. will also distort the recorded signal.

Some of the noise sources tested experimentally in a BSPM recording can be seen in Figure 3.5 with a corresponding plot of their respective frequency responses in Figure 3.6.

As described above, noise artifacts may occur in many different forms and magnitudes, making it an important task to reduce the noise in the BSPM where possible. Noise may also be so dominating in a channel that it is impossible to retrieve any real information from it. In these cases, the channel should be removed from the BSPM all together. In the next section, the most important task, drift reduction, will be discussed.

3.1.3 Description of the baseline drift removal problem

In ideal conditions, the parts of the BSPM where there are no sources of electrical activity in the heart (e.g. the PR and ST segments) should have zero amplitude (see Figure 2.3 on page 10). As described in Section 3.1.2 there are several sources to high amplitude slow varying noise (see the lower left plot in Figure 3.2). This type of noise in a signal will be referred to as baseline wander, baseline drift, or simply drift. The baseline wander can add several hundred millivolts to the amplitude of the signal. Since the pure BSPM amplitude normally varies within 1-3 mV, it is clear that the drift will have to be removed if the recording is to be of any use.

Removing baseline drift is a task of removing the drift without distorting the signal. When baseline wander is present in a signal, portions of the signal such as the PR segment that should have zero amplitude, will have amplitude equal to the amplitude of the drift at those parts. But at the other parts of the signal, such as the P and T wave and the QRS complex, it is not clear how much of the measurement is drift and how much is the actual signal.

3.2 Measuring ST and PR segment differences in rest and exercise recordings

As described in Section 2.4.1, some channels of the BSPM of a patient will change when the demand for blood exceeds the supply. This is often the case in

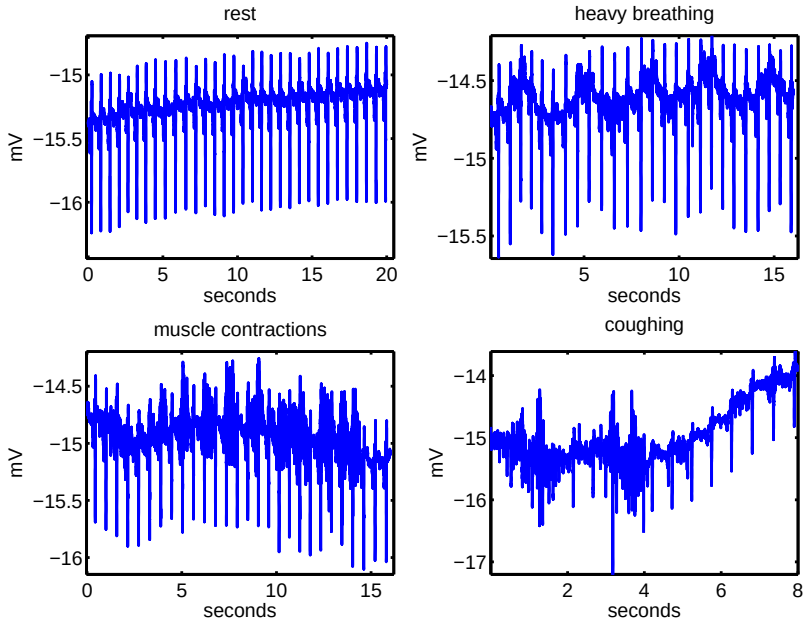

Figure 3.5: Upper left corner: a chest channel of the BSPM of a healthy patient during rest can be seen. Upper right corner: the same channel when the patient is breathing heavily. A regular oscillation of the signal in phase with the breathing can be observed. Lower left corner: the recording of the same patient contracting and relaxing chest and arm muscles. The BSPM has more noise content than the upper left one due to potentials generated by muscle contraction. The lower right corner: the recording when the patient is coughing. The coughing introduces disturbances to the BSPM, but it returns to normal when the patient settles down.

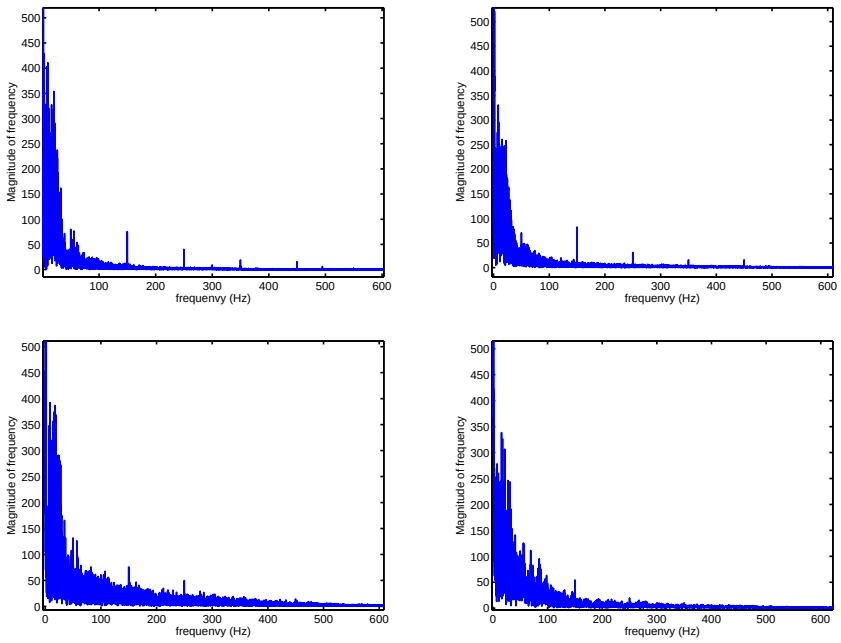

Figure 3.6: These figures show the frequency spectrums of the BSPM signals displayed in Figure 3.5. The upper left figure is the frequency spectrum of the BSPM during rest. The upper right shows when the patient is breathing. No significant additional high frequency content is added by the breathing. Lower left corner: notice how the magnitude of almost all the frequencies displayed is increased when the patient contracts his muscles. Lower right corner: a similar effect is seen in the frequency spectrum when the patient is coughing.

a person with ischemia during stress. The occluded arteries will provide enough blood to the heart muscles during resting periods, but not when the heart is working hard. Computing the difference in ST segment elevation/depression between rest and exercise can distinguish recordings of a patient with ischemia and a patient without.

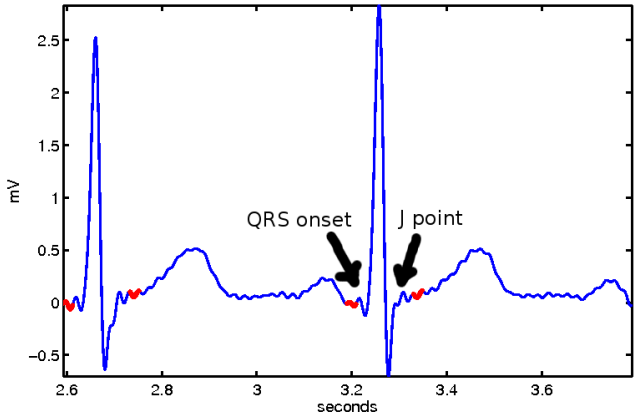

Figure 3.7: This figure shows two heartbeats from a BSPM of a healthy patient during rest. The onset of the QRS complex, and the J point right after the QRS complex is marked on the figure. The p value for this channel is computed as the mean of the area marked red right before the QRS complex onset. The s value for this channel is the mean of the marked area right after the J point.

The ST segment shifts are computed by subtracting a value on the baseline from a value in the ST segment. This segment is often defined relative to the J point, which is the point where the BSPM/ECG curve flattens between the QRS complex and the ST segment (see Figures 3.7 and 3.8). The value to use for the ST segment varies in the literature; [36, 31, 15, 5] respectively uses the points 60, 63, $60 - 80$ and $40ms$ after the J point. In this thesis, the mean of the signal in the period $50 - 70ms$ after the J point is used, with the J point being defined as $40ms$ after the QRS complex peak. The value on the baseline is computed by taking the mean of the signal in the period $30 - 10ms$ before the QRS complex onset. This section is used since it lies in the PR interval, and will in most cases not include values from the P wave or the QRS complex.

The BSPM recordings used in this thesis, were done on patients both during rest and while exercising on a stationary bike. The BSPM of a patient consists of 64 channels. These channels are called V^i, with $i = 1, \ldots, 64$ denoting the locations of the channels (see Figure 2.4 and Figure 2.5). The vector containing the jth heartbeat of channel i will be named V^i_j. For each heartbeat in a channel, a number s^i_j representing the ST segment elevation/depression and a number p^i_j representing the PR segment elevation/depression will be computed. The

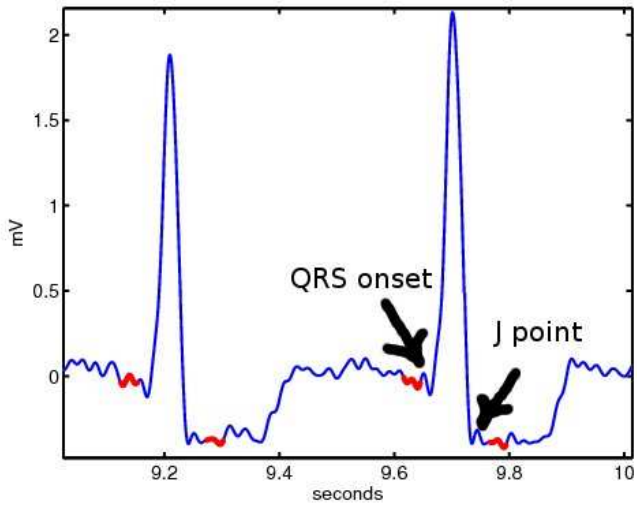

Figure 3.8: This figure shows two heartbeats from a BSPM of a patient with ischemia during stress testing. The onset of the QRS complex, and the J point right after the QRS complex is marked on the figure. The p value for this channel is computed as the mean of the area marked red right before the QRS complex onset. The s value for this channel is the mean of the marked area right after the J point. These heartbeats have depressed ST segments, which is characteristic for the BSPM of a patient with ischemia.

difference between these will be termed d_j^i:

$$\begin{aligned} s_j^i &= \frac{1}{L}\sum_{n=1}^{L} V_j^i(x_n), \text{ with } x_n \in \{50-70ms \text{ after the J point of } V_j^i\} \\ p_j^i &= \frac{1}{L}\sum_{n=1}^{L} V_{rest}^i(x_n), \text{ with } x_n \in \{30-10ms \text{ before QRS onset of } V_j^i\} \\ d_j^i &= s_j^i - p_j^i. \end{aligned} \tag{3.2}$$

In the above equations, L is the number of data points in the ST and PR segments. At this step, the mean difference between the ST and PR segment of channel i is created:

$$d_{(state)}^i = \frac{1}{H}\sum_{j=1}^{H} d_j^i. \tag{3.3}$$

H is the number of heartbeats in the channel V^i. The calculations in (3.2) and (3.3) are done for all channels V_{rest}^i in the rest recording, and V_{exc}^i in the exercise recording. This results in two vectors d_{rest} and d_{exc} with respective elements d_{rest}^i and d_{exc}^i with $i = 1, \ldots, 64$.

The vector d_{rest} is then subtracted from d_{exc} to get the differences between the recordings during exercise and the recordings during rest:

$$d = d_{exc} - d_{rest}. \tag{3.4}$$

After these computations on the BSPM of a patient, the resulting vector $d = [d^1, d^2, \ldots, d^{64}]$ contains the differences in ST segment shifts between exercise and rest for each of the 64 channels in the BSPM. These values will later be used to get an indication of whether a patient suffers from ischemia or not (see Section 2.4.2 and Chapter 6).

3.3 The Discrete Fourier Transform(DFT) and sampling

The electrical signals originating from the heart spread through the body continuously in time. Since computers work with discrete numbers, and not analog, the continuous analog signals need to be translated into discrete digital signals. To digitally process the analog electrical potentials recorded at the body surface, they need to be digitised. In this process the continuous signals are sampled at discrete time instants at a sampling frequency f_s. The resulting BSPM recording then consists of f_s discrete values per second. In this study, the BSPMs where recorded with a sampling frequency of $f_s = 2048$ Hz. According to Shannons sampling theorem [32] (page 28), the highest frequency that can be contained in a digital signal with sampling frequency f_s, is $\frac{f_s}{2}$. This means that the highest frequencies contained in the BSPM recordings used in this thesis is $f = \frac{f_s}{2} = \frac{2048}{2} = 1024$ Hz. All of this is done in the recording equipment described in Section 2.3.2, and will not be discussed further.

When working with BSPM signals, much of the modification and analysis will be on the frequency characteristics of the signal. When doing frequency analysis, it is convenient to convert the time-domain signal sequence to an

equivalent frequency-domain representation of the signal. This is done using the Discrete Fourier Transform(DFT). The DFT of a discrete time sequence $x(n)$ of length L is given by:

$$X(\omega) = \sum_{n=0}^{L-1} x(n)e^{-i\omega n}, \qquad 0 \leq \omega \leq 2\pi \tag{3.5}$$

where ω is the normalized frequency variable. Now, $X(\omega)$ is a discrete function sampled at equally spaced normalized frequencies $\omega_k = 2\pi k/L$, $k = 0, 1, 2, \ldots, L-1$.

Returning to (3.5), the frequencies f on the interval $0 \leq f \leq f_s/2$ corresponds to the normalized frequencies ω on the interval $0 \leq \omega \leq \pi$. Due to the symmetry properties of the DFT, $X(\omega)$ on the interval $\pi \leq \omega < 2\pi$ is just a mirror image of $X(\omega)$ on the interval $0 \leq \omega < \pi$. Using the relation $\omega = \frac{2\pi f}{f_s}$, (3.5) can be rewritten as

$$X(f) = \sum_{n=0}^{L-1} x(n)e^{-2\pi i f n/f_s}, \qquad 0 \leq f \leq f_s. \tag{3.6}$$

In fact, f is a discrete variable sampled at discrete points f_k, where $f_k = kf_s/L$, $k = 0, 1, 2, \ldots, L-1$. $X(f)$ represents the amplitude and phase of the different frequency components of the time sequence $x(n)$. $|X(f)|$ is the amplitude of the frequency components of $x(n)$. A plot of $|X(f)|$ over all frequencies f is

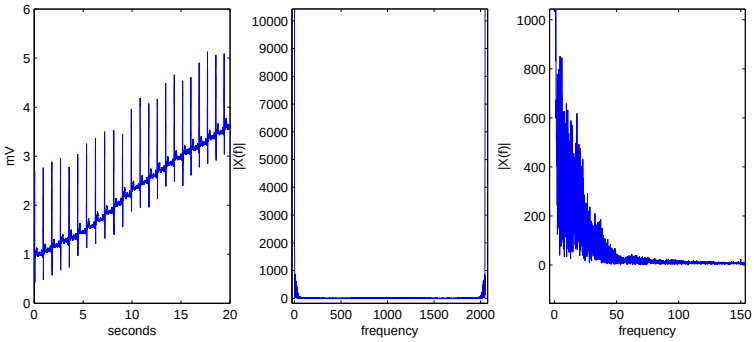

Figure 3.9: A 20 second segment of a BSPM recording, and its corresponding frequency spectrum. The right plot is the frequency spectrum zoomed in on frequencies in the interval $0 \leq f \leq 150$ since most of the frequency content in a BSPM recording are low frequencies.

called the frequency spectrum, and shows how much of each frequency f the signal $x(n)$ is composed of. A plot of a BSPM-recording and its corresponding frequency spectrum can be seen in Figure 3.9. For more reading on Discrete Fourier Transforms and sampling, see an introductory book on digital signal processing, for instance [32].

3.3.1 Filtering techniques

Throughout the thesis, frequency-selective linear time invariant (LTI) filters will be applied to the BSPM recordings. The filter characteristics of a digital LTI-

filter is determined by its impulse response $h(n)$. A filter with input $x(n)$ has output

$$y(n) = h(n) * x(n) = \sum_{k=-\infty}^{\infty} h(k)x(n-k),$$

where $*$ is the convolution operator. This is the time domain representation of a filter with impulse response $h(n)$. Since frequency-selective filters will be used, it is more convenient to express the output of a filter in the frequency domain. A property of convolution is the convolution theorem that states that convolution in the time domain is equivalent to multiplication in the frequency domain [32] (page 283). The frequency domain expression of the output of a digital filter is then

$$Y(\omega) = H(\omega)X(\omega), \tag{3.7}$$

where $Y(\omega)$, $H(\omega)$ and $X(\omega)$ are the Discrete Fourier Transforms of $y(n)$, $h(n)$ and $x(n)$ respectively.

When designing a frequency-selective filter, the desired frequency characteristics is given by the frequency response $H(\omega)$. Filters applied to BSPM-recordings need to have linear phase to avoid phase distortions in the output of the filter.

LTI filters with linear phase can be implemented both with Finite Impulse Response (FIR) or Infinite Impulse Response (IIR) characteristics. A filter of both of the two types could be designed for the tasks in this thesis. However, FIR filters are inherently stable, and much easier to design with linear phase characteristics. A drawback with FIR filters is that they generally require many more coefficients than an IIR filter, and hence are more computationally demanding. The advantages of using FIR filters was deemed greater than the disadvantages, and hence all filters used in this thesis will be FIR.

Ideal filters, i.e. filters that has infinitely sharp cut off frequencies such as

$$H(\omega) = \begin{cases} 1, & |\omega| \leq \omega_c \\ 0, & \omega_c < \omega \leq \pi, \end{cases}$$

cannot be realized in a FIR filter in practice due to the Paley-Wiener theorem [32] (page 656). An important result from the Paley-Wiener theorem is that such filters will require an infinite length impulse response $h(n)$, and hence be noncausal. To make a filter realizable, the infinite length impulse response need to be truncated at some point. A FIR filter of length M can be made by multiplying the desired impulse response $h_d(n)$ (infinite length) with a "window" $w(n)$ (finite length). $w(n)$ has the property that $w(n) = 0$ for $n > M-1$ and $n < 0$. This yields the impulse response

$$h(n) = h_d(n)w(n) \tag{3.8}$$

of length M.

The ideal filter $h_d(n)$ with infinitely sharp cut off frequnecy is in this thesis approximated using windowing techniques (3.8). There are two main consequences of using a causal approximation $h(n)$ to the noncausal $h_d(n)$: First, the transition between frequencies passed through the filter and frequencies removed is not infinitely sharp, but will change gradually. As an effect of this, there will be a band of frequencies, called the transition band, that are increasingly attenuated between the passed and stopped frequencies. Second, small disturbances

or ripples will be introduced in the frequency spectrum of both the passed and stopped frequencies of the filter. Thus, some parts of the "stopped" frequencies will be let through, and parts of the passed frequencies will change in amplitude. Designing filter windows is a task of reducing these ripples, and sharpening the transition band.

3.3.2 Filtering with Kaiser windows

In this thesis the window functions $w(n)$ used, will be Kaiser windows. This window type is chosen for its flexibility in adjusting the amount of ripples in the stop and pass bands, and the sharpness of the transition band. A length M Kaiser window used in designing the FIR filter impulse response $h(n)$ in (3.8), has time domain sequence

$$w(n) = \begin{cases} \dfrac{I_0\left[\alpha\sqrt{\left(\dfrac{M-1}{2}\right)^2 - \left(n - \dfrac{M-1}{2}\right)^2}\right]}{I_0\left[\alpha\left(\dfrac{M-1}{2}\right)\right]}, & 0 \leq n \leq M-1 \\ 0, & \text{elsewhere,} \end{cases} \tag{3.9}$$

and frequency domain sequence

$$W(\omega) = \frac{(M+1)sinh\left(\sqrt{\alpha^2 - \left(\dfrac{(M+1)\omega}{2}\right)^2}\right)}{I_0(\alpha)\sqrt{\alpha^2 - \left(\dfrac{(M+1)\omega}{2}\right)^2}}. \tag{3.10}$$

Here I_0 is the zeroth order modified Bessel function of the first kind, α is a parameter determining the shape of the window and M is the length of the window.

Generally, an increase in the filter length M will narrow the transition band. An increase in α will lower the amount of ripples in the pass and stop bands, but will also widen the transition band. Hence, the design of the filter is a compromise between the narrowness of the transition band, and the amount of disturbance in the kept and attenuated frequencies.

Chapter 4

Methods and algorithms

This chapter contains a description of many of the methods used and developed in this thesis. A combination of a selection of these will at a later point be made to form an automatic algorithm for processing BSPM recordings making them ready for ST segment shift measurements. The methods described serves different purposes:

Noise reduction: Notch filtering and lowpass filtering algorithms described in Section 4.1 were designed to reduce the noise content in a BSPM. These methods make use of frequency analysis and a priori knowledge of the noise frequency characteristics in a signal.

Drift reduction: Baseline drift is present in all BSPMs. Four different algorithms for removing this drift from a BSPM is described in Section 4.2

Removing corrupted signals: Some channels in a BSPM, or parts of a channel in a BSPM may still be too corrupted by noise or bad recording that no information can be extracted, even after noise and drift reduction algorithms have been applied. Section 4.3 contains description of algorithms to remove these signals.

QRS detection: Different parts of the BSPM signal need to be recognised. The QRS detection algorithm outlined in Section 4.4 is designed to find the QRS peaks in a BSPM. Other important features of the signal can be found once the QRS peaks are known.

The algorithms described in this chapter will be combined to form a complete method for improving BSPM signals.

4.1 Noise reduction algorithms

As described in Section 3.1.2, there are many sources of noise that can distort the recorded BSPM. Most of the distortions not classified as drift, are 50 Hz noise and white noise which will be present in all frequencies of the signal. It is these parts that make up the $BSPM_{noise}$ part of (3.1):

$$BSPM = BSPM_{signal} + BSPM_{noise} + BSPM_{drift}.$$

In many BSPM recordings, the most prominent noise is the 50 Hz powerline interference. Therefore the most important features of the noise reduction algorithms is to remove this powerline interference while causing minimal disturbance in the BSPM. In the algorithms described below; parts of a BSPM will be removed based on the assumptions of the frequency contents of signal and noise. Two algorithms are proposed; a notch filter for removing only 50 Hz contents of the BSPM, and a lowpass filter for removing all frequencies greater than a desired cutoff frequency.

It is assumed for simplicity that $BSPM_{noise}$ is made up of three components: $noise_{50Hz}$ and $noise_{white}$ and $noise_{other}$. The 50 Hz component should always be removed, as it may disturb the signal to a great degree if it is of large amplitude. Also, the removal of a small frequency band around 50 Hz will not disturb signals uncontaminated by 50 Hz noise, as will be seen in Section 5.1.1. As much of the rest of the noise, namely $noise_{white}$, is assumed to be white it will be of equal magnitude throughout the frequency spectrum. This means that the more frequencies are removed, the more of this noise is removed. For instance, a lowpass filter with cutoff frequency of 100 Hz will remove $\sim \frac{9}{10}$ of the white noise in the signal, since the frequency content is in the interval $0 - 1024$ Hz. Applying a lowpass filter to the signal may result in the filter removing important information contained in the BSPM. Choosing the correct cutoff frequency of a lowpass signal is therefore a compromise between the amount of noise removed, and the amount of distortions introduced to the BSPM.

These filters were designed using Kaiser windows as described in Section 3.3.1. Designing filters to remove parts of the signal with certain frequency components, is a compromise between sharpness of the transition band, and ripples in the pass and stop band of the filter. The two parameters α and M in (3.9) and (3.10), with M being the filter length, will determine the characteristics of the filter. The width of the transition band of the filter is the same as the distance from the peak to the first zero in the window's frequency domain sequence.

4.1.1 Use of notch filter to remove 50 Hz powerline noise

As proposed in [41] a notch filter can be used to remove 50 Hz powerline noise. The notch filter is a bandstop filter, which means that it will remove an interval of frequencies from the signal and keep the rest. A filter with stop band of 49-51 Hz will be used. The parameters α and M in the Kaiser window (3.9) and (3.10) is selected so that the transition bands in both the lowpass and highpass parts of the the filter is less than 1 Hz. With a filter of length $M = 1400$ and $\alpha = 1.5$, the above requirements are fulfilled. The 50 Hz component will in this example be removed, while frequencies between $49Hz$ and $51Hz$ will be attenuated. The frequency components less than $49Hz$ and greater than $51Hz$ will remain almost unchanged. If there is $50Hz$ powerline noise present in the signal, there will also be noise with frequency content as multiples of $50Hz$, i.e. $100, 150, \ldots Hz$. Similar notch filters for removing these frequencies are also applied to the signal.

4.1.2 Lowpass filter to reduce high frequency noise

While the notch filter will remove the $50Hz$ powerline noise, it will do nothing with the disturbances from the other high frequency noise sources. A lowpass filter will remove all frequencies greater than a cutoff frequency f_{cutoff}, and keep the lower frequency components of the signal. The problem with using such a filter, is that all non-noise components of the BSPM with frequency higher than f_{cutoff} also will be removed. According to [5, 39, 21] P and T wave frequencies generally lies between 0 and $10Hz$, and QRS complex spans over a greater range of frequencies, with most of the signal components in the range 4 to $20Hz$. [21] also states that most of the diagnostic information in ECGs is contained below $100Hz$ in adults, with the highest of these frequencies being in the QRS complex. Since the highest frequency contents of a BSPM signal is in the QRS complex, the removal of these should not affect the ST segment. Hence, removal of the higher frequencies, including some frequencies below $100Hz$, should improve the Signal to Noise Ratio (SNR) of the ST segment. Although the American Heart Association (AHA) [21] recommends a high-frequency cutoff of at least $150Hz$, lower f_{cutoff} frequencies will be used, since this thesis primarily focuses on the diagnostic information contained in the ST segment.

A low pass filter with parameters $\alpha = 2$ and length 1000 in equations (3.9) and (3.10) is an adequate FIR lowpass filter for this purpose. This filter will be tested on real BSPMs with different cutoff frequencies.

4.2 Drift reduction algorithms

In Chapter 3 the problem of baseline wander or drift in the BSPM recordings was described. Many ways of removing the drift in an ECG has been proposed in the literature. Four promising methods have been applied to the BSPM data in this thesis. Each of these will be described in this section, and evaluated in Section 5.2.

4.2.1 Drift reduction using splines

A spline is a function defined piecewise by polynomials. In spline interpolation, data points are connected by defining the spline to be equal to the data points, with polynomials connecting them. In this thesis splines will be used to make an approximation to the drift in the BSPM. This approximation will then be subtracted from the signal, producing a new BSPM with drift reduced. For further reading on spline interpolation, see e.g. [27, 23].

To get an approximation of the drift, the splines will be connected at one point per heartbeat called the knots. The points selected are in the PR segments $30ms$ before the onsets of the QRS complexes. Hence there should theoretically be no electrical sources in the heart creating baseline deviation at the knots. The magnitude of the BSPM here consist of baseline drift and noise, and should therefore be removed. The intervening values between the knots should be adjusted in a way that do not distort the signal, but still removes the baseline drift. The splines used are defined as follows:

The spline approximations are computed for the channels V^i, $i = 1, \ldots, 64$ of a BSPM one at a time. Let N be the number of data points in a channel V^i of a BSPM. V^i is then a collection of data values defined on an index set

$I = [1, 2, \ldots, N]$. A channel V^i containing H heartbeats will have H knots given by the partition $\Delta = [x_1, \ldots, x_j, \ldots, x_H]$ with $x_1 < x_2 < \ldots < x_H$, $x_j \in I$. One knot value is used per PR segment of the signal, as seen in Figure 4.1. The spline s approximating the drift is chosen to be the function described by $s(\Delta) = V^i(\Delta)$, and

$$s(x) = \begin{cases} s_0(x) & , x < x_1 \\ s_j(x) & , x_j < x < x_{j+1} \\ s_H(x) & , x_H < x \end{cases} \tag{4.1}$$

where each s_j is a polynomial, and $s_{j-1}(x_j) = s_j(x_j)$.

Two types of spline interpolation will be used to remove the baseline drift, and will be described in the next sections.

Linear splines

With linear splines, the spline connecting the knots will be a collection of straight lines (linear polynomials). The functions s_j in (4.1) are then on the form:

$$s_j(x) = V^i(x_j) + \frac{V^i(x_{j+1}) - V^i(x_j)}{x_{j+1} - x_j}(x - x_j).$$

These linear splines will interpolate the signal as shown in Figure 4.1. The drift

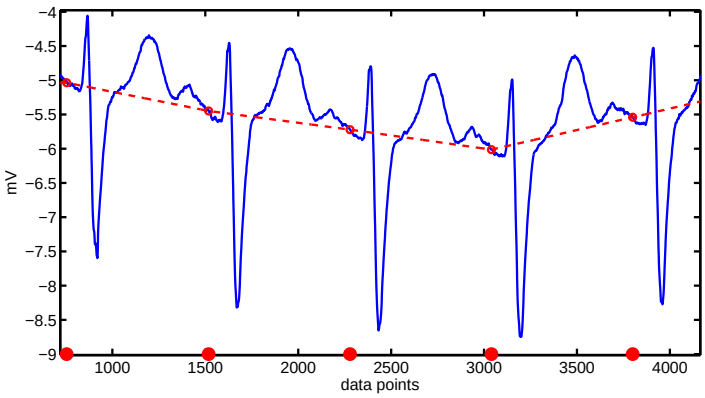

Figure 4.1: Linear spline approximation of the drift in a channel V^i of a BSPM. V^i is visualised in solid line, the approximation of the drift is marked with a dashed line. The knots $[x_1, x_2, \ldots, x_H]$ are marked as circles on the x axis. The knot values used are marked as circles connecting the linear functions in the drift approximation spline.

is now approximated by s. The drift is removed from V^i by subtracting the spline s from V^i. Using (3.1), this produces a new collection of data points $BSPM_{improved}$:

$$BSPM_{improved} = BSPM_{signal} + BSPM_{noise} + BSPM_{drift} - s$$

Now, if $s \approx BSPM_{drift}$ then $BSPM_{improved} \approx BSPM_{signal} + BSPM_{noise}$. In real recordings however, there will never be a true equality. Some drift will

always be present in $BSPM_{improved}$, and artifacts may also be introduced due to bad drift approximation.

Cubic splines

With cubic splines, the spline connecting the knots will be a collection of cubic polynomials satisfying the conditions given in Section 4.2.1. The functions s_j in (4.1) are chosen to be cubic polynomials on the form

$$s_j(x) = a_j x^3 + b_j x^2 + c_j x + d_j.$$

While the linear splines s needed no conditions other than those given in (4.1), some more restrictions will be given to the cubic splines. The cubic splines s are required to have two continuous derivatives, in other words $s \in C^2(\mathbb{R})$. Right sided derivatives are used, with the following definition:

$$s^{(n)}(x) := \begin{cases} s(x) & , n = 0 \\ \lim_{h \to 0^+} \frac{s^{(n-1)}(x+h) - s^{(n-1)}(x)}{h} & , n = 1, 2 \end{cases}$$

with $s^{(n)}(x)$ being the n-th derivative of s. Now the conditions set in (4.1) are expanded for the cubic splines to be:

$$s^{(n)}(x) = \begin{cases} s_0^{(n)}(x), & x < x_1 \\ s_j^{(n)}(x), & x_j < x < x_{j+1} \\ s_H^{(n)}(x), & x_H < x \end{cases} \tag{4.2}$$

for $n = 0, 1, 2$. A cubic spline s created with the conditions given in (4.1) and

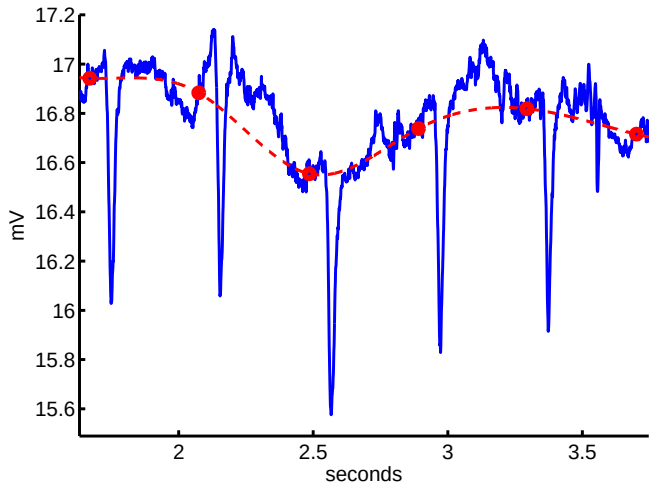

Figure 4.2: Cubic spline approximation of the drift in the channel of a BSPM. The approximation to the drift is visualised in a dashed line, with the knot values appearing as circles.

(4.2) will be an approximation to the drift in the channel V^i which it is based

on. These cubic splines will interpolate BSPMs in the way shown in Figure 4.2. Returning again to (3.1), a new dataset $BSPM_{improved}$ is created by subtracting s from the channel V^i:

$$BSPM_{improved} = BSPM_{signal} + BSPM_{noise} + BSPM_{drift} - s$$

If s is a good approximation to $BSPM_{drift}$, $BSPM_{improved} \approx BSPM_{signal} + BSPM_{noise}$.

Both the linear and cubic spline methods use the same knot values Δ when approximating the drift. In most cases the value of s between the knot values will be different in linear and cubic splines, since they use different polynomials. Generally, the cubic spline makes a smoother approximation to the drift, while the linear spline will make a more even approximation through each heartbeat.

Determining knot values

Even though the knots used in the two spline interpolation algorithms described above are chosen in the PR segment where there should ideally be no baseline deviation, low amplitude high frequency noise is present. This will influence the spline approximation to the drift, and this disturbance will be directly transfered to $BSPM_{improved}$. Two methods have been chosen to reduce this problem. The chosen methods are lowpass filtering, and using the mean of chosen neighbouring values of a knot point.

The lowpass filter is implemented using the lowpass filtering methods described in Section 4.1.2. A cutoff frequency of $49Hz$ is used to both reduce random white noise, and any $50Hz$ noise present in the signal.

Because of the noise present in all parts of the signal, the use of knot points as described in Section 4.2.1 will introduce a small randomness to the drift approximation. By instead using the median value of neighbouring points in close proximity to the original knot value (which is the point $30ms$ before the QRS complex onset) as the knot value, this randomness can be reduced (see Figure 4.3). 51 data points are used in the computation of the median value. Since the sampling rate is 2048 Hz, 51 points corresponds to $\frac{51}{2048\frac{1}{sec}} \approx 25ms$. With this time window the data points used in the calculation of the median knot value will in most cases be in the PR segment.

4.2.2 Highpass filtering

The spline interpolation methods described above removes the drift by subtracting an approximation of the drift from the BSPM. How precise the drift removal is, depends on the selection of knot points and the intervening polynomials. Highpass filtering is an alternative method to spline interpolation. Since the drift consist of slow varying high amplitude changes in the recorded signal, removing the low frequencies from the BSPM will reduce the drift. Unfortunately, parts of $BSPM_{signal}$ also contains low frequency components. Thus, filtering out low frequencies from the recorded signal can damage or change important information in the signal. The American Heart Association (AHA) [21]recommends a cutoff frequency below 0.5 Hz. This cutoff frequency will be used in the highpass filtering methods.

The highpass filter is designed using the techniques described in Section 3.3.1. Since the cutoff frequency is $0.5Hz$, the filter will need a transition band

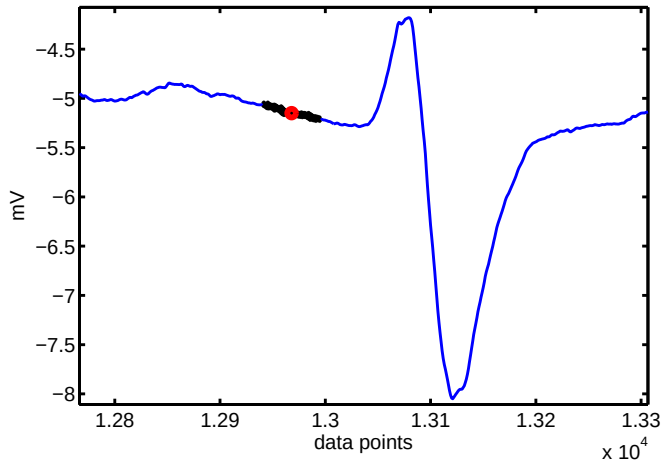

Figure 4.3: The selection of a knot value. The median of 51 data points is computed, and used as the knot value. The 51 data points are marked with 'x's, while the computed knot value is marked with an 'o'.

width of less than $0.5Hz$. A decrease in α and an increase in length M of the filter's window functions (3.9) and (3.10) will narrow the transition band. With $\alpha = 0$ the window will equal a rectangular window. To obtain a transition bandwidth of less than 0.5 Hz, the filter length has to be at least 4100. If α instead is set to 1 the filter will have smaller ripples in the passband, but will require a longer filter length. The window parameters for Equations (3.9) and (3.10) were selected to be length $M = 5000$ and $\alpha = 1$. This results in a FIR filter which removes frequencies below $0.5Hz$ while introducing minimal distortions to the frequency content higher than $0.5Hz$.

4.2.3 Filtering using Discrete Wavelet Transform

As an alternative to spline or highpass drift removal, other methods have been used in the literature. For instance Time-Varying Filtering [34], Short Time Fourier Transform [30] and Wavelet Transform based methods [6, 9, 40]. Of these the Wavelet Transform based methods seem most promising. A Wavelet Transform based baseline drift removal algorithm will therefor be implemented, and tested alongside the three other drift removal algorithms described in the above sections. A short description of the wavelet transform filter applied in this thesis is given below. Details on wavelet decomposition can be found elsewhere, for instance in [16, 11].

The wavelet transform filter bank works on each channel of a BSPM at a time. First, two symmetric filters are created from a mother wavelet. These filters splits the BSPM signal into a low frequency component and a high frequency component using lowpass and highpass filters and downsampling each part by a factor two. These components are represented by a scaling coefficient c_2 corresponding to the low frequency components of the signal, and a detail coefficient d_2 corresponding to the high frequency components of the signal. This process is repeated by splitting c_2 into a low frequency component c_3 and

a high frequency component d_3 and so on. This process is sketched in Figure 4.4 (a) and Figure 4.5. The process is repeated until the scaling coefficients represents sufficiently small frequencies, which can then be removed by setting the coefficient to zero.

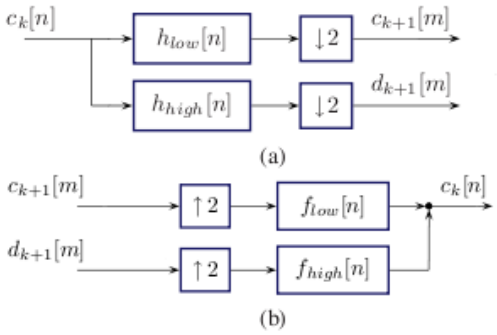

Figure 4.4: The decomposition (a) and recomposition (b) procedure of wavelet transformation.

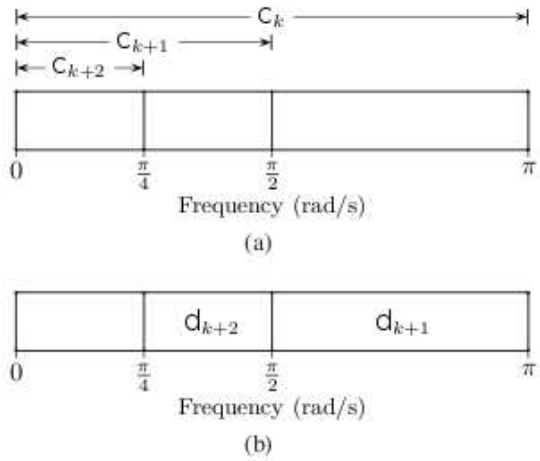

Figure 4.5: The frequency content of the scaling (a) and detail (b) subspaces at steps k, k+1, k+2 of the wavelet transform decomposition of the signal. The interval [0 , π] is the scaled frequency range of c_k.

In this thesis, the sampling frequency of the BSPM recordings used is $2048Hz$, so the highest frequency contents possible in the signal (the Nyquist frequency) is $\frac{2048Hz}{2} = 1024Hz$. As each step of the wavelet signal decomposition splits the signal's frequency components in two, the scaling coefficients c_2 and d_2 has frequency bands of width $512Hz$. With each step splitting the frequency band of c_k in two, with c_{k+1} containing the lower half of the frequency content, c_{12} will with this sampling frequency have a frequency content between 0 and $0.5Hz$. These frequencies are removed, in accordance with the AHA recommendations [21], by setting the scaling coefficient c_{12} to zero. The BSPM signal is then

reconstructed by setting $c_{11} = d_{12}$ (since $c_{12} = 0$), combining c_{11} and d_{11} to form c_{10} and so on until the BSPM signal is reconstructed with the frequencies between 0 and $0.5Hz$ removed. This reconstruction scheme is illustrated in Figure 4.4 (b). In the wavelet decomposition scheme used in this thesis, symlet wavelets are used.

4.3 Removal of corrupted signals

Some parts of a BSPM recording may be so corrupted that no usable information can be extracted from them. Including these parts in further calculations will only reduce the overall quality of the BSPM, and hence they should be removed. Both short time periods of a channel in a BSPM or a whole channel may need to be removed. The main causes of these corruptions are electrosurgical noise, malfunctioning equipment and loss of contact between skin and electrode. Figure 4.6 is an example of the latter.

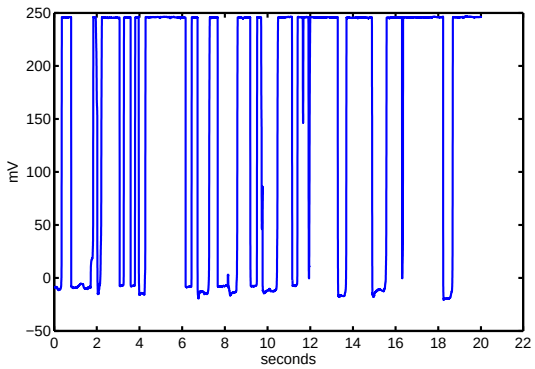

Figure 4.6: A BSPM recording destroyed by loss of contact between electrode and skin. Note the magnitudes on the y-axis.

The methods in this section were designed to completely remove BSPM channels or parts of BSPM channels so destroyed by noise that no information about the electrical activity in the heart could be extracted from them. This is the case when, after drift reduction and noise reduction has been applied to the signal, $BSPM_{noise}$ is still the dominating part in $BSPM = BSPM_{signal} + BSPM_{noise} + BSPM_{drift}$. In some cases, the recording may not contain electrical signals from the heart at all, and $BSPM \approx BSPM_{noise} + BSPM_{drift}$. This is the case for instance when there is loss in contact between skin and electrode, or when an electrode is malfunctioning. Four algorithms for removing the useless parts of BSPMs has been developed, and will be described next. Each algorithm takes a different approach to removing disturbances in a BSPM. A combination of these four algorithms will be made to get a complete method for identifying and removing bad parts of a BSPM. Drift and noise reduction must be applied to the signals before any of these four algorithms are applied to obtain the best results.

4.3.1 Removing destroyed channels

Some channels, like the one seen in Figure 4.6, are obviously of no use, since no information of the ECG characteristics can be found in them. A simple algorithm that makes use of the many channels in a BSPM and the fact that the characteristics in each channel should be similar is described in this section.

The ith channel of a BSPM will be denoted V^i. The median, V_{median}, of all channels in a BSPM is created by

$$V_{median}(x) = median_{i=1,\ldots,64}(V^i(x)) \qquad \text{for } x = 1, 2, \ldots, N,$$

where N is the number of data points in each channel of the BSPM. Now, each channel V^i is tested to see if it deviates more from V_{median} than an preset tolerance δ (See Figure 4.7). If it does, the channel is removed from the BSPM

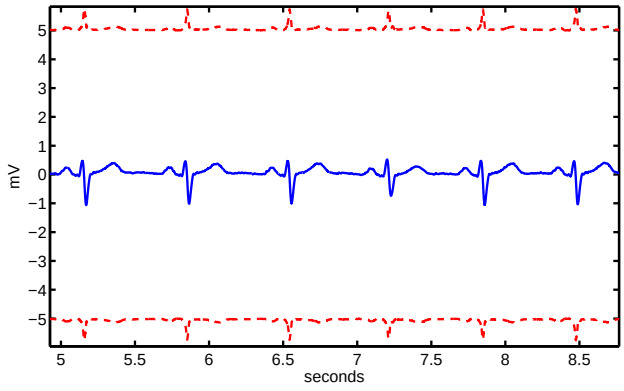

Figure 4.7: The middle graph of this figure shows parts of a channel of a BSPM. The upper and lower lines in this figure shows the *tolerance* of the test. If the BSPM signal at some point is greater than the upper line or lower than the lower line, the channel will be removed from the data set.

by setting it to zero:

$$V^i = \begin{cases} V^i, & \text{if } ||V^i - V_{median}||_\infty < \delta \\ 0, & \text{if } ||V^i - V_{median}||_\infty > \delta \end{cases} . \tag{4.3}$$

Here, $||\cdot||_\infty$ is the supremum norm defined by

$$||\mathbf{u}||_\infty = \max_{1 \le x \le N} \{u(x)\} \tag{4.4}$$

where $\mathbf{u}$ is an arbitrary vector with elements $u(x)$ and length N.

This algorithm is a fast and easy way to eliminate the worst channels in a BSPM, but is not suited to do a finer search for channels or parts of channels that need to be removed. More refined methods for doing this is described in the next sections.

4.3.2 Removal of varying segments

For each heartbeat V^i_j of a channel V^i of a BSPM, the shifts in the ST segment will be measured by calculating the difference in amplitude of $20ms$ segments

of the ST segment and the PR segment. The segments used are the same as the ones described in Section 3.2. These segments should normally not vary much during the $20ms$ segment, but will in some measurements do because of noise, T/P wave interruption and so on. The method described in this section will remove heartbeats V_j^i containing ST or PR segments with too large variation, as this probably is caused by noise or interference with T or P waves.

The method is simple: For each heartbeat V_j^i of a BSPM, the standard deviations σ_{st} and σ_{pr} of the ST and PR segment is computed. If these exceeds a tolerance value δ, the heartbeat is removed from the BSPM. Expressed more mathematically, the standard deviations are for each heartbeat:

$$\begin{aligned} \sigma_{st} &= \sqrt{\mathrm{Var}(V_j^i(X))} \\ \sigma_{pr} &= \sqrt{\mathrm{Var}(V_j^i(Y))}, \end{aligned} \tag{4.5}$$

with X and Y being index sets defined on the ST and PR segments of V_j^i. Then, the current heartbeat is kept if these standard deviations does not exceed the tolerance:

$$V_j^i = \begin{cases} V_j^i, & \text{if } \max\{\sigma_{st}, \sigma_{pr}\} < \delta \\ 0, & \text{if } \max\{\sigma_{st}, \sigma_{pr}\} > \delta \end{cases} . \tag{4.6}$$

4.3.3 Removal based on drift approximation

The changes in a BSPM labelled as drift can sometimes be quite abrupt, for example if the patient coughs or makes sudden movements. These and other disturbances in the BSPM can reduce the accuracy of the drift approximations. This section describes a method for removing the parts of a BSPM that have a too abrupt changing drift approximation created by the methods described in Section 4.2.1. Thus, this algorithm will only be applied to signals that have had the drift removed using a spline interpolation method. The method tests if the second derivatives of the drift approximation is greater than a given tolerance δ. If this is the case, these parts of the signal are removed while the parts with second derivatives smaller than δ are kept.

Using the QRS detection method described in Section 4.4.2 the indexes of the beginning of each heartbeat in the BSPM have been found. These are labelled $\Delta = [x_1, \ldots, x_j, \ldots, x_H]$, with H being the number of heartbeats in the BSPM. These knot points were used when making a spline based approximation to the drift. For each channel V^i, $i = 1, \ldots, 64$ of the BSPM, the splines in (4.1) were tied together at the knot values $V^i(\Delta)$ (Actually, values slightly differing from these were computed using the method described in Section 4.2.1, but this notation is used for notational convenience). A simple form of second derivative $D^{(2)}(\cdot)$ is calculated on these knot values:

$$\begin{aligned} D(V^i(x_j)) &= V^i(x_j) - V^i(x_{j-1}) \\ D^{(2)}(V^i(x_j)) &= D(D(V^i(x_j))) = \\ &= V^i(x_j) + V^i(x_{j-2}) - 2V(x_{j-1}). \end{aligned} \tag{4.7}$$

These second derivatives are computed for $j = 3, \ldots, H$. Then the absolute value of each second derivative is tested to see if it exceeds the set tolerance δ.

If $|D^{(2)}(V^i(x_j))| > \delta$, the heartbeats V^i_{j-2} and V^i_{j-1} are removed from the data set. This algorithm will remove heartbeats with too abrupt changes in the drift, and also artefacts introduced by the drift reduction algorithms.

4.3.4 Use of spatial information to test quality of signal

The electrical potential spreading from the heart through the body does so without discontinuities or abrupt changes. This is why the body can be viewed as a volume conductor. A consequence of this fact is that neighbouring channels should record similar signals. These properties of the BSPM is the background for the algorithm for identifying and removing noisy/bad signals described in this section. The spatial information provided by the BSPM is used to determine if the heartbeats V^i_j of each channel V^i fits in with the rest of the BSPM. For each heartbeat V^i_j in each channel the neighbouring channels will be used to predict several values from which V^i_j should not deviate more than a given tolerance δ. If V^i_j deviates from all these predicted values, it is considered a bad signal.

The algorithm works on one channel V^i at a time. For each channel, the algorithm is applied to each heartbeat V^i_j of that channel. The current heartbeat that the channel is working on will be called c for simplicity. The two channels above c are called o_1 and o_2, the two channels below are called u_1 and u_2, the two channels to the left are called l_1 and l_2 and the two channels to the right are called r_1 and r_2. Of course, not all these neighbours are available for all channels. The heartbeats V^{31}_j of channel V^{31} will for example only have the neighbours $o_1 = V^{30}_j$, $o_2 = V^{29}_j$, $u_1 = V^{32}_j$, $l_1 = V^{23}_j$ and $l_2 = V^{15}_j$, see Figure 2.4 and Figure 2.5. Figure 4.8 shows the example where a heartbeat from channel V^{20} is the current channel c.

Now a number s for the ST segment and a number p for the PQ segment of c is computed, as described in Section 3.2. This is also done for each of the neighbours of c, with their corresponding numbers being $s(u_1)$, $s(u_2)$, $p(u_1)$, $p(u_2)$ and so on. From each available direction, a predicted value of s and p is now computed in the following way, illustrated with $s(u_1)$ and $s(u_2)$:

$$ds(u) = \left\{ \begin{array}{ll} s(u_1) + \frac{(s(u_1)-s(u_2))}{2}, & \text{if both } s(u_1) \text{ and } s(u_2) \text{ available} \\ s(u_1), & \text{if only } s(u_1) \text{ available} \\ s + 2\delta, & \text{if neither } s(u_1) \text{ nor } s(u_2) \text{ available} \end{array} \right\}. \tag{4.8}$$

Similar computations are done with the other neighbours and the p values. This produces a set of two to four predicted s values for the channel c and two to four predicted p values, depending on the spatial location of c. The values s and p should now correspond with these predicted values. A test is applied to see if this is true:

$$\begin{aligned} \epsilon = \min\{&|s - ds(u)|, |s - ds(o)|, |s - ds(l)|, |s - ds(r)|, \\ &|p - dp(u)|, |p - dp(o)|, |p - dp(l)|, |p - dp(r)|, \}. \end{aligned} \tag{4.9}$$

If now $\epsilon > \delta$, the heartbeat c does not fit in with any of the predicted values from the neighbours, and is removed from the data set. If $\epsilon < \delta$, the ST or PQ segment of c fits in with at least one of the predicted values of the neighbours, and the heartbeat is kept.

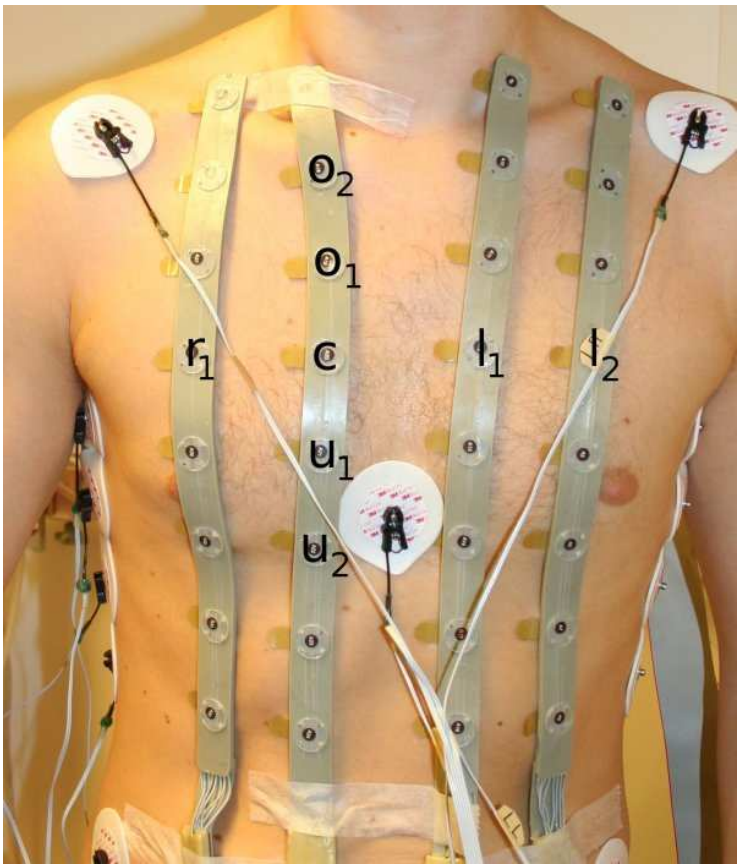

Figure 4.8: An illustration of the values used in the algorithm of Section 4.3.4. The channel marked c is the current channel. The channels marked o are the two neighbouring channels above c. The channels marked l are the two neighbouring channels to the left of c and so on. The closest of the two are given a subscript 1, the next a subscript 2.

4.3.5 Temporal quality test of PQ and ST segments

This method will make use of the principle that heartbeats occurring close to each other in time in the same channel should be similar. It creates median ST and PQ segments for each channel V^i of the BSPM, and compares the ST and PQ segment of each heartbeat V^i_j with their respective median. Heartbeats that contain ST or PQ segments that deviate more than a tolerance δ will be removed from the data set. This algorithm is to be implemented recursively, with each iteration possibly sorting out additional parts of the BSPM. The original channel V^i of the BSPM before any iterations of this algorithm has been run will be termed O^i.

The algorithm works on each individual channel O^i at a time. First, the reference ST and PR segment values are created from the ST and PR segments of each heartbeat in the channel V^i. These are created by first computing the mean value of the ST and PR segment of each heartbeat:

$$s^i_j(V) = \frac{1}{N}\sum_{n=1}^{N} V^i_j(x_n), \text{ with } x_n \in \text{ the ST segment of } V^i_j \tag{4.10}$$

$$p^i_j(V) = \frac{1}{M}\sum_{n=1}^{M} V^i_j(y_n), \text{ with } y_n \in \text{ the PR segment of } V^i_j, \tag{4.11}$$

and N, M being the number of data points in the ST and PR segments of the heartbeat respectively. Now median ST and PR segment values s^i and p^i are created, and their difference computed:

$$\begin{aligned} s^i &= median_{j=1,\ldots,H}(s^i_j(V)) \\ p^i &= median_{j=1,\ldots,H}(p^i_j(V)) \\ d^i &= s^i - p^i, \end{aligned}$$

with H being the number of heartbeats in the channel. Now that the reference numbers s^i and p^i have been created, the ST and PR segment numbers of each heartbeat O^i_j can be tested. These values $s^i_j(O)$ and $p^i_j(O)$ are created analogous to (4.10) and (4.11), using O^i_j instead of V^i_j. The difference d^i_j between the ST and PR segment of each heartbeat is computed, and compared to the median difference d^i:

$$d^i_j = s^i_j(O) - p^i_j(O).$$

If d^i_j deviates from d^i by more than a given tolerance δ, the heartbeat is removed from the BSPM:

$$V^i_j = \left\{ \begin{array}{ll} 0, & \text{if } |d^i_j - d^i| > \delta \\ V^i_j, & \text{if } |d^i_j - d^i| < \delta \end{array} \right\}.$$

4.3.6 Recursive combination of methods

In the above sections, four stand-alone algorithms for identifying and removing parts of a BSPM that contain too much artefacts or variation or deviates too much from the rest were described. As each method has their strengths and weaknesses, a combination of the above methods is formed. Below, an outline of the algorithm combination is given in a Matlab/Octave-like environment. In this

outline, `remove_second_derivative` and `delta_1` refers to the algorithm and corresponding tolerance described in Section 4.3.3. `remove_varying_segments` and `delta_2` refers to Section 4.3.2, `remove_spatial` and `delta_3` refers to Section 4.3.4 and `remove_temporal` and `delta_4` refers to Section 4.3.5.

`remove_spatial` and `remove_temporal` are implemented in a loop, with each element of the vectors `delta_3` and `delta_4` being stricter than the previous. These two algorithms compare the current signal to neighbouring signals in space and time. For each iteration of the loop, outliers of the BSPM has been removed. Thus, the heartbeats the signal is compared to have been improved for each iteration of the loop.

The method for removing deviating and corrupted channels is as follows:

```
remove_second_derivative(V,delta_1);
remove_varying_segments(V,delta_2);

O=V;

for i=1:5
    V=remove_spatial(V,delta_3(i));
    V=remove_temporal(O,V,delta_4(i));
end

V=remove_sparse_channels(V);
```

When a BSPM is used as the input `V` of the recursive algorithm, the output will be the BSPM with parts of the signal removed. The last step called `remove_sparse_channels` will remove channels in which only $\frac{1}{5}$ or fewer of the heartbeats are left after the corrupted heartbeats are eliminated.

4.4 QRS detection

An important task in ECG and BSPM signal processing is QRS complex detection. Since the QRS complex is the most prominent feature of the BSPM, it is used to locate the other signal characteristics. It is also used in a variety of BSPM signal processing algorithms and as diagnostic information. Knowing the QRS complex location is therefore of prime importance! An ideal algorithm for detecting QRS complexes should detect all QRS peaks in a BSPM, without returning any false peaks. Real BSPM recordings come with a great variety in shape, frequency and noise content. This makes it necessary for a QRS detection algorithm to be robust with respect to these variations. In this section, some results from the literature on QRS detection will be reviewed, and a new algorithm will be described.

4.4.1 Literature on QRS detection

A large number of QRS detection schemes are described in the literature. Friesen *et al* [14] tested nine different algorithms with respect to a variety of noise. No single algorithm in that study was clearly superior, but two algorithms were deemed better than the rest. The first of these is an algorithm based on digital

filtering, and is an adaption of the algorithm developed by Engelese and Zeelenberg [12]. It applies a differentiator and bandpass filtering to the signal, and scans it for amplitudes greater than a given threshold value. The second algorithm uses squaring of the signal and derivatives before scanning for parts that exceeds the threshold value. Qi Gao [33] tested eight different QRS detection algorithms, concluding that the algorithms based on amplitude and derivatives performed best.

Kannathal *et al* [5] suggests a QRS detection algorithm based on the commonly used algorithms developed by Pan *et al* [29] and the further development by Hamilton *et al* [18]. These algorithms are similar to the ones that performed best in the tests by Friesen *et al* [14] and Qi Gao [33]. These detection schemes were based upon analysis of slope, amplitude and width of the ECG. Common for these three articles is to propose an algorithm involving the following five steps: First, the ECG is bandpass filtered with a 5-15 Hz passband. Second, the signal is differentiated (using a five point derivative) to get information about the slope of the signal. Third, the signal is squared to make the signal positive and amplify the high frequencies. Then a moving integrator is applied to the signal to detect the QRS complexes. Last, the QRS peaks are detected using adaptive thresholds. The adaptive thresholds detect peaks above the given value, and adjusts this value to detect QRS complexes with different amplitudes.

Chen *et al* [10] proposes a simpler algorithm that makes use of bandpass filtering, squaring and a moving summation window, but no derivatives. The correct detection rate of this algorithm was about the same as the ones described in [5] ($\sim 99.5\%$).

[39] concluded that a bandpass filter with centre frequency of 17 Hz maximises the QRS energy relative to other disturbances.

4.4.2 A proposed QRS detection algorithm

The algorithms mentioned in the previous section were designed for traditional 12-lead ECG. Many of them were also intended for real time usage, which limits the computational complexion of the algorithms. The QRS algorithm proposed in this thesis is inspired by the ones in described in [5], [14], [10]. This algorithm is not intended for real time usage. Hence more computationally demanding methods can be used to improve the algorithm. Moreover, advantage of the increased number of channels in a BSPM will be taken. A 7 step QRS detection algorithm was developed. The input to the algorithm is an unmodified BSPM. A sample channel of an unmodified BSPM can be seen in Figure 4.9. The output of the algorithm is a vector containing the QRS values. All the changes made to the BSPM during these seven steps are temporary, and only the QRS values will be used in further processing.

Step 1: Lowpass filtering is applied to all the channels in the BSPM. This lowpass filter is described in Section 4.1.2, and has a cutoff frequency of 49 Hz. This filter removes the high frequency noise content of the BSPM. Although a 5-15 Hz bandpass filter is used in many of the most popular algorithms, it will not be used in this one. One reason for this is that the AHA [21] states that the QRS complex contains higher frequencies than this. (In addition, both averaging and smoothing will be applied to the signal in later steps.)

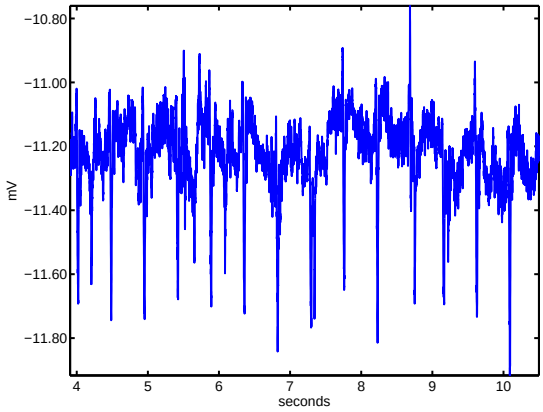

Figure 4.9: A channel of a BSPM before any processing steps has been applied. It is clear from this figure that automatic detection of QRS complexes in this channel is difficult without modifications to the BSPM.

Step 2: Highpass filtering is applied to all the channels. In addition to removing the drift and DC component in the BSPM, the highpass filter is intended to increase the magnitude of the QRS complex relative to the other parts of the BSPM. Since the T-wave primarily consists of frequencies in the range 1-2 Hz [21] and the QRS complex primarily consists of frequencies in the range 5-20 Hz [21], [39] a highpass filter with cutoff frequency 5 Hz is used. The highpass filter used is the same as the one described in Section 4.2.2, but with filter length $M = 3000$ and a different cutoff frequency. The result of the two first steps on the sample channel

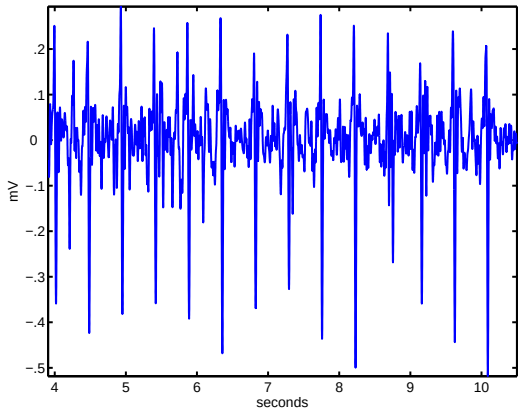

Figure 4.10: This figure shows the BSPM channel from Figure 4.9 after step 1 and step 2 of the QRS detection algorithm has been applied.

of a BSPM can be seen in Figure 4.10. Although this channel is suited for detecting QRS complexes, not all channels in a BSPM will be. The

next step is therefore to identify and remove those channels when using the QRS detection algorithm.

Step 3: Removal of disturbing channels. Some channels in a BSPM will be too noisy to provide information about the location of the QRS complexes. The step after this one will involve creating an average BSPM sequence from the channels in the BSPM. Channels with too much noise and too high amplitude, such as the one in Figure 4.6 will aggravate this average. For this reason, all channels too deviant from the median of the BSPM will be removed from the dataset before the rest of the algorithm is applied. The method described in Section 4.3.1 is used for this step.

Step 4: Absolute value and averaging. The absolute value of each channel that passed through the previous step is now computed to make all the data points in the signal positive. The electromagnetic signals originating from the heart propagates at high speed through the body. The signals will therefore reach the electrodes at different places on the body surface at, for all practical and computational purposes, the same time. Thus each channel of the BSPM will have the QRS complexes at the same times, which is shown in Figure 4.11. The average BSPM is cre-

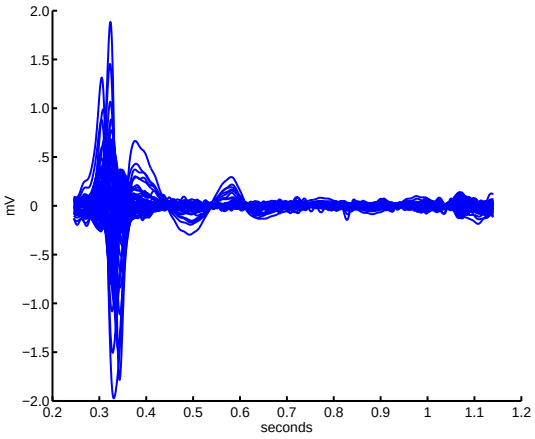

Figure 4.11: This is a plot of a single heartbeat from all 64 channels in a BSPM. Although both the form and amplitude varies much from channel to channel, all QRS complexes occur roughly at the same time.

ated from all the channels V^i that by now contains only positive values: $BSPM_{average}(x) = \frac{1}{N}\sum_{i=1}^{N} V^i(x)$, where N is the number of channels included in the computation of the average and $V^i(x)$ is the channel i of the BSPM at index x. This average will have differences in amplitude in the QRS complexes reduced, and will also have less random variations than each individual channel. At this point, the QRS complexes have been amplified and equalised, while the other parts of the signal has been suppressed.

Step 5: Moving average filtering. A moving average filter is applied to the

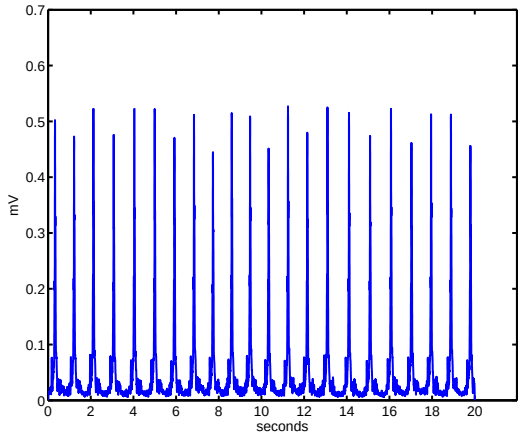

Figure 4.12: The $V_{average}$ computed by applying steps 1-4 of the QRS detection algorithm.

BSPM returned from the previous step of this algorithm, to create a new signal sequence $BSPM_{smoothed}$. The duration of a normal QRS complex is 60-100 ms. The length of the moving average filter is selected to be 101 points, which with a sampling rate of 2048 Hz corresponds to 49.3 ms. This is long enough to keep the high QRS peaks, without the high values from the QRS peaks creating falsely high P and T waves. This smoothing will, in addition to further evening the amplitude of the QRS complexes, remove many local maxima that could disturb the detection of the QRS complexes.

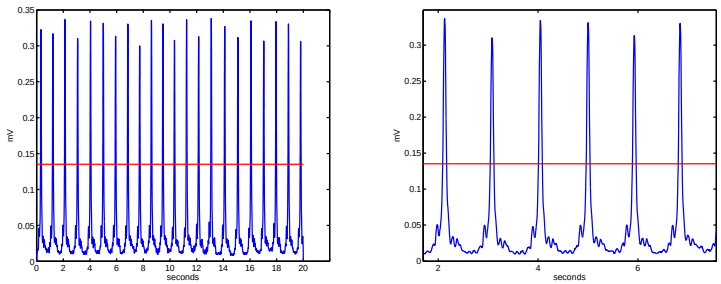

Figure 4.13: The smoothed average BSPM obtained by applying step 1-5 of the QRS detection algorithm to a BSPM. The horizontal line is the threshold value of $0.4 \cdot max(BSPM_{smoothed})$.

Step 6: Finding values larger than the threshold value. Now the smoothed BSPM is searched for values exceeding a preset threshold value to find potential QRS candidates. The threshold value is chosen to be $0.4 \cdot \max(BSPM_{smoothed})$ and is frequently used in other QRS detection algorithms [33], [14], [18]. Both averaging over the BSPM channels and

smoothing of the average have evened the amplitude of the QRS peaks, so a QRS complex is unlikely to be lower than 0.4 times the largest QRS complex in any dataset. The algorithm searches for periods where all consecutive data points in $BSPM_{smoothed}$ for $40ms$ or more is higher than the threshold value. When such a period is found the algorithm stores it as $interval_{start}$. Then it starts to search for $40ms$ of consecutive data points which is lower than the threshold value and stores it as $interval_{end}$. This produces an interval with high values of $BSPM_{smoothed}$, where a QRS value is located. Now the max value of $BSPM_{average}$ is found in that interval, and the index in the vector $BSPM_{average}$ in which this max value is located is stored in $\Delta(i)$. In other words, the vector Δ is the indexes of the maximum elements of $BSPM_{average}$ in all the found intervals $[interval_{start}, interval_{stop}]$.

After a QRS complex is found, the algorithm continues it's search $200ms$ after that QRS complex , since there is a physiological refractory period about this long [18]. After this search has been conducted on the entire signal, the QRS complexes of $BSPM_{average}$ has been found. The elements of the vector Δ then contains the temporal location of the QRS complexes. Since the QRS complex occurs at the same time for all channels of a BSPM, these QRS complexes are the QRS complexes of each channel of the BSPM as well (See Figure 4.11). Figure 4.14 shows the same time segment of the BSPM channel from Figure 4.9 , with the QRS complexes marked. Note that although the correct QRS complexes has been identified, they have not been located exactly at the peak of the complex in this case. Although the electric signal reaches each channel at the same time, the channels will record the signals differently.

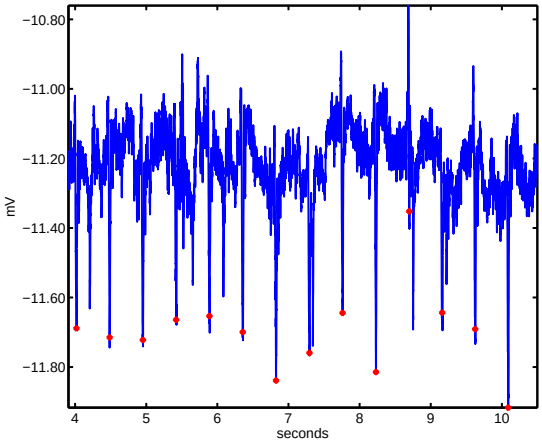

Figure 4.14: This is a short time segment of a BSPM, with the found QRS complex values marked with a dot. As the figure shows, the correct QRS complex was found even when there were neighbouring peaks of high amplitude.

Step 7: Although the six previous steps will find all the QRS complexes in a BSPM in most cases, abnormal T waves or other unpredicted sources may

produce false positives. These need to be sorted out. This last step of the QRS detection algorithm will make use of the fact that the time between each heartbeat should be about the same length[1].

The median distance between the detected QRS complexes is computed, and is termed L. The temporal location of the QRS complexes found in step 6 of the algorithm is collected in the vector Δ, with each element of Δ being the estimated location of a QRS complex. In this last step of the algorithm, two candidates for each QRS complex is tested against each other: The previously found values in Δ, and predicted values using the median distance L. The new vector consisting of the locations of the QRS complexes is given the name Δ_{new}.

The first element is set equal to the one found using step 1-6; $\Delta_{new}(1) = \Delta(1)$. Determining the rest of the QRS complex values is a bit more complicated. Assuming $\Delta_{new}(i)$ is found, $\Delta_{new}(i+1)$ is found the following way: Two candidates for the value is computed. The first, called Δ_o is picked from the previously found set of QRS complex locations Δ at a suitable location:

$$\Delta_o = \min_{j=1,\ldots,H}\{\Delta(j) > (\Delta_{new}(i) + 300)\}, \tag{4.12}$$

where H is the number of QRS complexes in Δ. This essentially picks the first value of Δ located 300 data points or more after $\Delta_{new}(i)$. The second candidate Δ_p for $\Delta_{new}(i+1)$ is predicted using the knowledge of the median distance between the previously found QRS complexes:

$$\begin{aligned} \Delta_p &= \text{the index of } \max_{x\in[a,b]}\{BSPM_{average}(x)\} \\ \text{with } a &= \Delta_{new}(i) + L - 200 \\ \text{and } b &= \Delta_{new}(i) + L + 200. \end{aligned} \tag{4.13}$$

Thus, the value Δ_p found in (4.13) is the temporal location of the maximum value of $BSPM_{average}$, in the interval where a QRS complex should occur.

Now the two candidates Δ_o and Δ_p for the QRS complex location $\Delta_{new}(i+1)$ has been found. $\Delta_{new}(i+1)$ is then set equal to Δ_o if $BSPM_{average}(\Delta_o) > BSPM_{average}(\Delta_p)$, and equal to Δ_p otherwise.

This is continued for increasing values of i until the end of the signal $BSPM_{average}$ is reached. Δ_{new} now contains the final QRS complex locations that will be used in later computations. This last step of the algorithm will work well in correcting sets of found QRS complexes in which there are a few false positives or undetected QRS complexes.

The output of the QRS detection algorithm is a vector containing the QRS peak's temporal location . All the steps in the algorithm was just steps toward obtaining the QRS values. Thus all changes made to the BSPM during the QRS detection algorithm were temporary, and will not be used in further processing of the BSPM.

[1] This is only the case in patients with normal heart rhythm. Patients with heart conditions such as arrhythmia will have heartbeats of uneven duration. This algorithm is designed to work in these cases as well.

Chapter 5

Evaluation of methods and algorithms

In Chapter 4 a number of algorithms for performing several BSPM processing tasks were presented. This chapter contains an evaluation of the performance of these algorithms. Where multiple algorithms for performing the same task were presented, a comparison will be made. It is important to note that all the algorithms have been evaluated with one goal at hand: To improve BSPMs for detecting ischemia by measuring differences in ST segment shifts.

5.1 Noise reduction in signal

Two algorithms were proposed to remove high frequency noise from BSPMs. A notch filter was designed to remove the 50 Hz powerline noise that is present in some BSPMs. A lowpass filter was also designed to remove all frequencies above a desired cutoff frequency. These filters were applied to several real patient recordings. The results of applying the filters to BSPMs is given below, together with a description of what these results indicate.

5.1.1 Notch filter to remove powerline noise

The notch filter has been tested on BSPMs with little to none 50 Hz powerline noise. Figure 5.1 shows a plot of a channel of such a BSPM before and after the notch filter has been applied. As expected, the BSPM is almost identical before and after the filter was applied. This is because there was very little 50 Hz frequency present in the BSPM before filtering, and removing these very small parts of the recording will only result in minor changes.

In Figure 5.2 the notch filter was applied to a BSPM with much 50 Hz powerline noise present. The figure shows a smoother BSPM with less random fluctuations after the notch filter has been applied. A look at Figure 5.3 confirms that only the frequency components close to 50 Hz has been removed, and thus the Signal-to-Noise Ratio has been improved.

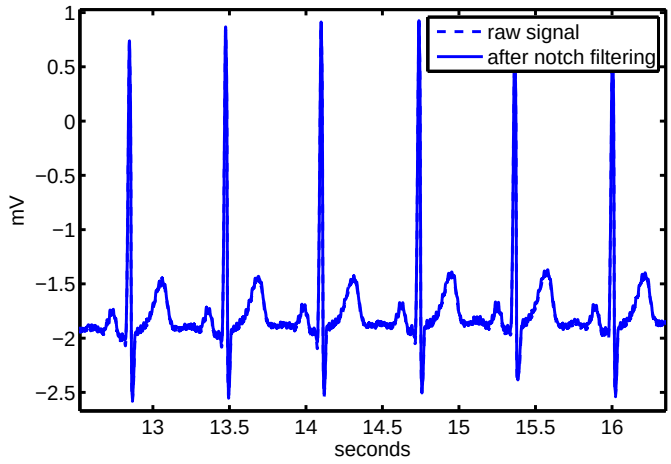

Figure 5.1: The dashed line shows a channel of a BSPM with little 50 Hz power line noise. The solid graph shows the BSPM after a notch filter has been applied to remove the 50 Hz components of the BSPM. They are clearly almost identical.

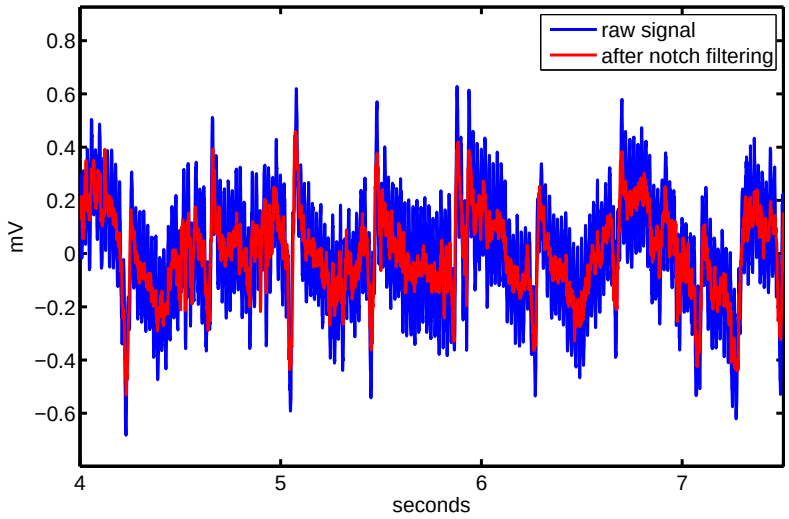

Figure 5.2: The blue graph shows a channel of a BSPM contaminated with 50 Hz power line noise. The red graph shows the BSPM after a notch filter has been applied to remove the 50 Hz components of the BSPM.

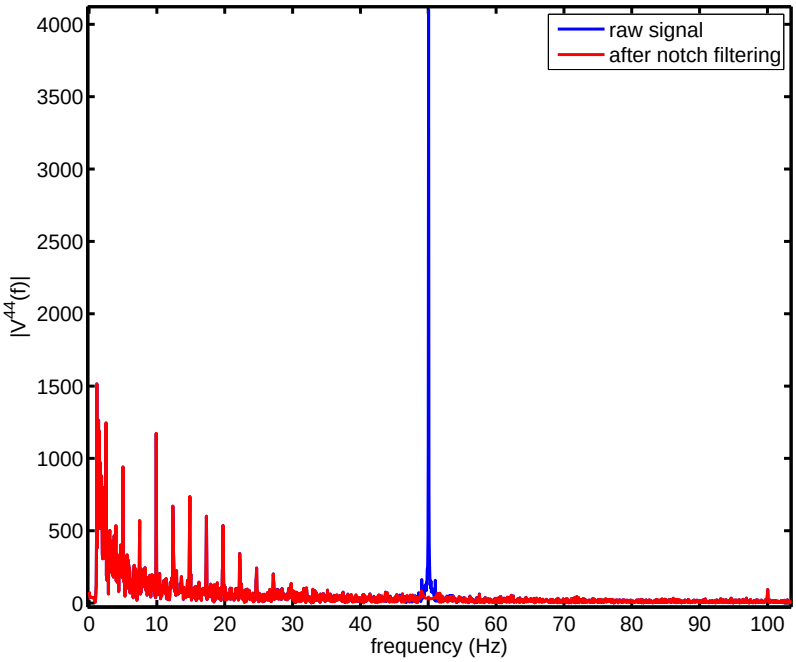

Figure 5.3: Parts of the frequency spectrum of a BSPM contaminated by 50 Hz powerline noise. The blue graph shows a BSPM contaminated with 50 Hz power line noise. The red graph shows the BSPM after a notch filter has been applied to remove the 50 Hz components of the BSPM. As the figure shows, the notch filter causes near to no distortions in other frequencies than those in the immediate neighbourhood of 50 Hz.

5.1.2 Lowpass filter to remove high frequency noise

The lowpass filter with cutoff frequency $49Hz$ has been applied to the same nice signal as was used in Figure 5.1. Little of the content of the BSPM was in frequencies above 50 Hz, and removing these frequencies should therefore result only in minor changes in the BSPM. The result can be seen in Figure 5.4. It is clear that the lowpass filter produced no significant distortions in this nice BSPM.

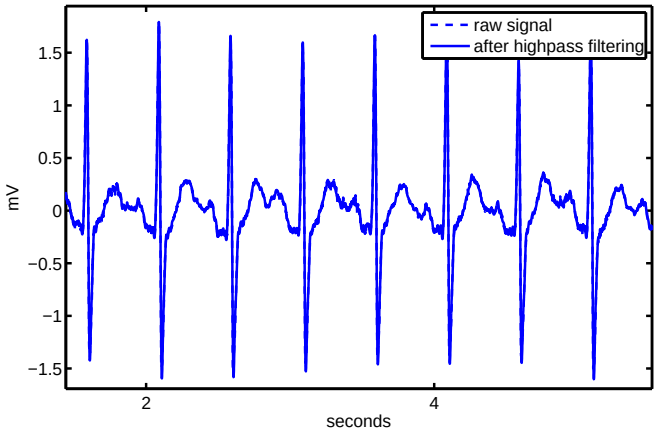

Figure 5.4: The dashed line shows a BSPM with little 50 Hz power line noise or other high frequency noise. The solid line shows the BSPM after the lowpass filter with cutoff frequency of 49 Hz has been applied to remove the high frequency components of the BSPM. They are clearly almost identical.

In Figure 5.5 the lowpass filter was applied to a BSPM with much high frequency content. The result of the filtering is a much smoother BSPM with less abrupt variations in amplitude. Not only is this much nicer visually, it is also more useful for doing calculations on the different phases of the signal since the randomness has been reduced. The danger with applying this lowpass filter is that it is difficult to know if only noise is removed, or if parts of $BSPM_{signal}$ also is removed. That the lowpass filter introduces no significant changes to BSPMs with low noise contents like the one in Figure 5.4, is a good indication that it will not introduce significant changes in the $BSPM_{signal}$ part of BSPMs with higher noise content. Similar results were achieved when applying the lowpass filter with a cutoff frequency of 49 Hz to other BSPMs as well.

5.1.3 Results from noise reduction

To test the noise reduction algorithms further, six real BSPMs were used, with both exercise and rest recordings from each of the six. The recording in channel i of a BSPM will be called V^i. As a validation that the noise removed does not contain important information about $BSPM_{signal}$, the noise will be correlated with a reference signal. The reference signal is chosen to be the median heartbeat V^i_{median} of each channel V^i. An illustration of such a V^i_{median} can be seen in Figure 5.6.

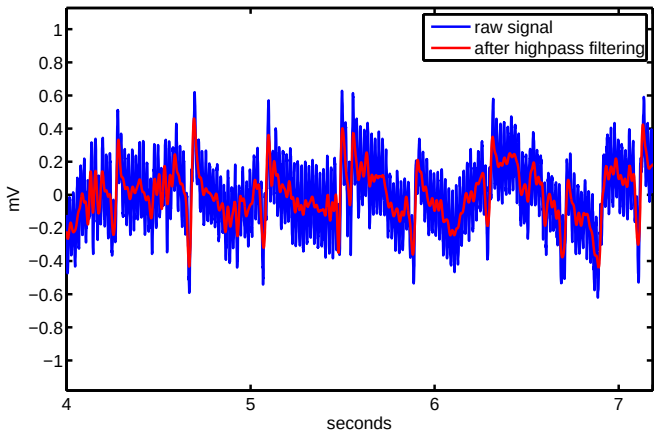

Figure 5.5: The blue graph shows a BSPM with much high frequency content. The red graph shows the BSPM after the lowpass filter with cutoff frequency of 49 Hz has been applied to remove the high frequency components of the BSPM.

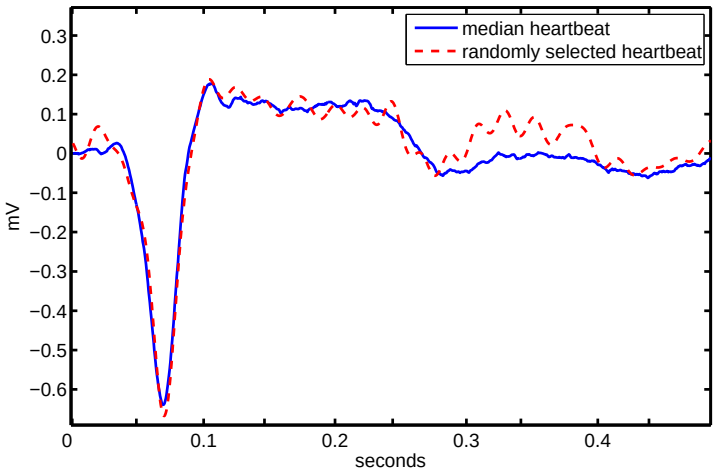

Figure 5.6: The median heartbeat of a BSPM in solid line, and a randomly selected heartbeat from the same BSPM in the dashed line. As can be seen, the abrupt random variations is reduced in the median heartbeat.

Before the noise reduction algorithms were applied, the drift was removed from the recordings using the highpass filtering methods described in Section 4.2.2. Thus, each recording used consisted mainly of $BSPM_{signal}$ and $BSPM_{noise}$ before noise reduction was applied. Also, the recordings in which no useful information could be contained were removed.

For each heartbeat V_j^i, the noise removal algorithms removed a part n_j^i that was labelled as noise. To test if this really was noise, or contained information important to $BSPM_{signal}$, n_j^i was correlated with the reference heartbeat V_{median}^i in the following way:

$$\rho_i = \frac{1}{H} \sum_{j}^{H} corr(n_j^i, V_{median}^i),$$

where H is the number of heartbeats in the current channel i. The correlation number $\rho = \frac{1}{64} \sum_1^{64} \rho_i$, with 64 being the number of channels in a BSPM, was computed for each patient. Each ρ describes how correlated the noise removed from the BSPM is with the medians of the corresponding channels. This resulted in correlation numbers representing how correlated the noise removed is with the median heartbeats, and can be seen in Table 5.1.

Patient	state	notch filter	lowpass filter 50 Hz	lowpass filter 100 Hz
patient1	rest	0.0715	0.1102	0.0010
patient1	exercise	0.0085	0.0169	0.0017
patient2	rest	0.0340	0.0764	0.0157
patient2	exercise	0.0024	0.0102	0.0026
patient3	rest	0.0444	0.0799	0.0185
patient3	exercise	0.0052	0.0118	0.0054
patient4	rest	0.0018	0.0192	0.0000
patient4	exercise	0.0728	0.0177	0.0013
patient5	rest	0.0122	0.0084	0.0058
patient5	exercise	0.0076	0.0051	0.0025
patient6	rest	0.0148	0.0210	0.0107
patient6	exercise	0.0112	0.0190	0.0064

Table 5.1: The correlation number between the noise removed from the signal, and the median heartbeat. As can be seen, there is not much correlation between the median heartbeats and the noise removed.

As Table 5.1 shows, both the notch filter and 100 Hz cutoff lowpass filter removes elements that are very little correlated with the median heartbeat. This indicates that the parts that are removed consists mainly of random noise, and not signal. Also the 50 Hz cutoff lowpass filter removes elements that are little correlated with the median heartbeat. In some cases, the correlation number between the median and the parts removed with 50 Hz lowpass filter shows some degree of correlation. Since the highest frequencies contained in $BSPM_{signal}$ is in the QRS complex, the parts removed will probably not introduce disturbances to the ST segment.

5.2 Drift reduction

The four drift reduction algorithms discussed in Section 4.2 were tested on various BSPM recordings. Since there is such large variations in the drift in different BSPM recordings, this section will take a look at the performance of the four methods on a large range of different BSPMs. The most desired properties of a drift reduction algorithm is that it will work equally well on all kinds of BSPMs. It should also introduce minimum distortions to the ST and PR segments while removing as much of the drift as possible.

In all the following tests in this section, 20 second segments of recording will be used. Some figures will display smaller parts of the segments for illustrational purposes. Testing the performance of the drift reduction algorithms on real BSPM recordings is difficult, since there is no a priori knowledge on how the drift should be in each case. Therefore the results will be analysed in many representative cases, and a conclusion will be drawn on the all round performance. As a minimum requirement the algorithms should be able to remove slow varying drift from a nice and tidy signal.

5.2.1 Drift reduction on nice BSPMs

If an algorithm performs poorly when removing the simplest forms of drift, it will probably not be good at more complex cases. This section will take a look at the performance on BSPMs with little noise disturbances. Since it is easiest to see the precision of the drift approximation in the simplest cases, bad performance here will be a good indication of bad performance in more complex cases. Figure

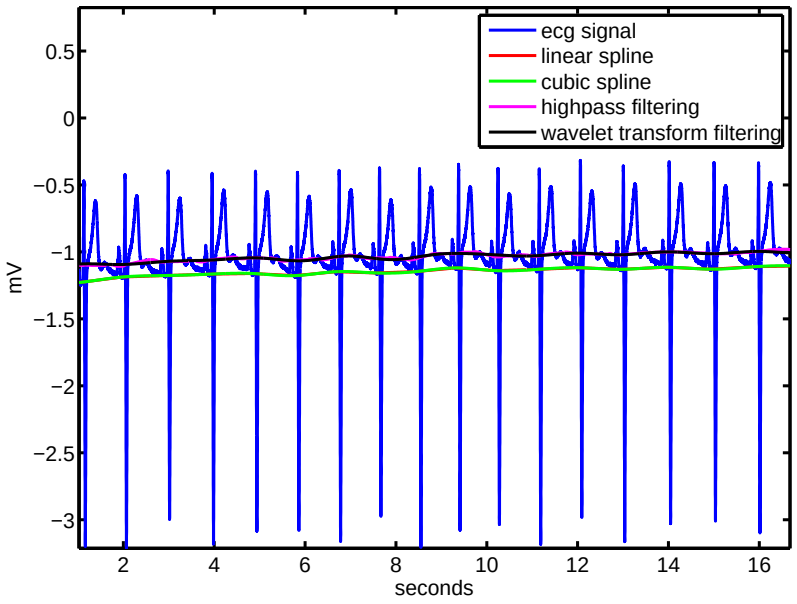

Figure 5.7: The four different drift reduction algorithms' approximation to the drift in a nice BSPM channel from a healthy person.

5.7 is a typical example of a nice BSPM with slow varying drift. The drift has been approximated by the four drift reduction algorithms, and plotted on the BSPM. There is a difference in the amount of drift removed between the frequency based and the spline based drift approximations. However, the four plots of the drift approximations are close to parallel, which means that they will give similar results when calculating ST PR differences.

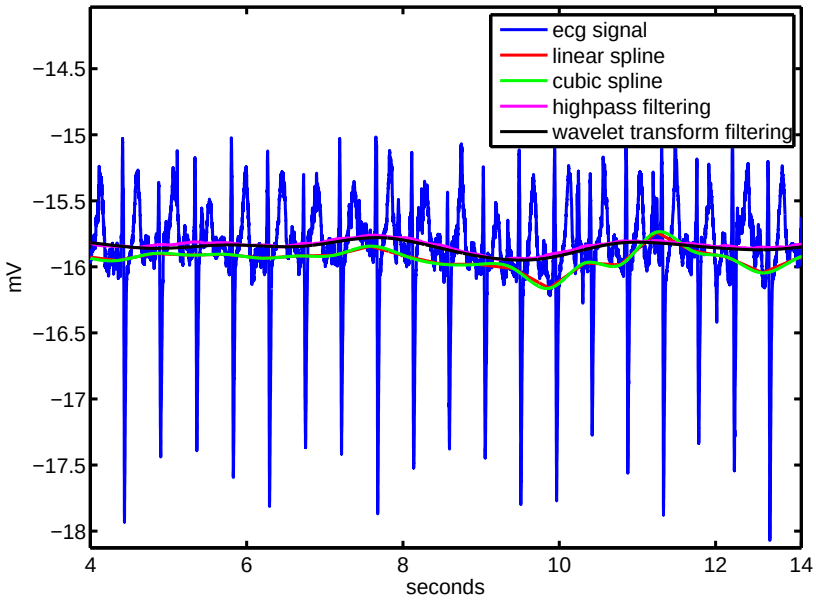

Figure 5.8: The approximation of the drift by the four different drift reduction algorithms in a nice BSPM from a healthy person during exercise.

Figure 5.8 shows the drift approximations to the drift in a nice BSPM channel from a healthy person during exercise. The heartbeat rate is greater than the one in Figure 5.7. Small deviations from the baseline with a period of a heartbeat or less will therefore not be caught up by the frequency based algorithms, since these use a cutoff frequency of 0.5 Hz. When the heartbeat rate is this high, the spline methods will give a straighter baseline after drift reduction, while the frequency based methods will remove a smoother drift approximation from the BSPM. This can also be seen in Figure 5.9, where the spline drift approximations follow the abrupt parts of the drift to a greater degree than the frequency drift approximations does.

5.2.2 Drift reduction on noisy BSPMs

As seen above, the drift reduction algorithms all worked quite well on BSPMs with little high frequency noise present. Since the algorithms need to work well on all kinds of BSPMs, they have also been tested on noisier BSPM recordings. Figure 5.10 shows the drift approximations to a BSPM with much noise present.

As expected, the spline methods' drift approximations are more sensitive to

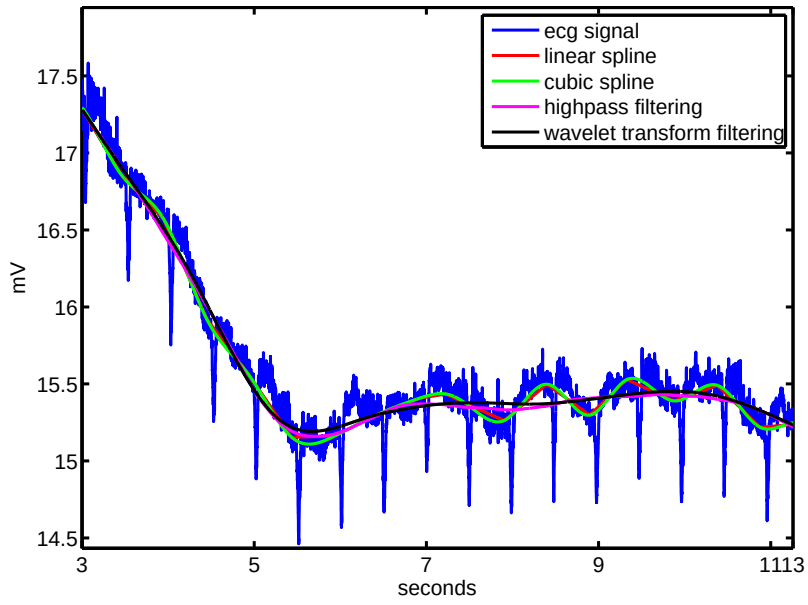

Figure 5.9: The four different drift reduction algorithms' approximation to the drift in a BSPM with little noise and much drift.

high frequency noise. The deviation from baseline in the knot values increases as the amount of high frequency noise increases, and results in a decrease in the precision of the splines' drift approximations. The frequency based drift approximation methods' performance will not be affected by the noise present, since they operate purely on the low frequencies of the BSPM.

The drift reduction algorithms was also applied to noisy BSPMs with more complex drift. Much noise present in a BSPM can reduce the precision of the spline based drift reduction algorithms, though not much. Because of the method used when calculating the knot values in the splines, the algorithms can handle much noise before anything more than minor faults occur (see Figure 5.12) Still, this illustrates the importance of removing the high frequency noise from the BSPM before applying spline based drift reduction algorithms.

5.2.3 The impact of drift reduction on phase difference calculations

So far, the precision of the four drift reduction algorithms has been tested and discussed. Extra focus will now be turned to the property of the algorithms that is of most importance to this study. The processed BSPMs will be used to calculate ST PR differences to diagnose ischemia. Hence it is vital that the ST and PR segments of the BSPM is preserved as true as possible after drift reduction has been applied. The BSPM of a patient with ischemia with drift removed using the four methods can be seen in Figure 5.13. An important property for the drift reduction algorithms to have, is that they do not distort

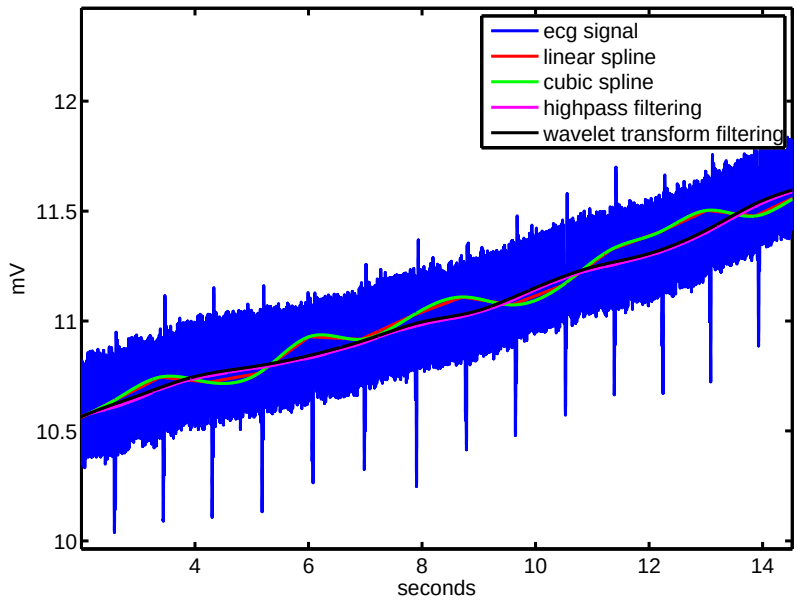

Figure 5.10: A BSPM channel with a lot of high frequency noise present, and a slow varying drift. The drift approximations computed by the four drift reduction algorithms are displayed on top of the BSPM. It is clear that the drift computed by the two spline based algorithms deviates randomly from the actual drift at some points. This decrease in precision is a result of the high frequency noise present, and will only affect the spline based algorithms

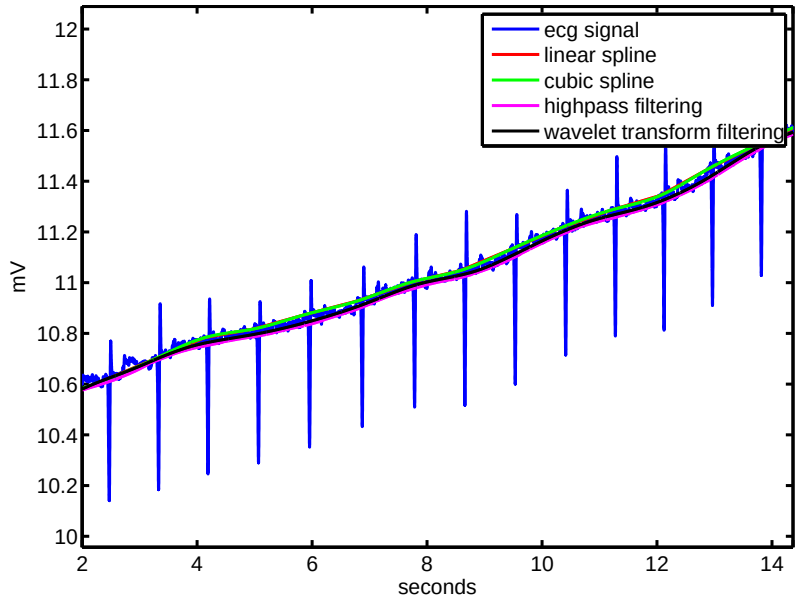

Figure 5.11: The same BSPM as in Figure 5.10, but with noise removed using a 49 Hz cutoff lowpass filter. With the high frequency noise removed, an improvement in the two spline based drift approximations can be seen.

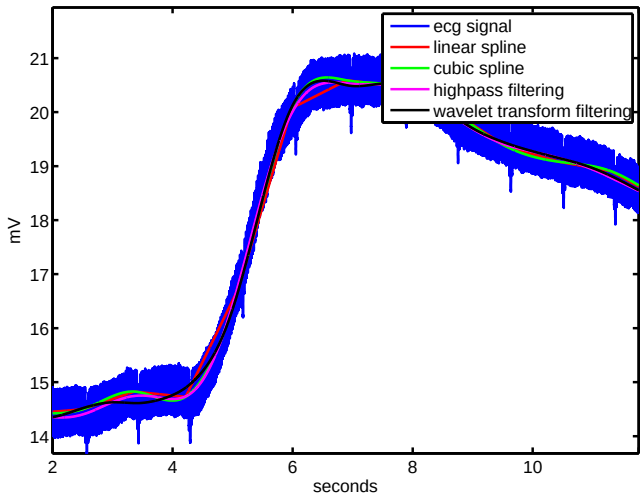

Figure 5.12: An BSPM with high frequency noise present, and a complex drift. Approximations to the drift is shown on top of the BSPM. The noise causes minor disturbances to the spline base drift approximations, but they still yield good results.

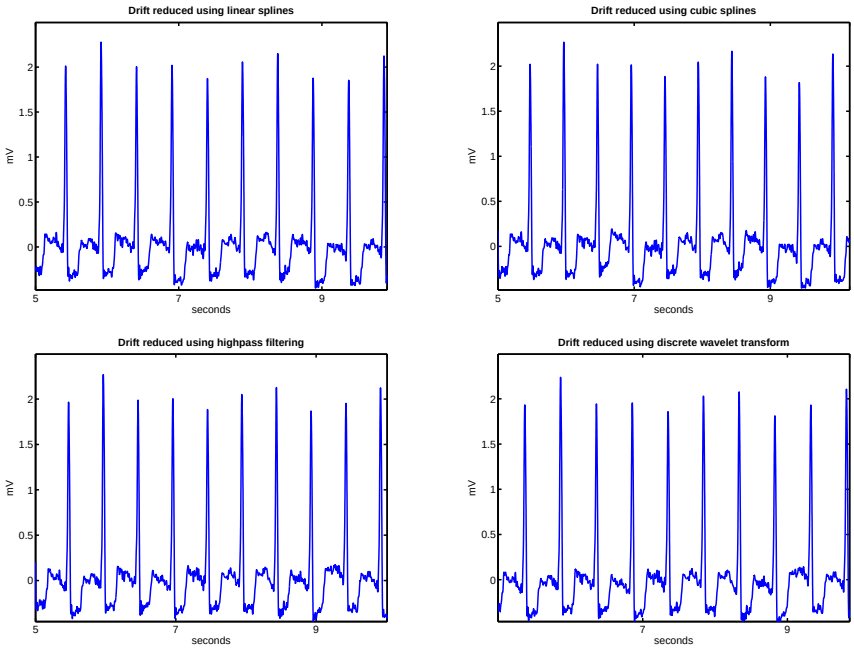

Figure 5.13: The drift reduction algorithms has been applied to the exercise BSPM of a person with ischemia. The characteristic lowered ST segments are preserved with all of the four algorithms.

the ST and PR segments of the signal. In most cases, like in Figure 5.13, the four methods performed equally well. In some other cases, like those seen in Figure 5.9 and 5.8 the frequency based algorithms will not give a good approximation to the faster varying drift, which may cause some segments of the signal to deviate more from the baseline than it should. In the following section, a method will be picked in favour of the three other.

5.2.4 Conclusions on drift reduction

All of the four drift removal algorithms implemented in this thesis made good approximations to the drift in BSPM signals. Two frequency based algorithms (highpass filtering and wavelet transform filtering) and two spline interpolation based algorithms (linear and cubic) were used to approximate the drift in a signal. The frequency based algorithms had similar performance, and the two spline based performed similar to each other while different from the frequency based algorithms.

The major advantage of the frequency based algorithms is that their performance will not be affected by higher frequency noise in the BSPM. They will also remove exactly the same frequencies from all BSPMs. Their drawback is their inability to remove drift with frequency components higher than $0.5Hz$ that is often present in BSPMs recorded during exercise. Thus, when the approximated drift has been removed from the BSPM, there will still be some baseline deviations in some signals.

The spline based algorithms will deal better with this problem, as the approximation created by them will follow the drift in the signal to a greater degree. Thus a BSPM improved with one of the spline based drift removal algorithms will have a straighter baseline with fewer deviations. The major drawback of the spline based methods, is that their performance relies on the selection of knot values right before the onset of each QRS complex. A robust QRS complex detection algorithm and good methods for removing high frequency and $50Hz$ noise components will minimise the effect of this drawback.

All over, the four algorithms performed well. Each algorithm has advantages and drawbacks compared to the others. While it is difficult to draw a definite conclusion, there were some indications that some algorithms performed better than others. The cubic spline interpolation method is considered the best of the four in the tasks required for this thesis. The ability to approximate drift with faster variations than $0.5Hz$ was the ability weighted the most. Also, the cubic version was selected over the linear because of its smoother approximations to the drift. This makes it the most robust of the four methods, as it will perform well on BSPMs with fast heartbeat rates as well as slow ones. The good performance of the QRS complex detection algorithm and noise reduction algorithms were helping factors in this decision.

5.3 Results from removing corrupted signals

Even after noise and drift reduction algorithms have been applied to a BSPM, there will often be noise and artefacts present. In Section 4.3 four different methods for removing corrupted and deviating parts of a BSPM were presented. All of these methods improve the recorded BSPM by removing parts that is deemed corrupted with respect to a given tolerance. It is obvious that the amount of signals classified as corrupted depends on the strictness of the set tolerance.

With the limited number of BSPMs available for testing, it is not possible to provide ideal parameters for these methods. Parameters that result in the best removal of corrupted or noisy heartbeats of the BSPMs available at this point, may not be ideally fit for other BSPMs. When determining the parameters used in this thesis, the six available BSPMs where split into training and test sets. A training set of four BSPMs and a test set of two were used. The parameters were selected to fit the four datasets in the training set, and tested to see if they fitted the test sets. Then new test and training sets consisting of different permutations of BSPMs were formed. This procedure was repeated, and suitable parameters were found. Not using too strict tolerances was deemed most important in this process.

With a larger number of BSPMs available than at the present time, the parameters performing best on an arbitrary BSPM can be found. A similar method of using training and test sets is a possible way of doing this. With these sets being significantly larger than at this point, one can be more certain that the found parameters fits BSPMs recorded at a later point.

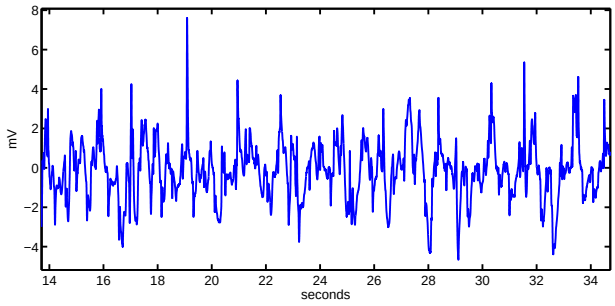

Figure 5.14: An example of a channel in which the whole channel was removed by the sorting algorithm.

5.3.1 Results from Removing destroyed channels

In this section, the method described in Section 4.3.1 will be evaluated. The method removes whole channels if parts of it deviates too much from the median of all channels. Some QRS complexes in otherwise nice signals can have amplitude several mV greater than the average QRS complex. Thus a large tolerance should be used with this method. When the algorithm is used as one of the first steps in the QRS detection algorithm, a tolerance of about $5mV$ should do. This way, most signals will be kept while corrupted channels and channels with abnormally high QRS complex peaks will be removed. While this is a good method for sorting out channels in one of the first steps of a QRS detection algorithm, other less coarse methods will be better in improving an arbitrary BSPM.

5.3.2 The performance of the combined sorting algorithm

In Section 4.3.6 a recursive combination of the four methods described in Section 4.3 (excluding that of Section 4.3.1) was proposed. As mentioned earlier, too few body surface potential mappings were available to determine the ideal tolerances. Instead, some examples of the performance of the combined sorting algorithm will be given. The tolerances were found using training and testing sets from the few date sets available.

In the combined sorting algorithm, four tolerances were used. After testing, these were set to `tol_1` $= 2$, `tol_2` $= 0.05$, `tol_3` $= [0.7, 0.6, 0.5, 0.4, 0.3]$ and `tol_4` $= [0.14, 0.13, 0.12, 0.11, 0.10]$. Some illustrations of the algorithm's performance is given in Figure 5.14 - 5.16.

The parameters used was a good combination for keeping as much information as possible, while also sorting out the too noisy or corrupted heartbeats. If less than $\frac{1}{5}$ of the original number of heartbeats in a channel was left after the sorting, the whole channel was removed. The choice of this value was a compromise between having enough heartbeats left in a channel to get a reliable measurement of the ST segment and the need to have ST segment shift values for as many points on the body surface as possible. By increasing this number, ST segment shifts from fewer channels of the BSPM may be computed, but these will in turn be more trustworthy. The sorting algorithm was applied

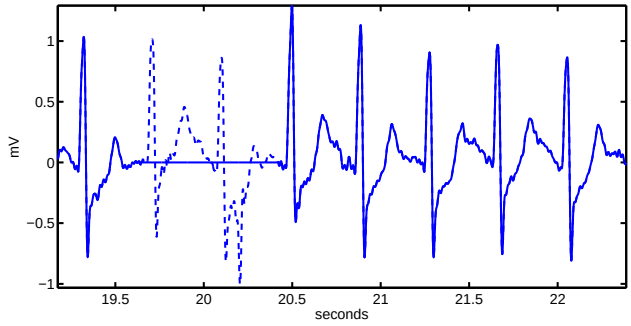

Figure 5.15: An example of two heartbeats (dashed line) that have been removed because their ST and PR segment deviates too much from the rest of the BSPM channel (solid line).

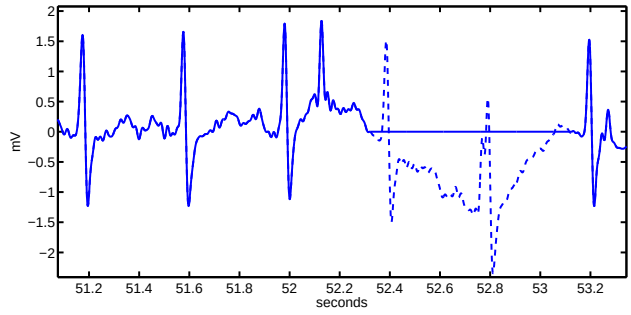

Figure 5.16: In this figure, an abnormally wide QRS complex resulted in an artificial shift in the signal was introduced by the spline drift removal algorithm. The two heartbeats plotted with a dashed line was removed by the method based on the drift approximation's second derivatives.

to six real BSPM recordings. In the "nicest" of these only two channels were completely removed. In the BSPM with the noisiest or worst signals, 9 whole channels were completely removed.

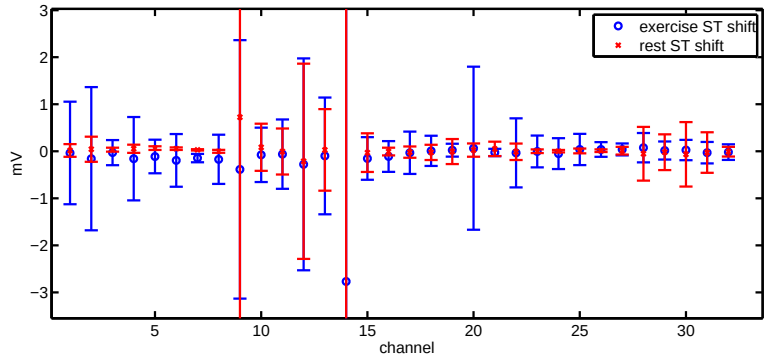

Figure 5.17: The mean ST segment shift values of the 32 first channels both during rest and during exercise, with corresponding standard deviations. This is the mean ST segment shifts of a patient computed before the sorting algorithm has been applied. Note the high standard deviations in most channels.

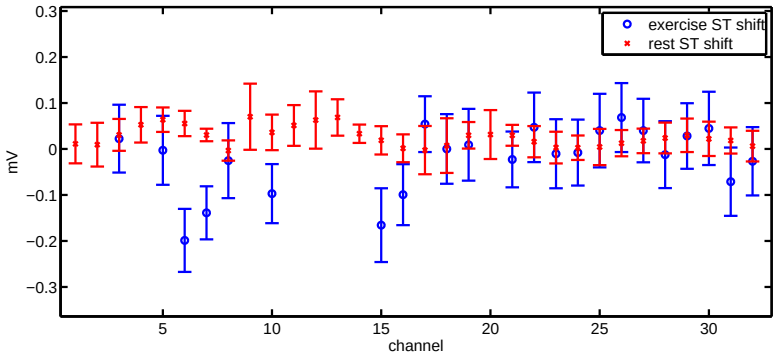

Figure 5.18: The mean ST segment shifts of both exercise and rest recording with corresponding standard deviations. This is the values for the same patient as is plotted in Figure 5.17, but after the sorting algorithm has been applied. Note that the standard deviations has been greatly reduced.

By removing the noisy, corrupted and deviating heartbeats, the standard deviation in the measured ST segment shifts is greatly reduced. Figure 5.17 and Figure 5.18 shows the mean ST segment shift of the 32 front channels of the noisiest of the six BSPMs. The figures show both the ST segment shift and the channels standard deviation, for both rest and exercise recordings. By reducing the standard deviation this much, the sorting algorithm provides more correct measures of the ST segment shift.

5.4 QRS detection on real BSPMs

And now to something completely different: In Section 4.4.2 a QRS detection algorithm was proposed. Here the performance of this algorithm will be discussed, and some results presented. Step 1 to 6 of the algorithm detects QRS complexes in a wide range of BSPM signals. Abnormally large P or T waves, or high amplitude noise may produce false positives. Step 7 of the algorithm is designed for correcting this, by making use of information about when a QRS complex should occur.

The QRS detection algorithm was applied to both the rest and exercise recording of the six BSPMs available. From each patient, 60 seconds of exercise recording and 60[1] seconds of rest recording was used. This made a total of 690 seconds of BSPM recordings for the QRS detection algorithm to be tested on. The algorithm detected 1287 out of 1289 QRS complex peaks, and produced no false positives. In this limited test, the algorithm thus had a sensitivity of 99.8% and a specificity of 100% (specificity being the percentage of detected QRS peaks that are real QRS peaks). These are promising results, but testing on much larger data sets is required to confirm the effectiveness of this algorithm. For the purpose of detecting ischemia from ST segment shift differences, a high specificity is more important than the sensitivity. A falsely detected QRS complex may lead to a false ST segment shift being computed. An undetected QRS complex however, will only reduce the number of heartbeats available for ST segments measuring by one. Thus, if later testing shows a decrease in specificity, measures should be taken to increase it. Increasing the treshold value or using adaptive thresholds may increase the specificity, but may also lead to a decrease in sensitivity.

[1] For one of the patients, only 30 seconds of rest recording were available.

Chapter 6

The complete algorithm and results

In Chapter 4 many algorithms for performing different processing tasks on a BSPM were presented. In Chapter 5 these algorithms were evaluated one at a time. In this chapter a discussion is made on how these algorithms are put together to form a complete BSPM processing algorithm. The complete BSPM processing algorithm is automatic, so it takes raw data as input. The output of the algorithm is a vector of numbers describing the differences in ST segment elevation/depression. These numbers can, when viewed properly, give an indication on whether a patient suffers from ischemia or not. Among other things, the output can also be used as input to methods computing the electrical activity in the heart, as an inverse problem. Manual choosing of ST segment shift differences is very time consuming and inaccurate. This is the main reason for creating an automatic algorithm for doing this, utilising the methods developed in this thesis.

The processed BSPMs will be inspected to see if they provide good data for recognising signs of ischemia in a patient. The processed data provide clearer and more trustworthy data for this kind of testing, as will be seen towards the end of this chapter.

6.1 The final BSPM processing algorithm

When there is suspicion that a patient suffers from ischemia, a BSPM of that patient can be recorded. The recording is done of the patient both during rest and exercise. The difference in ST segment between these two recordings can give an indication of whether the patient suffers from ischemia or not. The BSPM is a recording of the potential differences in the electrical signals propagating from the heart to 64 points on the body surface. Unfortunately, a variety of other signals are also recorded. These are classified as noise and baseline drift. The total recording in a BSPM has been modelled as (3.1):

$$BSPM = BSPM_{signal} + BSPM_{noise} + BSPM_{drift}.$$

The main goal of the automatic BSPM processing algorithm is to minimise the amount of $BSPM_{noise}$ and $BSPM_{drift}$ present in all kinds of BSPM record-

ings, while keeping $BSPM_{signal}$ unchanged. The algorithm is a combination of methods developed and discussed earlier in this thesis, and will produce an improved recording called $BSPM_{improved}$. A simplified model of the algorithm is given:

$$\begin{aligned} BSPM_{improved} = BSPM_{signal} + BSPM_{noise} + BSPM_{drift} \\ -A_{noise} - A_{drift} - A_{deviants}, \end{aligned} \tag{6.1}$$

where A_{noise} and A_{drift} are approximations to the noise and drift in the signal and $A_{deviants}$ is the corrupted channels and heartbeats that is removed. When the BSPM has been cleaned of artefacts and noise, ST segment shift differences is calculated from $BSPM_{improved}$.

All the methods included in the automatic algorithm has been described in detail in previous chapters. Hence, this section will only include an overview of how these methods are combined. The process of the algorithm is split into five steps, each producing an output that is used as input to the next step.

6.1.1 Noise reduction

The first step of the automatic BSPM processing algorithm is noise reduction. The performance of the noise reduction methods is not affected by the other steps in the algorithm, but several of the other steps perform better if noise reduction has been applied first. The algorithms described in Sections 4.1.1 and 4.1.2 are applied. The lowpass filter will use a cutoff frequency $f_{cutoff} = 49Hz$. All changes made in the BSPM by this step of the algorithm is kept for the later stages. This improves the BSPM recording by removing parts of the signal A_{noise} classified as noise:

$$BSPM_{noiseimproved} = BSPM_{signal} + BSPM_{noise} + BSPM_{drift} - A_{noise}.$$

6.1.2 QRS complex detection

After noise reduction has been applied to the BSPM, the time has come to detect the QRS complexes. All the later steps of the BSPM processing algorithm require information about the location of the QRS complexes or heartbeats. The method used for detecting the QRS complex peaks of each heartbeat is described in detail in Section 4.4.2. Although the BSPM is modified in different ways to detect the QRS complex peaks, none of these modifications are kept for later stages of the BSPM processing algorithm. The output of this step in the algorithm is the location of the QRS peaks, and from this information of where each heartbeat in the channels of the BSPM starts and ends.

6.1.3 Drift removal

The cubic spline interpolation method for removing drift in the BSPM was deemed the best of the four methods for drift removal tested in this thesis. Using the output of the last step in the BSPM processing algorithm, the cubic spline interpolation method for drift removal described in Section 4.2.1 can now be applied. The method makes an approximation A_{drift} to the drift in the BSPM, and subtracts it from the data:

$$BSPM_{driftimproved} = BSPM_{noiseimproved} - A_{drift}.$$

The changes made to the BSPM during this step of the algorithm are kept for later stages.

6.1.4 Identifying and removing corrupted parts of signal

At this stage in the algorithm, both noise reduction and drift removal has been applied. If $A_{noise} \approx BSPM_{noise}$ and $A_{drift} \approx BSPM_{drift}$, the signal $BSPM_{driftimproved}$ used at input to this step of the algorithm is

$$BSPM_{driftimproved} \approx BSPM_{signal}.$$

Unfortunately this is rarely the case. In most BSPMs there will be parts of individual channels, or even whole channels, which are still distorted by noise or simply do not contain any heart signal information at all! These parts of the BSPM are removed in this step of the algorithm. For removing the corrupted and deviant parts of $BSPM_{driftimproved}$, the recursive algorithm described in 4.3.6 is used. After this step is applied, the final $BSPM_{improved}$ in (6.1) is obtained.

6.1.5 Computing the ST segment elevations/depressions

The output $BSPM_{improved}$ of the previous step of the algorithm is the BSPM signal with noise and drift reduced, and corrupted and deviating parts of the signal removed. As $BSPM_{improved}$ is a cleaner dataset that is more close to the actual $BSPM_{signal}$ than the recorded raw data. $BSPM_{improved}$ can, with some modifications, be used in many tasks where a processed BSPM dataset is required. In this thesis, the processing algorithm is applied to both recordings $BSPM^{rest}$ during rest and recordings $BSPM^{exc}$ during exercise for each patient, creating two processed datasets $BSPM^{rest}_{improved}$ and $BSPM^{exc}_{improved}$. For each patient, these two datasets will be used in computing the ST segment shift differences between rest and exercise. The method described in Section 3.2 is used for this. Equation (3.4) in this method produces a vector d of length 64. Each element d^i, $i = 1, \ldots, 64$ is a number representing the difference in ST segment shift between rest and exercise for the channel i of the BSPM.

6.2 Comparison of BSPM and ECG

The traditional 12-lead ECG consists of six electrodes placed on the chest, with corresponding leads called V1-V6, in addition to the reference limb electrodes. Of these six leads, V1, V3 and V5 are placed at approximately the same position as V^{20}, V^{13} and V^{6} respectively in a BSPM (see Figure 2.2 and Figure 2.4). The ECG of one of the two healthy patients has been recorded, and will be compared to the processed resting BSPM of the same patient. The ECG and BSPM of the three channels placed at approximately the same position on the thorax can be seen in Figure 6.1. In this patient, the BSPM electrode V^{20} was placed approximately $3cm$ away from the location of electrode V1 of the ECG. The other two pair of electrodes were closer to each other, but still with deviation in location. Generally, these three pairs of electrodes from ECG and BSPM are the ones placed closest to each other. In addition to the electrodes being placed at slightly different spatial locations, the difference in the recording

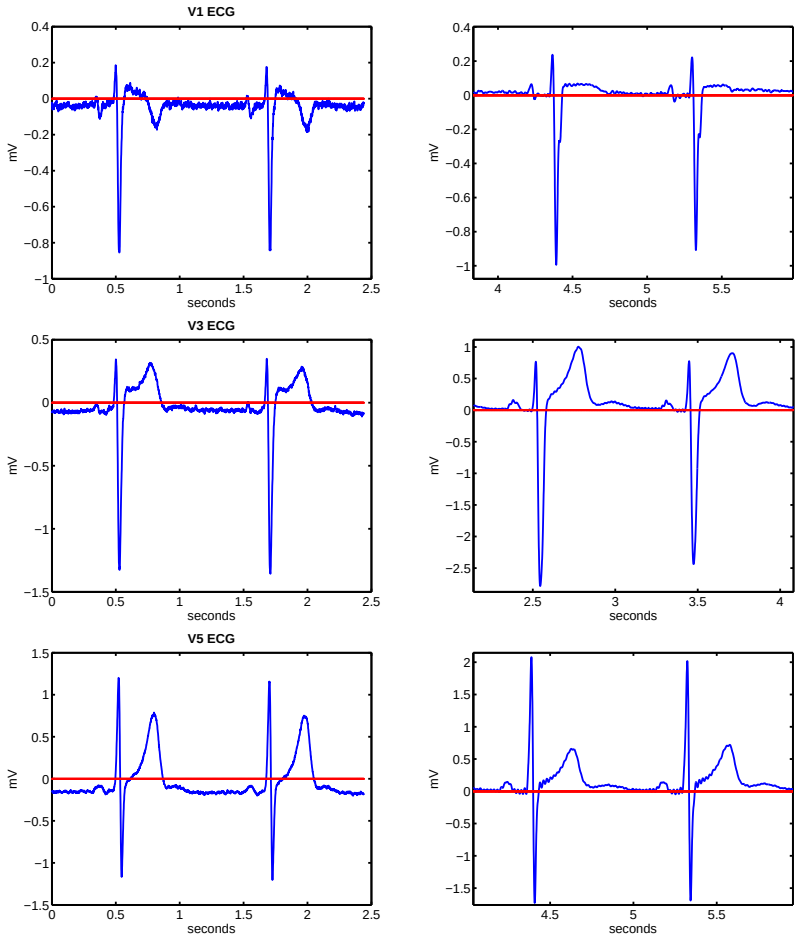

Figure 6.1: The left column contains the ECG of channel V1, V3 and V5 of a healthy patient. Along the right column is the resting BSPM of channel V^{20}, V^{13} and V^{6} of the same patient. As each pair of ECG and BSPM recording are recorded by electrodes placed at approximately the same position on the chest and both recordings are rest recordings, each pair should show similar ECG/BSPM morphology. The ECGs are quite similar to their corresponding BSPMs. Notice the difference in amplitude in the two lower pairs. The amplitude of the BSPM channel V^{13} is almost twice that of ECG channel V3.

equipment and signal processing may also be a cause of differences in the ECG and BSPM recordings. In this example, the recordings were done with over a year in between. As expected, the ECG and BSPM recordings were quite similar. There are some changes in morphology that may have been caused by the above mentioned or other reasons. One interesting difference is the amplitude differences, especially between V3 of the ECG and V^{13} of the BSPM.

For this patient, the difference between the ST and PR segments was computed in the above mentioned electrode locations using (3.2) and (3.3). The

ECG		BSPM	
V1	0.08mV	V^{20}	0.06mV
V3	0.15mV	V^{13}	0.3mV
V5	0.13mV	V^{6}	0.18 mV

Table 6.1: The ST segment shifts in the ECG and BSPM of a healthy patient during rest in three corresponding locations at the chest.

results can be seen in Table 6.1. Comparing the amplitude of the channels (Figure 6.1) and the magnitude of the ST segment shifts in the table, it seems that the larger amplitude in the BSPM channels results in a higher magnitude in the ST segment elevations in this recording. The amplitude of the exercise BSPM is similar to that of the resting BSPM for this patient, indicating that no falsely high ST shift difference between rest and exercise should be introduced by this. The most important sources for the deviation between the ECG and BSPM recording is the difference in recording equipment and spatial placement of the electrodes, as there are only small differences in morphology other than the amplitude of the signal. The recording in these leads in the BSPM and ECG should be similar, as they are recordings of essentially the same kind done at about the same locations. On this one patient, these expected similarities were present with some deviations. There will always be deviations between different recordings like these, due to the above discussed or other reasons. Despite the differences, channel V^{20}, V^{13} and V^{6} will be considered equivalent to the ECG channels V1, V3 and V5 for the remainder of this thesis.

6.3 Visualisation of results

An informative way of visualising the differences in ST segment depression/ elevation of a patient between rest and exercise computed as shown in equations (3.2), (3.3) and (3.4) on page 25 will be introduced in this section. The output of the automatic BSPM processing algorithms described in Section 6.1 is 64 numbers d^i, $i = 1, \ldots, 64$, each describing the difference in ST segment shift in a point on the body surface. These numbers are assigned colours according to their value, and plotted at their correct location at the body surface. An example of this visualisation is shown in Figure 6.2.

Although the visualisation of the ST segment differences in Figure 6.2 shows the differences d^i at their location on the upper body, other visualisations may be better for seeing the BSPM results as a whole. In Figure 6.3 the same vector d as in Figure 6.2 has been used. The values in d has been connected using linear interpolation to better see the floating differences between the numbers

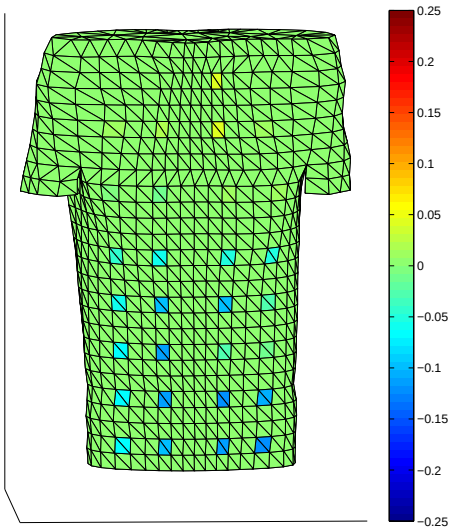

Figure 6.2: The ST segment shift difference between the rest and exercise recording has been computed for each of the 64 channels in a BSPM. Each of these values are assigned a colour according to their value. These values are plotted at the location of the electrodes at the body surface.

d^i of each electrode. These smooth coloured mappings of the ST segment shift differences in a patient will from this point on be termed "Body Surface ST segment Mapping" (BSSTM). This BSSTM has been laid upon a picture of a patient wearing the recording equipment for the purpose of illustration. Figure 6.4 is the same BSSTM, without the illustrating picture of the upper body. This way of visualising the ST segment shift differences can be valuable both as a tool for evaluating BSPM signal processing algorithms, and as a diagnostic tool.

The BSSTM of a patient will show the changes in ST segment elevation/ depression between rest and exercise at both the front and back of a patient. With knowledge of which degrees of difference at which points is characteristic for a patient with ischemia, this mapping can be viewed to easily get an idea of whether the patient suffers from ischemia or not. Since the body has the property of a volume conductor, signals should propagate smoothly through the body. Thus, signals recorded at the body surface should not differ much from other points recorded in close proximity. If too abrupt changes are present in the BSSTM of the body surface (such as in Figure 6.8), there is probably much noise present in some of the channels since the signals from the heart itself will not produce such a BSSTM. This is useful in evaluating the performance of the complete BSPM processing algorithm. A good algorithm will be able to sort out changes that are too abrupt and produce a smoother BSSTM.

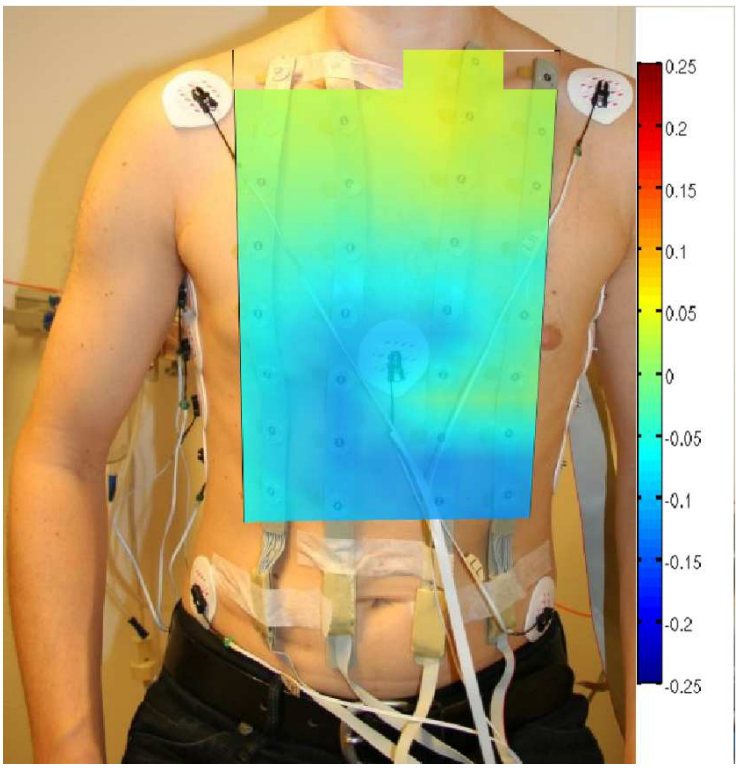

Figure 6.3: The Body Surface ST segment Mapping shown in Figure 6.4 laid upon a picture of a patient wearing the BSPM recording equipment. Note which parts of the colourmap corresponds to which channels of the BSPM.

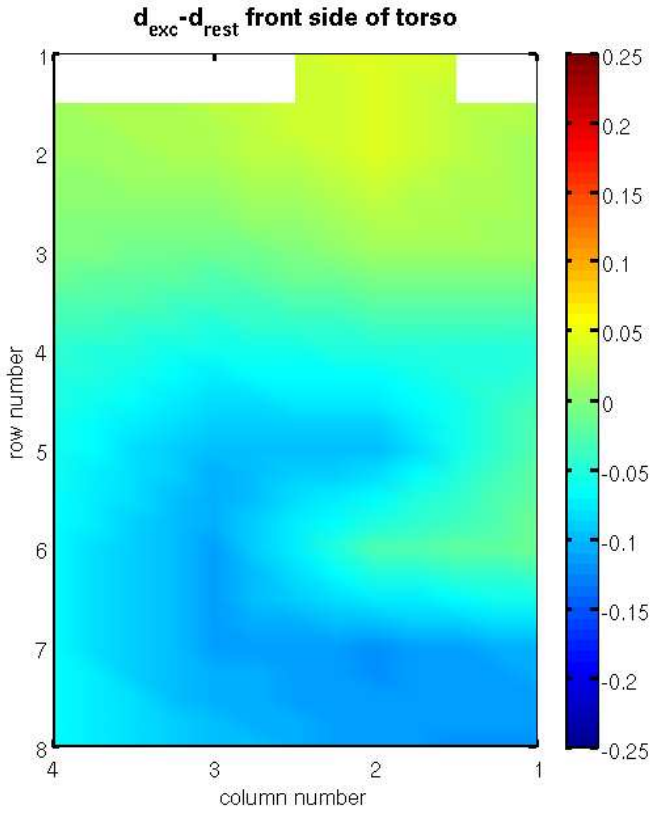

Figure 6.4: An example Body Surface ST segment Mapping. This is the same mapping as shown in Figure 6.3 and consists of the 32 first values of d^i. These values has been interpolated to create a smooth mapping of the ST segment shift differences in the BSPM.

6.4 Results on real data

The automatic algorithm outlined in Section 6.1 has been implemented on several real BSPM recordings. These results are presented in this section. As there is only a limited number of BSPM recordings available for testing, the algorithm's performance on these data sets can not serve as a statistical "proof" that it will work well on all BSPMs. But the performance on these actual recordings will be an indication to it's accuracy on future BSPM recordings. For each patient, a 60[1] seconds of consecutive recording has been used as the rest recording, and 60 seconds as the exercise recording. In Appendix A, the BSSTMs of all the BSPMs processed by the automatic algorithm are shown. These are the plots of the vector d computed by (3.2),(3.3) and (3.4) for each patient. An example of a healthy patient and a patient with ischemia will be viewed in the next two sections for illustration.

6.4.1 Algorithm tested on a healthy patient

This is a discussion of the algorithm's performance on one of the healthy patients. Since this patient is not suffering from any heart conditions, it is expected that the vector d computed in (3.4) in the last step of the automatic algorithm should have values close to zero. The elements of d should not differ much from each other. In Figure 6.5 the vector d has been computed using the raw data of the patient as the input $BSPM_{improved}$ to the last step of the automatic algorithm (See Section 6.1.5). The BSSTM is quite smooth, but with maximum ST shift $-0.129mV$ in channel 2. By visually inspecting the BSPM plots of each channel of this recording, it has been confirmed that the recording consists mainly of nice BSPM signals with little noise and artefacts present. Hence, the automatic BSPM processing algorithm should not make many alterations to these data. The BSSTM of the same patient after the automatic algorithm has been applied is shown in Figure 6.6. In this figure, the data has been processed by the algorithm described in Section 6.1 and the new vector d is displayed in the BSSTM. It is clear that there is little difference between Figure 6.6 and Figure 6.5. Only the channels which differed much from the rest of the BSSTM in the raw data has been altered more than a few μV in the processed version. Thus the algorithm performed very well on this BSPM. It removed some deviating channels, while the rest of the channels remained nice. After processing, the maximum ST shift is of $-0.09mV$ in channel 13. The shift of $-0.129mV$ in channel 2 that was present in the raw data has been reduced to a mere $-0.035mV$ shift in the processed version.

6.4.2 Algorithm tested on a patient with ischemia

The algorithm has also been tested on several patients with confirmed ischemia, with results displayed in Appendix A. In this section, one of these will be studied closer as an example of the automatic algorithm's processing of an ischemic patient. First, the vector d containing the differences in ST segment shift between rest and exercise is computed from the raw data in the same way as was done in Section 6.4.1. This d has been visualised in a BSSTM shown in Figure

[1] Except patient4, which had only 30 seconds of rest recording available.

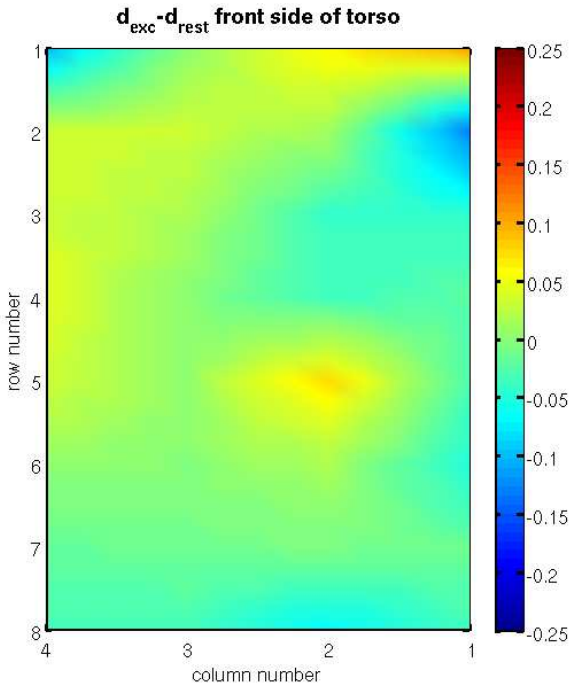

Figure 6.5: The BSSTM of the front of a healthy patient. The raw data recordings has been used when making this BSSTM. It is quite smooth even before any processing has been done. Only the 32 front channels are included in this BSSTM.

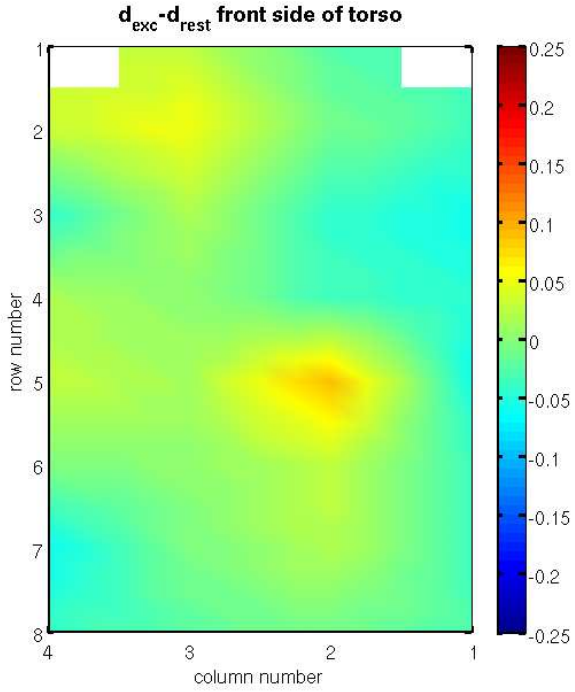

Figure 6.6: The front BSSTM of processed data of the same patient as in Figure 6.5. The BSPM and BSSTM of this patient where quite nice before any processing algorithms were applied, and hence few changes has been made. Notice that some of the channels was deemed too bad to be included in the final BSSTM.

6.8. Several abrupt changes and irregularities can be seen in the figure, especially in the left part. Figure 6.7 shows the vector d from the raw data of the patient computed from one randomly selected heartbeat instead of the mean heartbeat of each channel. The abrupt changes in ST segment shift differences

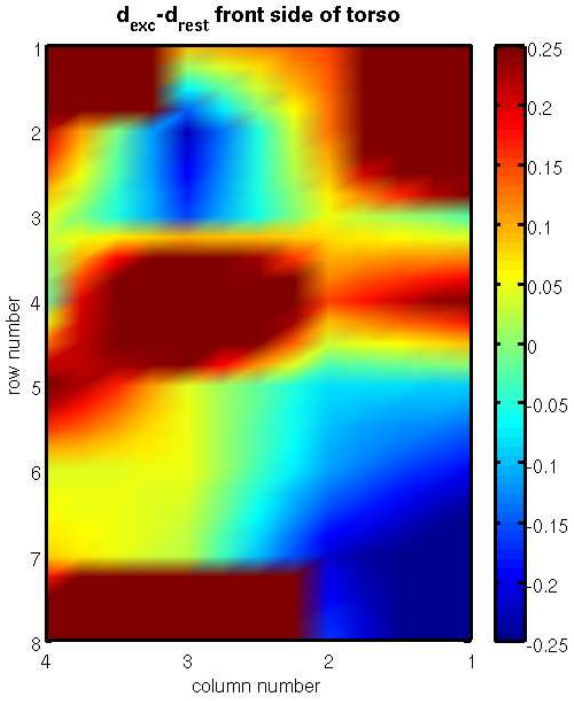

Figure 6.7: The BSSTM of a randomly selected heartbeat of the front of a patient suffering from ischemia. This is the BSSTM of the raw data recorded, and irregularities and abrupt changes in the BSSTM are visible.

in neighbouring channels seen in these two figures is not physically possible. Hence there is much noise and artefacts present in several of the channels in this BSPM.

The automatic BSPM processing algorithm has been applied to this BSPM, and the output of the algorithm can be seen in Figure 6.9. Several changes from the BSSTM of the raw data (Figure 6.8 and especially the BSSTM of one heartbeat shown in Figure 6.7) can be seen. The algorithm deemed several channels too distorted to be included in the data set. All the deviating channels has been either removed or corrected so that they fit in with the rest of the BSPM. This leaves a smoother BSSTM, which fits better with the physical model of electrical signals propagating from the heart through the body. There is still a region in the lower right area of the processed BSSTM with large (greater than $0.2mV$) differences in ST segment shifts between the rest and exercise recording. It is mainly in this area that the ischemia is visible in this BSPM. Thus the algorithm managed to sort out much of the corrupted parts of the signal, while at the same time keeping the information that makes it possible to diagnose the patient.

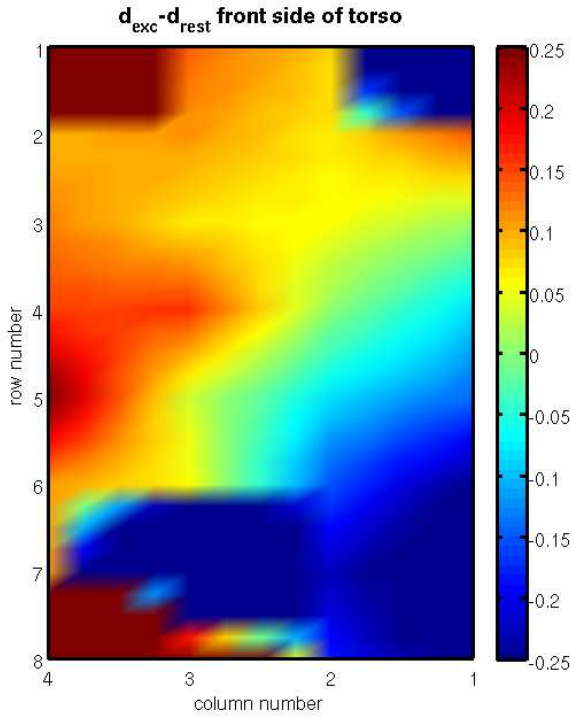

Figure 6.8: The BSSTM of the front of a patient suffering from ischemia. This is the BSSTM of the raw data recorded. The mean ST and PR segments of each channel has been used in computing the differences in ST shift between exercise and rest, resulting in a smoother surface than the one in Figure 6.7. Although some of the random effects have been removed by using the mean channels of the raw data instead of a randomly selected heartbeat, abrupt changes and unnaturally high ST shift values are clearly visible. The upper corners of the BSSTM and an area to the lower left shows signs of being contaminated by high noise or baseline drift levels.

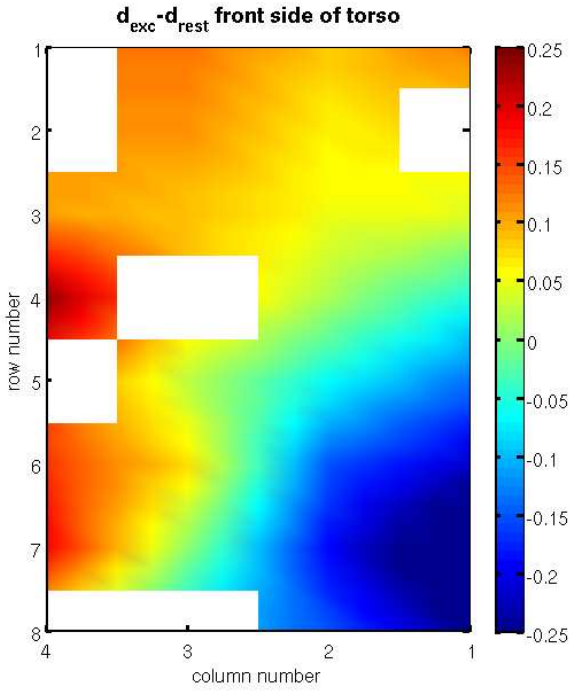

Figure 6.9: This is the BSSTM of the processed data of the same patient as in Figure 6.8. Note how the areas that were "unphysical" in Figure 6.8 and Figure 6.7 have been either corrected, or removed from the BSPM. Note also the great depression in the lower right part of the BSSTM, which is different from the rest of the BSSTM. This is characteristic for a patient suffering from ischemia.

6.4.3 Data produced by the automatic algorithm

It is a difficult task to evaluate the correctness of the complete BSPM processing algorithm developed in this thesis. There are no given answers to how the BSPM recordings should be after processing, as the only information available is the raw BSPM data and the knowledge of whether the patient has an ischemia or not. Each step of the algorithm has been evaluated earlier in Chapter 5, but here, light will be shed on the complete output. In Section 6.5 a discussion will be made of whether or not it is possible to separate the processed BSPM of a healthy patient from that of an ischemic patient. First, the processed BSPMs will be investigated for strengths and weaknesses in the processing algorithm.

In the two example patients discussed above (see figures 6.5 - 6.9), the BSPMs became smoother after processing. The same can be seen on all the processed BSSTMs presented in Appendix A. There are no channels deviating much from the rest, and most ST shift values in neighbouring areas are similar. This is coherent with the laws of physics that implies that the signal spreading from the heart through the body should not deviate much in locations close to each other. Thus the outputs of the automatic algorithm are BSPM datasets that are physically closer to what the electrical signals from the heart should look like on the body surface, than the raw data is.

All the processed BSPMs have a quite small standard deviation in all channels not removed by the algorithm (see Appendix A). Assuming that the measured ST shifts are Gaussian distributed around the measured mean, the majority of the measured values are close to this value. Also, a large amount of data are still present after processing, making the computed values for the ST segment shifts trustworthy.

6.5 Using output to separate healthy and ischemic patients

ST shifts in exercise ECG testing is a well known method of detecting ischemia. The criteria for a positive test of ischemia varies in the literature [25, 22, 19, 15, 31]. The most common criteria, the one in the American Heart Association guidelines, is depression or elevation of at least $0.1mV$ in one or more of the ECG leads. Other propose a maximum shift of $0.2mV$ or more, or require a shift in several consecutive channels of a BSPM.

Data from all the BSPMs processed by the automatic algorithm are presented in Table 6.2. In Section 6.2 it was established that channels V^{20}, V^{13} and V^{6} of the BSPM are located at approximately the same positions as V1, V3 and V5 of the 12-lead ECG. Applying the $\geq 0.1mV$ criteria to these three channels of each patient's BSPM, the following is found: Both healthy patients will be recognised as healthy (though just barely for one of them), while three of the four ischemic patients will be recognised as ischemic. The fourth ischemic patient is not recognised, but the ST shift difference value of channel V^{6} is missing since the channel was sorted out by the processing algorithm.

Looking at the maximum ST shift in each patient, the maximum shift of one of the healthy patient's BSPM shows some depression. Three of the four ischemic patients show a depression greater than $-0.2mV$, while the fourth also have a quite large depression of $-0.154mV$. With a criteria to the magnitude

Patient	ST shift difference between exercise and rest in mV				
	V^{20}	V^{13}	V^{6}	min ST shift	max ST shift
patient5	0.003	0.090	-0.033	-0.062 in V^{31}	0.090 in V^{13}
patient6	-0.061	-0.098	-0.013	-0.119 in V^{15}	0.043 in V^{9}
patient1	–	–	-0.254	-0.254 in V^{6}	0.067 in V^{57}
patient2	-0.012	-0.154	-0.138	-0.154 in V^{13}	0.108 in V^{17}
patient3	–	-0.063	-0.216	-0.328 in V^{7}	0.24 in V^{28}
patient4[a]	0.071	0.026	–	-0.216 in V^{16}	0.105 in V^{36}

[a]Due to a recording error, no resting BSPM was available for this patient. The BSPM recording done a couple of minutes after the exercise have been used as a substitute for the rest recording for this patient. This may have resulted in falsely low differences between the rest and exercise ST segment shifts, since it takes some time for the BSPM signal to normalise after a stress test.

Table 6.2: This table shows ST segment shift differences between exercise and rest recordings as computed by (3.4). All data are from the BSPMs processed by the automatic algorithm. Along each row is the ST shift differences in selected channels of a patient. The first three data columns show the shift in the three channels V^{20}, V^{13} and V^{6} which are located at approximately the same positions as the 12- lead ECG leads V1, V3 and V5 respectively, as mentioned in Section 6.2. The two last columns shows the greatest depression and elevation in each BSPM.

of the maximum ST shift $\geq 0.1mV$, all ischemic and one of the healthy patients will be identified as ischemic. With ST shift $\geq 0.15mV$ all the ischemic and healthy patients will be identified correctly, while a criteria of ST shift $\geq 0.2mV$ will identify three of the four ischemic patients correctly and the rest as healthy. Table 6.3 summarises the outcome of some of the criteria applied to the processed BSPMs. As seen in Table 6.3, it is possible to separate the healthy and

Patient	Outcome of test (Positive(P)/Negative(N))			
	ST shift$\geq$ $0.1mV$ in V^{20}, V^{13} or V^{6}	max ST shift $\geq$ $0.1mV$	max ST shift $\geq$ $0.2mV$	True values
patient5	N	N	N	N
patient6	N	P	N	N
patient1	P	P	P	P
patient2	P	P	N	P
patient3	P	P	P	P
patient4	N	P	P	P

Table 6.3: This table summarises the response of the processed BSPMs to three different criteria. A positive (P) response means that the BSPM fulfils the criterion, while a negative (N) means that it does not.

ischemic patients using different criteria to the computed ST segment shift differences. In addition to set criteria like these, the BSPM opens the possibility of looking for whole areas of the torso with ST segment depression/elevation.

6.5.1 The performance of the automatic algorithm

In the previous section, the ST shift values of all the processed BSPMs were discussed. These were correctly identified as either ischemic or healthy, with the exception of one healthy patient 'patient6' which showed ST depressions slightly larger than what would be expected from a healthy patient. The insecurity of this patient could either be due to weaknesses in the automatic algorithm, an occurrence of a healthy patient with correctly measured relatively large ST depression, or some other causes. Which of these reasons that contribute to the large ST depressions in this patient is investigated below:

The performance of each step of the automatic algorithm was evaluated in Chapter 5. If the ST shift differences of this patient were introduced by the automatic algorithm, it most likely must have been the drift removal step as the other steps only removes outlying or noisy parts of the signal. While this is a possibility, it is unlikely. Neither the parts of the patient's BSPM with smaller ST shift nor any of the other patients' BSPMs show signs of artefacts being introduced by the drift removal method.

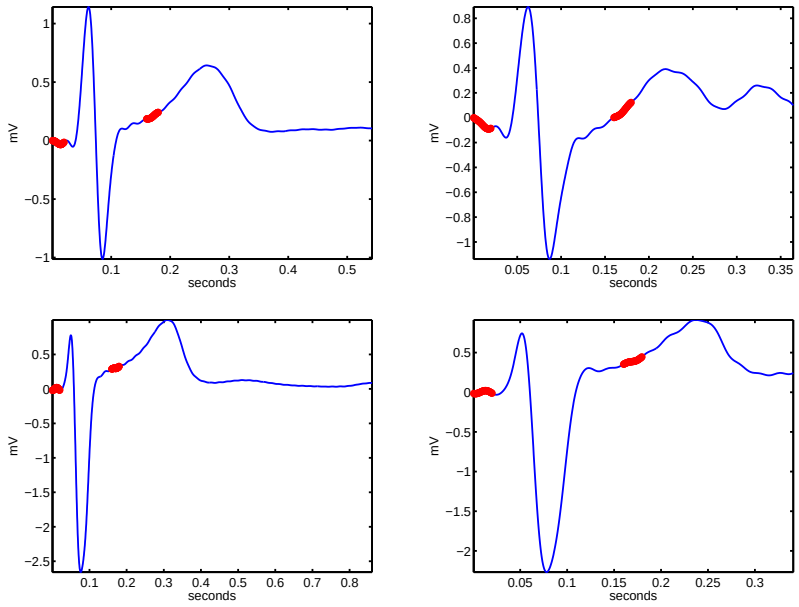

Figure 6.10: The BSPM morphology of selected channels of the two healthy patients. Comparison of BSPM morphology between rest and exercise in the channels with the greatest ST shift between rest and exercise. The left column displays plots of the resting BSPMs, while the right column displays the exercise BSPMs. The upper pair is the mean channels of patient6, while the lower pair is the mean channels of patient5.

Another possibility is that these ST segment shift differences between rest and exercise naturally occurs in this patient's BSPM. The AHA summarised from 58 studies of exercise ECG testing that the mean sensitivity of these tests was 67%, and the specificity 72% [15] (sensitivity being the percentage of patients with a disease having an abnormal test, and specificity the percentage of

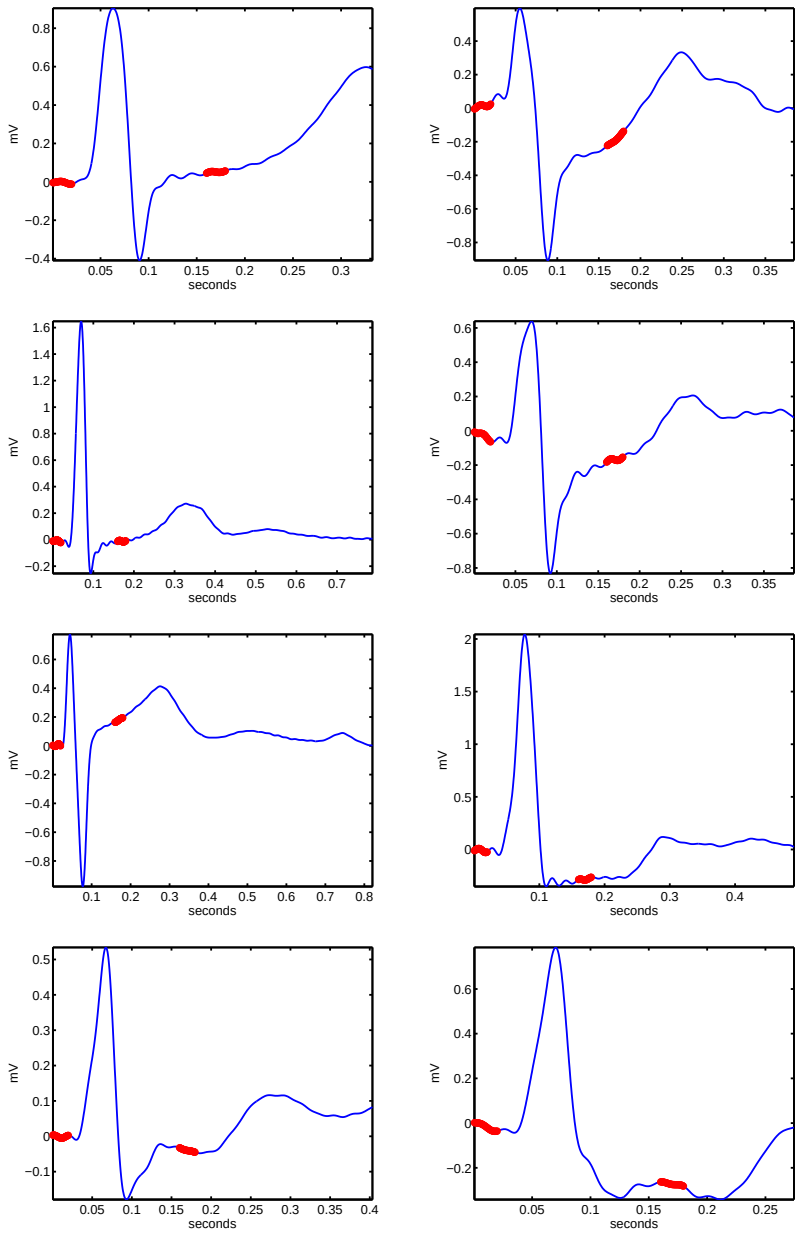

Figure 6.11: The BSPM morphology of selected channels of the four ischemic patients. Comparison of BSPM morphology between rest and exercise in the channels with the greatest ST shift between rest and exercise. The left column displays plots of the resting BSPMs, while the right column displays the exercise BSPMs. The plotted pairs are, from top to bottom, of patient1, patient2, patient3 and patient4.

healthy patients having a normal test). It is thus quite common that healthy patients show ST shift larger than $0.1mV$ in exercise tests. In Figure 6.10 and Figure 6.11, the rest and exercise BSPM channel with the largest ST shift difference of the healthy and ischemic patients are displayed. Now, the morphology of the signal with the highest ST segment shift for patient6 and the ischemic patients can be compared. It can be seen that the ST segment difference of $\approx 0.1mV$ between rest and exercise in patient6 is due to an elevation during rest that has been reduced during exercise. The BSPM of e.g. patient3 has a distinct morphology characteristic of ischemia during exercise, while the BSPM of patient6 has similar morphology during both rest and exercise. Inspection of the data shows that patient6 most likely is processed correctly. Large ST segment shifts is recorded in healthy patients from time to time, and this is one such occurrence.

Inspecting Figure 6.10 and Figure 6.11 further, it can be seen that the BSPMs of the healthy patients does not show much change in morphology between rest and exercise. The BSPMs of the ischemic patients on the other hand, all show a clear change in morphology between rest and exercise. Both the ST segments and the QRS complexes in the displayed channels of the BSPMs changed between rest and exercise.

6.6 Summary of results

At the start of this chapter, the automatic algorithm for processing BSPM data was formed using the methods developed in Chapter 4 and evaluated in Chapter 5. A tool, named the BSSTM, for visualising the ST segment shift differences between rest and exercise was introduced. All the processed BSPMs are presented in Appendix A, and two example BSPMs were discussed more thoroughly. Finally, the data was investigated, to see if the BSPMs of ischemic patients could be distinguished from those of healthy patients.

Before processing, it was not possible to know which channels of a BSPM could be trusted, and which was noisy or filled with artifacts. There was a high standard deviation in many measured ST shifts. Some channels contained very high ST shifts, and there were great differences between some neighbouring channels of several BSPMs. This makes the information obtained from the raw data faulty and insecure, and it is also difficult to distinguish a BSPM of a healthy patient from that of an ischemic patient.

After processing by the automatic algorithm presented in this chapter, all BSPMs have become smoother and more physically realistic. Channels deviating too much from their neighbours have been removed or corrected. The standard deviations in the ST shift measurements have been decreased to an acceptable level, though it is still quite high for most of the BSPM channels. Looking at the BSSTMs of the processed data, clear spatial trends can be seen as depressions or elevations in neighbouring channels. This in addition to the relatively low standard deviations is a good indication that the ST shift values can be trusted. The large number of data points in each BSPM confirms this further.

After processing, the BSPMs can be distinguished as healthy or ischemic by looking at the ST shift differences. Both magnitude and spatial distribution of the ST shifts provide information that can be used to get an indication of ischemia in the patient. The six BSPMs processed in this thesis separated

correctly into two groups of healthy and ischemic. The distinction was not very clear though, with some degree of ST shift also in the healthy subjects. As discussed in this chapter, this can be attributed to the ST shift measurement not being a precise measure of ischemia. There are good indications toward that the ST segment shifts measured in each processed BSPM are close to the actual signals sent from the heart. The ST shifts measured after processing are definitively better than those measured from the raw data. It is not possible to exclude that the algorithm introduces artifacts or fails to remove noisy or false signals. The results from the six tested BSPMs indicate that such weaknesses in the algorithm are small if present at all. With a larger dataset available for testing, more secure results on the performance of the algorithm can be obtained. The ability of the computed ST segment shifts to separate ischemic and healthy patients could also be tested more extensively.

6.6.1 Advantages and disadvantages in BSPM over ECG

Although the ECG is the traditional instrument for exercise testing of patients to detect ischemia, there are several advantages in the BSPM over the 12-lead ECG confirmed by the results found in this thesis: The increased spatial sampling lessens sensitivity to noise and drift, as each channel can be compared to spatially neighbouring channels. This has been used to sort out deviating heartbeats from BSPM datasets. Also, the sensitivity of an ECG recording suffers even with only a couple of channels removed due to noise. Two channels removed from a BSPM will not significantly change it's diagnostic power as the missing channels can be replaced by neighbouring values. In four of the six BSPMs, the greatest ST shifts were at other locations than the location of 12-lead electrodes. Thus the BSPM can detect changes of greater magnitude than the ECG and possibly improve the diagnostication of ischemia. When viewing results from a BSPM recording, one can look for areas of ST shifts rather than a few single leads as is done with ECG recordings. This makes the BSPM a much more robust device, and it greatly improves the possibility of looking for consecutive points with ST shift as a sign of ischemia.

There are some potential disadvantages in using BSPM instead of ECG. First, the BSPM equipment consists of a great number of electrodes which makes it more time consuming to put on and take off compared to the practical 12-lead ECG. Second, the traditional ECG provides sufficient information in many applications, for instance monitoring the heartbeat rate. Thus the use of a BSPM over an ECG is not preferable in many applications. Third, the BSPM is relatively new compared to the ECG. While the ECG is a well known and much used tool for most medical personnel around the world, the BSPM is not. Finally, ECG recording equipment is cheaper than BSPM equipment, and is already available in most hospitals and medical institutions.

6.6.2 The reliability of ST shift as measure of ischemia

In the above sections, the results obtained by applying the automatic post processing algorithm to real BSPMs have been discussed. The results indicate that the algorithm does not introduce significant errors in these BSPMs. Assuming that the algorithm processes the data correctly, the presence of ST shift differences $\geq 0.1mV$ in a healthy patient means that ST shift differences is

not an accurate measure of ischemia. This has been discussed elsewhere in the literature [15, 22, 19].

There is additional information other than the ST segment shifts in the processed BSPM that can improve the detection of ischemia. As seen in Figure 6.10 and Figure 6.11, there was no significant change in morphology between rest and exercise in the healthy patients' BSPM, while in ischemic patients' BSPM there will most likely be change in the channels with the most ST shift. Looking at the BSPM morphology of the channel with the largest ST shift difference will help separating ischemic from healthy patient in the six BSPMs used in this thesis, and it will probably improve the distinction also in future BSPM recordings. The slope of the ST segments can also improve the diagnostication of ischemia from a processed BSPM [15]. In most cases of ischemia the BSPM will show an alteration in the slope of the ST segment, while a healthy patient's ST slope should show no significant changes. Information beyond what is in a BSPM recording will also improve the diagnostication. [13] states that probability before the test, the subject's age, time since last meal, known diseases, symptoms and use of medication should be taken into account when drawing conclusions based on an ECG stress test.

The BSPMs of different patients are recordings of signals that have travelled through different bodies before reaching the recording electrodes. This results in differences in the BSPMs due to differences in the bodies of the patients in addition to the heart signals being different. One result of this is differences in signal amplitude between patients, as the signal amplitude depends on the distance between the heart and the electrode [35]. Viewing the ST shift differences relative to the amplitude of the signal (measured at the QRS complex, T wave or otherwise) can to some degree cancel this effect, possibly increasing the differences between the ST shift measurements of healthy and ischemic patients. This may also introduce errors in form of falsely high or low ST shift values. A much bigger dataset than the six BSPMs available at this point is needed to test if this can improve the detection of ischemia.

While some improvements to the methods of using BSPM data and ST shifts to detect ischemia were suggested above, these need to be tested on bigger data sets to be confirmed. The processing algorithm developed in this thesis will provide equally good output for the ischemia detection methods discussed above, as it does for the computation of ST segment shifts used here. Processed BSPM data and ST segment shifts are also useful as input to cardiac computation methods, such as inverse problems [28], which does not utilise the additional information provided for example by the slope or morphology of a BSPM. Thus, post processing and ST segment shift computation has been the focus of this thesis.

Chapter 7

Conclusions and further work

7.1 Summary of the thesis

The body surface potential mapping has been proposed as a better tool than traditional 12-lead ECG in detecting ischemia using ST segment exercise testing. As the raw data of a BSPM recording contains noise and artefacts, a post processing algorithm was developed in this thesis to provide more accurate and secure ST segment shift measurements. A quick review of the designed and tested methods is given:

First the noise, baseline drift and artefacts present in a BSPM recording were classified. A simple model of the content of a BSPM recording was proposed:

$$BSPM = BSPM_{signal} + BSPM_{noise} + BSPM_{drift}.$$

Noise and drift reduction methods were developed and tested to improve the quality of the recording, by using the knowledge of the noise and drift content in a BSPM signal. A QRS detection algorithm was developed, and used to split the signal into individual heartbeats and finding important segments of the BSPM. For the final step of improving a BSPM recording, heartbeats still dominated by noise or artifacts are removed. For doing this, several methods were designed and tested, and put together in a recursive algorithm. Finally a visualisation tool for viewing the ST segment shifts over the upper body was presented. From the processing methods tested throughout the thesis, a complete BSPM post processing algorithm was formed. The algorithm is designed to be automatic, by taking the raw data of an exercise and rest BSPM as input. As output, both the processed BSPM and it's corresponding ST segment shift differences are provided.

7.1.1 The automatic BSPM processing algorithm

An outline of the automatic BSPM processing algorithm developed in this thesis is given, step by step:

- As the first step of the BSPM processing algorithm, a lowpass filter is applied to remove high frequency content of the recording. It was concluded that a lowpass filter with cutoff frequency of $49Hz$ is best suited for this.

- Next, the QRS complex peaks are detected, and used both for splitting the signals into heartbeats and locating the PR and ST segments of each recording.
- To remove the baseline drift, an approximation to the drift using cubic spline interpolation is made and subtracted from the recording. The cubic spline interpolation method was chosen to be the best of the four drift removal methods tested.
- Heartbeats too deviating in a temporal or spatial sense are sorted out from the data set, leaving a more consistent BSPM free of severe artifacts.
- After the processing part is complete, the ST segment shift differences between the rest and exercise recording are computed.
- These shifts are visualised as body surface ST segment maps, and both the processed BSPM and ST segment shifts are given as output of the algorithm.

7.1.2 Discussion of the algorithm

Each step of the automatic algorithm has been evaluated and discussed. A summary of these discussions is given:

Noise reduction: The noise reduction part will work on all kinds of BSPMs and for all purposes. It introduces no artifacts or distortions to the kept frequency band of the signal. With the current cut off frequency though, parts of the QRS complex will be removed. The cut off frequency should be increased if the method is applied in a setting where the QRS complex morphology is important.

QRS complex detection: A good algorithm for the task of processing BSPMs for ischemia diagnostication. It proved to be a robust method detecting the QRS peaks in BSPMs with various noise and heartbeat rates. It detected 1287 out of 1289 QRS complex peaks with no false positives in the testing set. More testing on a larger dataset is required to get statistical significant proof that the algorithm works well. Adaptive thresholding or derivative based detection could be added to the method, but are unlikely to improve the performance significantly.

Baseline drift removal: The drift removal algorithm performed well on the tested data, and was deemed a robust method for drift removal. It is though dependent on good selection of knot values, and shows a slight reduction in performance when applied to noisy data. All drift reduction algorithms may introduce artefacts and distortions to the signal, but this algorithm was deemed best out of the four tested with respect to this. This step also requires more testing on a larger dataset to confirm it's good performance.

Sorting out corrupted heartbeats: With the chosen parameters the outliers and corrupted parts of the testing BSPMs were removed, while keeping a sufficient amount of information. With a larger data set, training

and testing sets can be used to obtain the optimal parameters fitting various demands on the outcome. The spatial sorting can be more refined, as can the temporal, e.g. with least squares surface fitting prediction to sort out spatial outliers.

Computing ST segment shift differences: A more refined way of choosing PR and ST segments could be made. In this thesis, the segments used were defined as a fixed distance from the QRS peak. With a good QRS detection algorithm, this provides a robust method prone not to compute false ST and PR segment values.

7.2 Results of the algorithm applied to six test BSPMs

Six BSPM recordings of real patients were available for testing. Of these, four were known to suffer from ischemia, while two were healthy. Using the computed ST shift differences from the automatic algorithm, it was possible to classify each patient as either healthy or ischemic. While it was possible to classify the patients using only the electrode locations of the 12-lead ECG, the increased number of sampling points of the BSPM provide more information. Four of the six patients had maximum ST shift values in locations outside the traditional ECG lead locations. The limited number of leads makes the standard ECG vulnerable to noise and corrupted channels. When looking for signs of ischemia using ST shifts, both the magnitude and locations of these shifts provided by the BSPM should be utilised for maximum effect. In the four BSPMs of ischemic patients it was possible to see clear signs of the presence of ischemia, while the BSPMs of the two healthy patients showed indications that they belonged to healthy patients. This is a sign of strength in the processing algorithm. Regardless of noise level in the raw data, all the processed BSPMs were both smooth and rich enough on data to make decisions based on them.

The distinction was not very clear however, especially with one healthy patient showing ST segment depressions close in magnitude to those of the ischemic patients. No signs were found in the processed BSPM that these shifts were due to weaknesses in the processing algorithm, but rather a not so uncommon occurrence of a healthy patient with ST shifts in exercise testing. This patient's BSPM had no change of morphology between rest and exercise that is characteristic for an ischemic patient. This indicates that ST shift differences alone is not the ideal measure of ischemia, which has been supported in the literature [13, 22, 15]. It should rather be combined with other information such as the ST slope, T wave amplitude, shift relative to signal amplitudes, information about the patient's health and age etc. On the other hand, a simple matrix of numbers, such as the ST shifts, is required in many applications or cardiac computation methods, such as solving inverse problems. A method for automatically computing these from raw BSPM data is therefore necessary.

7.3 Conclusions

Shifts in the ST segment of an exercise ECG test is a sign of ischemia. The BSPM is a better suited tool for these tests, as the increased spatial sampling provides richer information than the traditional 12-lead ECG. In this thesis, a complete automatic algorithm for post processing BSPM recordings was developed. The algorithm was applied to the BSPM recordings of two healthy and four ischemic patients. The algorithm made the BSPMs more consistent, greatly reduced the deviations in the measured ST shift values and returned a more physically realistic BSPM for all the six data sets. After processing it was possible to separate the BSPMs into recordings of healthy patients and recordings of ischemic patients solely based on the ST shift values computed by the automatic processing algorithm. However, there was no clear distinction between the ischemic and healthy patients. It was judged that this is a diagnostic weakness of measuring ST segment shifts, rather than false values being introduced in the processing. While this shows that the developed algorithm performed well on this limited set of six patients, further testing with bigger data sets is required to confirm the results of this thesis.

It was found that the magnitude of ST segment shifts between rest and exercise recordings alone is not the ideal way of diagnosing ischemia based on a BSPM exercise recording. Other morphological signs in a BSPM recording that can improve the detection of ischemia were described. The computation of reliable ST segment shift differences is important in other applications as well. Solving inverse problems for locating ischemic regions in the heart [28] for instance, utilise the magnitude of ST segment shifts alone when identifying ischemic heart disease.

7.4 Further work

The algorithm developed in this thesis showed promising results on the six BSPM recordings available. Further testing on a larger dataset is required to get statistical significant results on the performance of the algorithm. A larger set of BSPMs also opens for other interesting research, some ideas will be presented here: Other methods of improving the detection of ischemia, as discussed in Section 6.6.2, could be evaluated. With a bank of BSPMs from a diversity of patients available, a BSPM could be compared to the BSPMs in this bank for instance by using adaptive filtering techniques to see which BSPM in the bank it is closest to. The patient could then be diagnosed the same.

To better the use of spatial information to sort out deviating and corrupt channels, least mean square surface fitting on the ST segment values can be used to predict the ST value a channel should have according to the surrounding channels. The same techniques can be used to replace ST segment values for channels that have been removed from the data set.

The algorithms developed in this thesis have not been optimised with respect to computational demands. At this point, the CPU time needed by the automatic algorithm is of no importance, but it may be in some later applications. Another interesting project would be to redesign the whole or parts of the algorithm for real time implementation. In doing this the accuracy of some of the methods may need to be toned down, but a functioning adaption made

for real time implementation should be possible.

Appendix A

Appendix: Figures from completely processed BSPMs

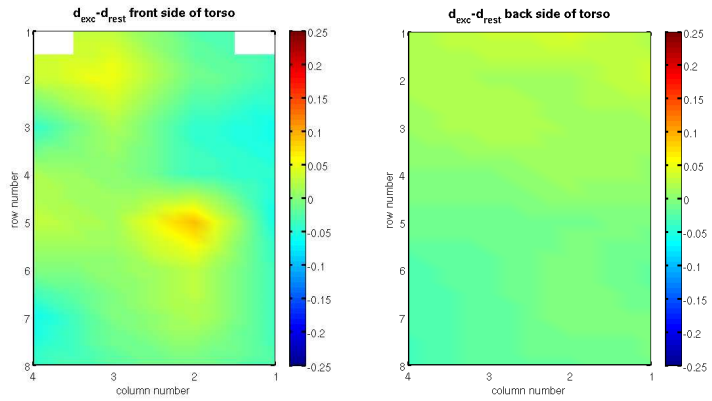

Figure A.1: The BSSM of patient5 after the BSPM has been processed. The left figure shows the front of the patient, the right figure shows the back of the patient.

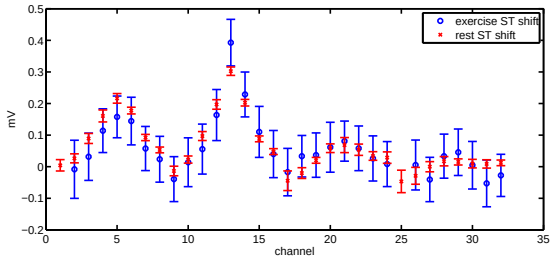

Figure A.2: The ST shifts in the processed rest and exercise recordings of patient5 plotted on top of each other. The standard deviation in the ST shift measurement is included. This is the 32 channels on the front of the patient.

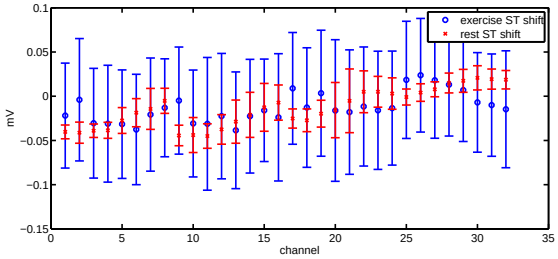

Figure A.3: The ST shifts in the processed rest and exercise recordings of patient5 plotted on top of each other. The standard deviation in the ST shift measurement is included. This is the 32 channels on the back of the patient.

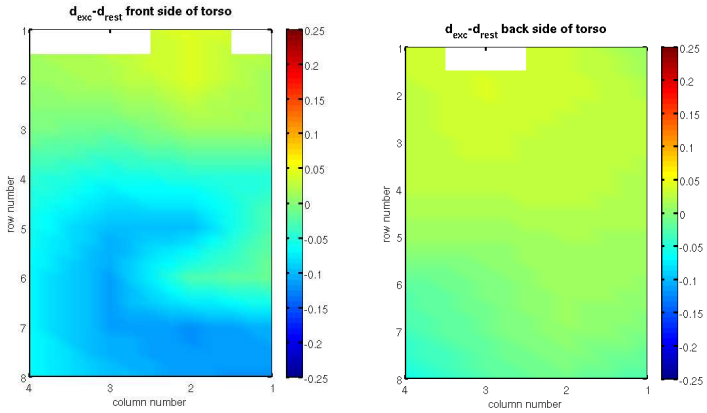

Figure A.4: The BSSM of patient6 after the BSPM has been processed. The left figure shows the front of the patient, the right figure shows the back of the patient.

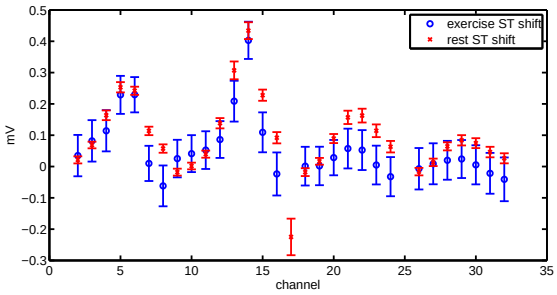

Figure A.5: The ST shifts in the processed rest and exercise recordings of patient6 plotted on top of each other. The standard deviation in the ST shift measurement is included. This is the 32 channels on the front of the patient.

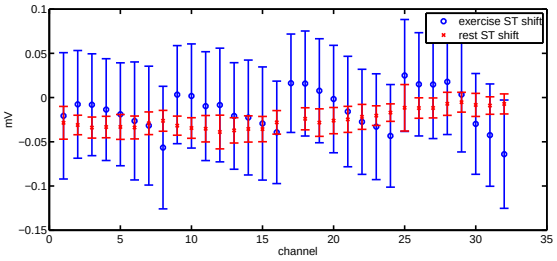

Figure A.6: The ST shifts in the processed rest and exercise recordings of patient6 plotted on top of each other. The standard deviation in the ST shift measurement is included. This is the 32 channels on the back of the patient.

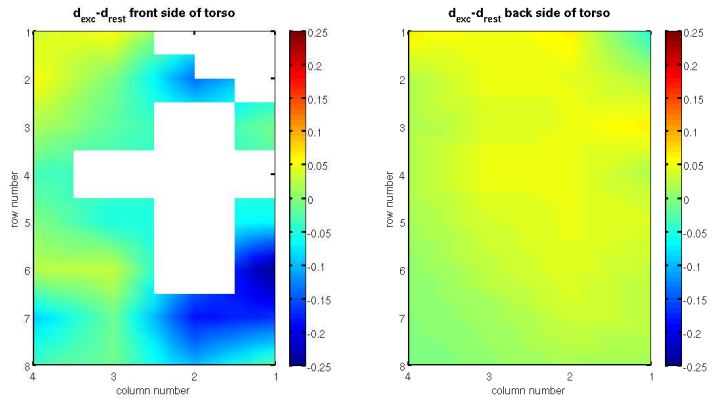

Figure A.7: The BSSM of patient1 after the BSPM has been processed. The left figure shows the front of the patient, the right figure shows the back of the patient.

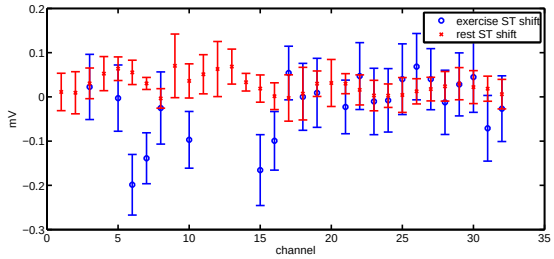

Figure A.8: The ST shifts in the processed rest and exercise recordings of patient1 plotted on top of each other. The standard deviation in the ST shift measurement is included. This is the 32 channels on the front of the patient.

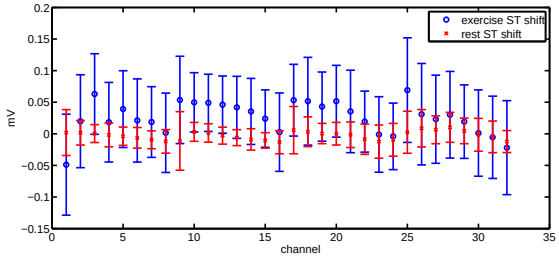

Figure A.9: The ST shifts in the processed rest and exercise recordings of patient1 plotted on top of each other. The standard deviation in the ST shift measurement is included. This is the 32 channels on the back of the patient.

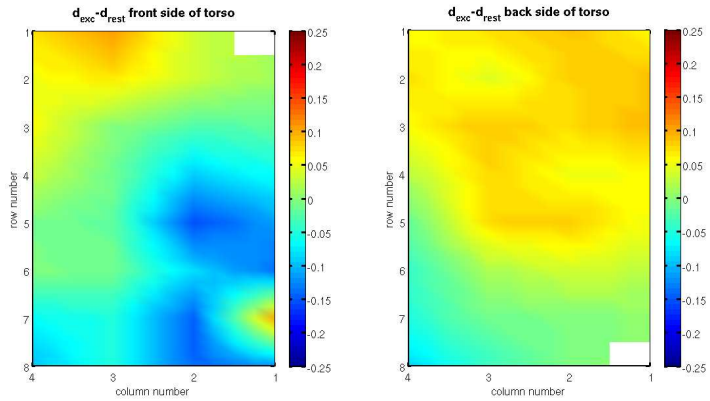

Figure A.10: The BSSM of patient2 after the BSPM has been processed. The left figure shows the front of the patient, the right figure shows the back of the patient.

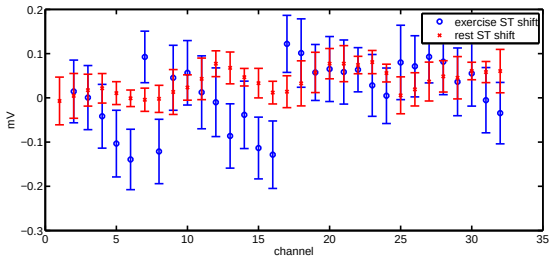

Figure A.11: The ST shifts in the processed rest and exercise recordings of patient2 plotted on top of each other. The standard deviation in the ST shift measurement is included. This is the 32 channels on the front of the patient.

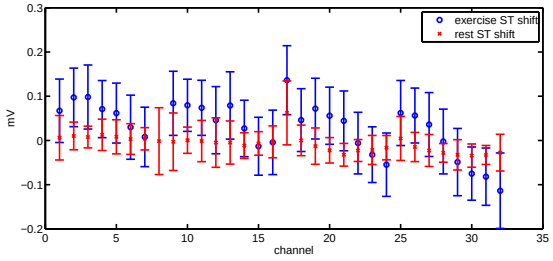

Figure A.12: The ST shifts in the processed rest and exercise recordings of patient2 plotted on top of each other. The standard deviation in the ST shift measurement is included. This is the 32 channels on the back of the patient.

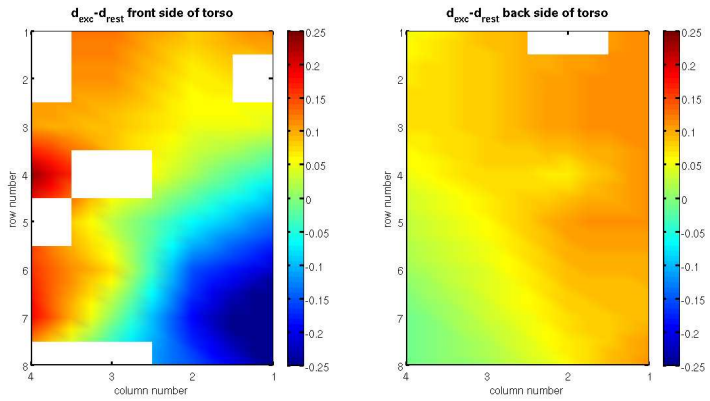

Figure A.13: The BSSM of patient3 after the BSPM has been processed. The left figure shows the front of the patient, the right figure shows the back of the patient.

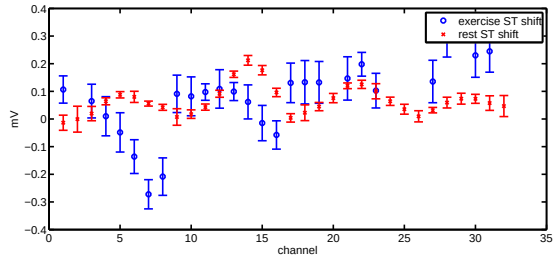

Figure A.14: The ST shifts in the processed rest and exercise recordings of patient3 plotted on top of each other. The standard deviation in the ST shift measurement is included. This is the 32 channels on the front of the patient.

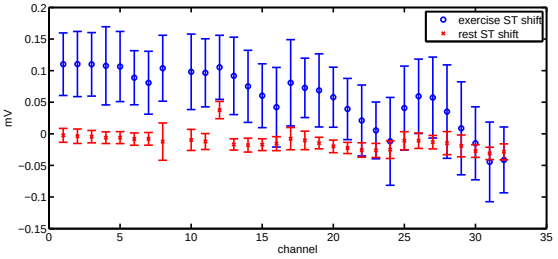

Figure A.15: The ST shifts in the processed rest and exercise recordings of patient3 plotted on top of each other. The standard deviation in the ST shift measurement is included. This is the 32 channels on the back of the patient.

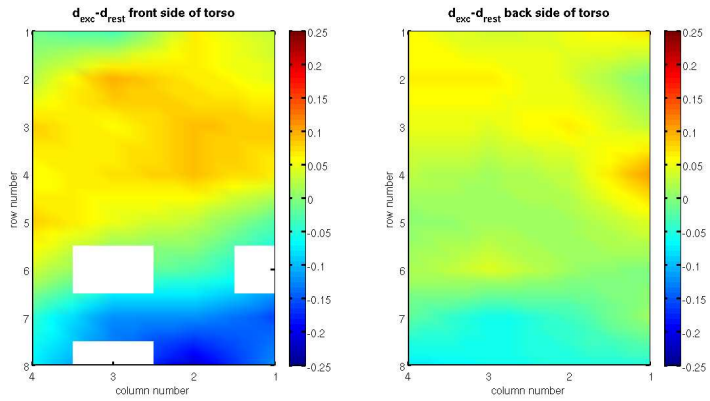

Figure A.16: The BSSM of patient4 after the BSPM has been processed. The left figure shows the front of the patient, the right figure shows the back of the patient.

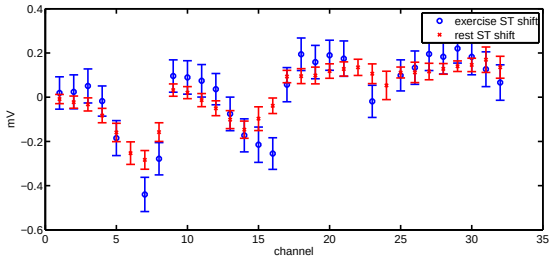

Figure A.17: The ST shifts in the processed rest and exercise recordings of patient4 plotted on top of each other. The standard deviation in the ST shift measurement is included. This is the 32 channels on the front of the patient.

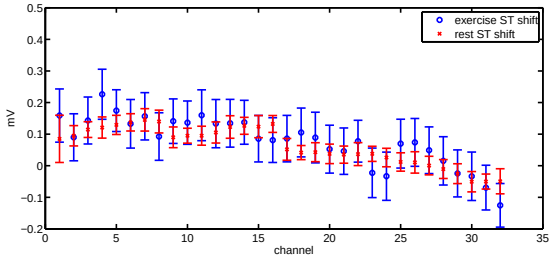

Figure A.18: The ST shifts in the processed rest and exercise recordings of patient4 plotted on top of each other. The standard deviation in the ST shift measurement is included. This is the 32 channels on the back of the patient.

Bibliography

[1] http://www.rikshospitalet.no. Web page.

[2] http://www.simula.no. Web page.

[3] http://www.biosemi.com/strip_electrode.htm. Web page, accessed aug 13, 2008.

[4] http://www.pdsheart.com/glossary.html. Web page, accessed feb 20, 2008.

[5] U. R. Acharya, J. S. Suri, J. A. E. Spaan, and S. N. Krishnan, editors. *Advances in Cardiac Signal Processing*. Springer, 2007.

[6] J. P. Agante and Marques de Sa. ECG Noise Filtering Using Wavelets with Soft-tresholding Methods. *IEEE Computers in Cardiology*, 1999.

[7] A. A. Agateller. http://en.wikipedia.org/wiki/image:sinusrhythmlabels.png. Web page, accessed jan 12.

[8] Biosemi. http://www.biosemi.com/products.htm. Web page, accessed aug 13, 2008.

[9] R.F. Borries, J. H. Pierluissi, and H. Nazeran. Wavelet Transform-Based ECG Baseline Drift Removal for Body Surface Potential Mapping. In *Proceedings of the 2005 IEEE Engineering in Medicine and Biology 27th annual conference*, 2005.

[10] H. C. Chen and S. W. Chen. A Moving Average based Filtering System with its Application to Real-time QRS Detection. *IEEE Computers in Cariology*, 2003.

[11] I. Daubechies. The Wavelet Transform, Time-Frequency Localization and signal analysis. *IEEE Transactions on Information Theory*, 36, 1990.

[12] W. A. H. Engelese and C. Zeelenberg. A single scan algorithm for QRS-detection and feature extraction. *IEEE Computers in Cardiology*, 1979.

[13] G. Erikssen, J. Bodegard, and J. Erikssen. Arbeids-EKG. *Tidsskrift for Den norske legeforening*, 124, 2004. (In norwegian).

[14] G. M. Friesen, T.C. Jannett, M. A. Jadallah, S. L. Yates, S. R. Quint, and H. T. Nagle. A Comparison of the Noise Sensitivity of Nine QRS Detection Algorithms. *IEEE Transactions on Biomedical Engineering*, 1990.

[15] R. J. Gibbons, G. J. Balady, J. T. Bricker, B. R. Chaitman, G. F. Fletcher, V. F. Froelicher, D. B. Mark, B. D. McCallister, A. N. Mooss, M. G. O'Reilly, and W. L. Winters. ACC/AHA 2002 guideline update for exercise testing: a report of the American College of Cardiology/American Heart Association Task Force on Practice Guidelines (Committee on Exercise Testing). *American College of Cardiology Web site.*, 2002. Available at: www.acc.org/clinical/guidelines/exercise/dirIndex.htm.

[16] A. Graps. An introduction to wavelets. *IEEE Computational Science and Engineering*, 2, 1995.

[17] L. S. Green, R. L. Lux, and C. W. Haws. Detection and localization of coronary artery disease with body surface potential mapping in patients with normal electrocardiograms. *Circulation*, 76, 1987.

[18] P. S. Hamilton and W. J. Tompkins. Quantitative Investigation of QRS Detection Rules Using the MIT/BIH Arrythmia Database. *IEEE Transactions on Biomedical Engineering*, BME-33(12), 1986.

[19] H. Hänninen, P. Takala, J. Rantonen, M. Mäkijärvi, K. Virtanen, J. Nenonen, T. Katila, and L. Toivonen. ST-T Integral and T-wave Amplitude in Detection of Exercise-induced Myocardial Ischemia Evaluated With Body Surface Potential Mapping. *Journal of Electrocardiology*, 36, 2003.

[20] J. Keener and J. Sneyd. *Mathematical Physiology*. Springer, 1998.

[21] P. Kliegfield, L. S. Gettes, J. J. Bailey, R. Childers, B. J. Deal, E. W. Hancock, G. van Herpen, J. A. Kors, P. Macfarlane, D. M. Mirvis, O. Pahlm, P. Rautaharju, and G. S. Wagner. Recommendations for the standardization and interpretation of the electrocardiogram: part I: the electrocardiogram and its technology: a scientific statement from the American Heart Association Electrocardiography and Arrhythmias Committee, Council on Clinical Cardiology; the American College of Cardiology Foundation; and the Heart Rhythm Society. *J Am Coll Cardiol*, 2007.

[22] F. Kornreich, T. J. Montague, and P. M. Rautaharju. Body surface potential mapping of st segment changes in acute myocardial infarction. Implications for ECG enrollment criteria for thrombolytic therapy. *Circulation*, 1993.

[23] T.J. Lyche. Lecture Notes for Inf-Mat 3350/4350 2006. http://www.ifi.uio.no/~tom/book2006.pdf, 2006.

[24] P. E. McSharry, G. D. Clifford, L. Tarassenko, and L. A. Smith. A dynamical model for generating synthetic electrocardiogram signals. *IEEE Transactions on Biomedical Engineering*, BME-50(3), 2003.

[25] I. B. A. Menown, J. Allen, J. McC. Anderson, and A. A. J. Adgey. ST depression only on the initial 12-lead ECG: early diagnosis of acute myocardial infarction. *European Heart Journal*, 22, 2001.

[26] D. M. Mirvis. Current status of body surface electrocardiographic mapping. *Circulation*, 75, 1987.

[27] K. Mørken and T.J. Lyche. Lecture notes for Inf-Mat 5340-Spline methods. http://www.uio.no/studier/emner/matnat/ifi/INF-MAT5340/v07/undervisningsmateriale/komp.html, 2007.

[28] B.F. Nielsen, M. Lysaker, and A. Tveito. On the use of the resting potential and level set methods for identifying ischemic heart disease: An inverse problem. *Journal of Computational Physics*, 220, 2007.

[29] J. Pan and W. J. Tompkins. A Real-Time QRS Detection Algorithm. *IEEE Transactions on Biomedical Engineering*, BME-32(3), 1985.

[30] S. V. Pandit. Ecg baseline drift removal through STFT. In *18th Annual international conference of the IEEE Engineering in medicine and biology society, Amsterdam*, 1996.

[31] J. Pekkanen, A. Peters, G. Hoek, P. Tiittanen, B. Brunekreef, J. Hartog, J. Heinrich, A. Ibald-Mulli, W. G. Kreyling, T. Lanki, K. L. Timonen, and E. Vanninen. Particulate Air Pollution and Risk of ST-Segment Depression During Repeated Submaximal Exercise Tests Among Subjects With Coronary Heart Disease: The Exposure and Risk Assessment for Fine and Ultrafine Particles in Ambient Air (ULTRA) Study. *Circulation*, 106, 2002.

[32] J. G. Proakis and D. G. Manolakis. *Digital Signal Processing.* Prentice Hall, 4th edition, 1996.

[33] G. Qi Gao. Computerised detection and classification of five cardiac conditions. Master's thesis, Auckland University of Technology, 2003.

[34] L. Sörnmo. Time-varying filtering for removal of baseline wander in ECGs. *IEEE*, 1992.

[35] L. Sörnmo and P. Laguna. *Bioelectrical signal processing in cardiac and neurological applications.* Elsevier Academic Press, 2005.

[36] G. W. Stone, J. Webb, and D. A. Cox et al. Distal Microcirculatory Protection During Percutaneous Coronary Intervention in Acute ST-Segment Elevation Myocardial Infarction: A Randomized Controlled Trial. *Journal of the American Medical Association*, 293, 2005.

[37] J. Sundnes, G. T. Lines, X. Cai, B. F. Nielsen, K. A. Mardal, and A. Tveito. *Computing the electrical activity in the heart.* Springer, 2006.

[38] P. Takala, H. Hänninen, J. Montonen, M. Mäkiäjrvi, J. Nenonen, L. Oikarinen, K. Simelius, L. Toivonen, and T. Katila. Magnetocardiographic and Electrocardiographic Exercise Mapping in Healthy Subjects. *Annals of Biomedical Engineering*, 29, 2001.

[39] N. V. Thakor, J. G. Webster, and W. J. Tompkins. Estimation of QRS Complex Power Spectra for Design of a QRS Filter. *IEEE Transactions on Biomedical Engineering*, BME-31(11), 1984.

[40] M. A. Tinati and B. Mozaffary. A Wavelet Packets Approach to Electrocardiograph Baseline Drift Cancellation. *International Journal of Biomedical Imaging*, 2006, 2006.

[41] J. A. van Alste and T. S. Schilder. Removal of Base-Line Wander and Power-Line Interference from the ECG by an Efficient FIR Filter with a Reduced Number of Taps. *IEEE Transactions on Biomedical Engineering*, BME-32(12), 1985.

[42] WHO. The World Health Report 2004: changing history. *Geneva:World Health organisation*, 2004.

[43] F. Yanowitz, G. Vincent, R. Lux, M. Merchant, L.S. Green, and J.A. Abildskov. Application of body surface mapping to exercise testing; ST-isoarea maps in patients with coronary artery disease. *American Journal of Cardiology*, 50, 1982.